Final Report

EXPERIMENTAL INVESTIGATION OF SKEWED ELASTOMERIC EXPANSION BRIDGE BEARINGS

by

Gregory D. Allen
and
Thomas M. Murray
Principal Investigator

Sponsored by

Oklahoma Department of Transportation
Reasearch and Development Division

in cooperation with

Federal Highway Administration

Report No. FSEL/ODOT 86-01

August 1986

FEARS STRUCTURAL ENGINEERING LABORATORY
School of Civil Engineering and Environmental Science
University of Oklahoma
Norman, Oklahoma 73019

TECHNICAL REPORT STANDARD TITLE PAGE

1. REPORT NO. FHWA/OK 86(5)	2. GOVERNMENT ACCESSION NO.	3. RECIPIENT'S CATALOG NO.
4. TITLE AND SUBTITLE Experimental Investigation of Skewed Elastomeric Expansion Bridge Bearings		5. REPORT DATE August, 1986 6. PERFORMING ORGANIZATION CODE
7. AUTHOR(S) Gregory D. Allen and Thomas M. Murray		8. PERFORMING ORGANIZATION REPORT
9. PERFORMING ORGANIZATION NAME AND ADDRESS Fears Structural Engineering Laboratory University of Oklahoma 303 E. Chesapeake St. Norman, OK 73019		10. WORK UNIT NO. 11. CONTRACT OR GRANT NO. Agreement #34, 84-11-2
12. SPONSORING AGENCY NAME AND ADDRESS Research and Development Division Oklahoma Department of Transportation 200 NE 21st Oklahoma City, OK 73105		13. TYPE OF REPORT AND PERIOD COVERED Final 14. SPONSORING AGENCY CODE

15. SUPPLEMENTARY NOTES in cooperation with

Federal Highway Administration, US Department of Transportation

16. ABSTRACT Twelve skewed elastomeric expansion bridge bearings were supplied by the Oklahoma Department of Transportation. To evaluate the performance of these skewed bearings, the following six phases of testing were conducted on each of the twelve bearings: I. Shear and compressive stiffness tests, II. Fatigue cycles representing 50 years of service with parallel bearing surfaces, III. Shear and compressive stiffness tests, IV. Shear stiffness tests with bearings at sub-freezing temperatures, V. Fatigue cycles representing 50 years of service with rotated bearing surfaces, and VI. Shear stiffness tests. Phase I formed the basis of comparison with the post-fatigue results from Phases III and VI, and the low temperature tests from Phase IV. It was found that the fatigue loading with parallel bearing surfaces had very little effect on the compressive and shear stiffnesses of the skewed bearings. Some degradation of shear stiffness was found after the fatigue loading with rotated bearing surfaces, Phase V. However, the combined degradation due to both fatigue loadings was considered insignificant.

It was found that the simple shear equation for estimating the shear stiffnesses of the twelve bearings was very conservative and no correlation was evident between predictions and the experimental results of Phase I. In general, the shear stiffness changed more rapidly than the change in bearing area as the skew angle decreased from 90° (rectangular) to 30°.

As an outgrowth of the experimental work, design expressions for determining the effective shear stiffnesses of both skewed and rectangular bearings with turned axes were developed. Excellent correlation was found between shear stiffness predictions from the proposed equations and the experimental results.

17. KEY WORDS skew, bearings, elastomeric, bridges, shear stiffness, expansion device, shear modulus	18. DISTRIBUTION STATEMENT no restrictions		
19. SECURITY CLASSIF. (OF THIS REPORT) none	20. SECURITY CLASSIF. (OF THIS PAGE) None	21. NO. OF PAGES 139	22. PRICE

This publication was printed and issued by the Oklahoma Department of Transportation as authorized by V. O. Bradley, Director. 55 copies have been prepared and distributed at a cost of $184.35.

ABSTRACT

Twelve skewed elastomeric expansion bridge bearings were tested to evaluate their performance when subjected to shear fatigue and low temperature loadings. The following six phases of testing were conducted for each of the twelve bearings:

I. Shear and compressive stiffness tests.

II. Fatigue cycles representing 50 years of service with parallel bearing surfaces.

III. Shear and compressive stiffness tests.

IV. Shear stiffness tests with bearings at sub-freezing temperatures.

V. Fatigue cycles representing 50 years of service with rotated bearing surfaces.

VI. Shear stiffness tests.

Phase I formed the basis of comparison with the post-fatigue results from Phases III and VI, and the low temperature tests from Phase IV. It was found that the fatigue loading with parallel bearing surfaces had very little effect on the compressive and shear stiffnesses of the skewed bearings. Some degradation of shear stiffness was found after the fatigue loading with rotated bearing surfaces, Phase V. However, the combined degradation due to both fatigue loadings was considered insignificant.

It was found that the simple shear equation for estimating the shear stiffnesses of the twelve bearings was very conservative and no correlation was evident between predictions and the experimental results of Phase I. In general, the shear stiffness changed more rapidly than the change in bearing area as the skew angle decreased from 90° (rectangular) to 30°.

As an outgrowth of the experimental work, design expressions for determining the effective shear stiffnesses of both skewed and rectangular bearings with turned axes were developed. Excellent correlation was found between shear stiffness predictions from the proposed equations and the experimental results.

METRIC CONVERSION FACTORS

Approximate Conversions to Metric Measures

Symbol	When You Know	Multiply by	To Find	Symbol
		LENGTH		
in	inches	*2.5	centimeters	cm
ft	feet	30	centimeters	cm
yd	yards	0.9	meters	m
mi	miles	1.6	kilometers	km
		AREA		
in^2	square inches	6.5	square centimeters	cm^2
ft^2	square feet	0.09	square meters	m^2
yd^2	square yards	0.8	square meters	m^2
mi^2	square miles	2.6	square kilometers	km^2
	acres	0.4	hectares	ha
		MASS (weight)		
oz	ounces	28	grams	g
lb	pounds	0.45	kilograms	kg
	short tons (2000 lb)	0.9	tonnes	t
		VOLUME		
tsp	teaspoons	5	milliliters	ml
Tbsp	tablespoons	15	milliliters	ml
fl oz	fluid ounces	30	milliliters	ml
c	cups	0.24	liters	l
pt	pints	0.47	liters	l
qt	quarts	0.95	liters	l
gal	gallons	3.8	liters	l
ft^3	cubic feet	0.03	cubic meters	m^3
yd^3	cubic yards	0.76	cubic meters	m^3
		TEMPERATURE (exact)		
°F	Fahrenheit temperature	5/9 (after subtracting 32)	Celsius temperature	°C

*1 in = 2.54 (exactly). For other exact conversions and more detailed tables, see NBS Misc. Publ. 286, Units of Weights and Measures. Price $2.25, SD Catalog No. C13.10:286

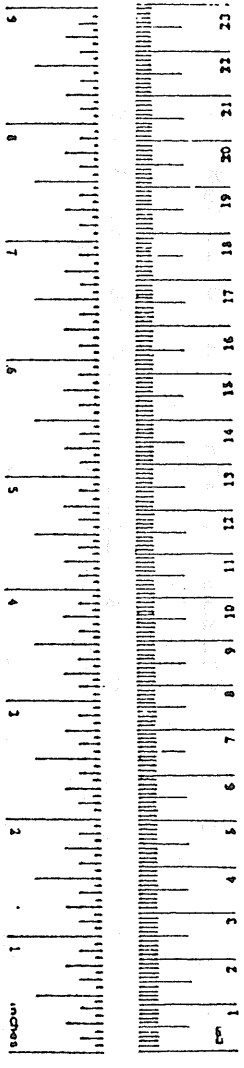

Approximate Conversions from Metric Measures

Symbol	When You Know	Multiply by	To Find	Symbol
		LENGTH		
mm	millimeters	0.04	inches	in
cm	centimeters	0.4	inches	in
m	meters	3.3	feet	ft
m	meters	1.1	yards	yd
km	kilometers	0.6	miles	mi
		AREA		
cm^2	square centimeters	0.16	square inches	in^2
m^2	square meters	1.2	square yards	yd^2
km^2	square kilometers	0.4	square miles	mi^2
ha	hectares (10,000 m^2)	2.5	acres	
		MASS (weight)		
g	grams	0.035	ounces	oz
kg	kilograms	2.2	pounds	lb
t	tonnes (1000 kg)	1.1	short tons	
		VOLUME		
ml	milliliters	0.03	fluid ounces	fl oz
l	liters	2.1	pints	pt
l	liters	1.06	quarts	qt
l	liters	0.26	gallons	gal
m^3	cubic meters	35	cubic feet	ft^3
m^3	cubic meters	1.3	cubic yards	yd^3
		TEMPERATURE (exact)		
°C	Celsius temperature	9/5 (then add 32)	Fahrenheit temperature	°F

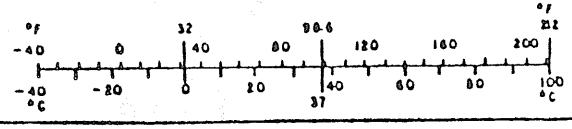

TABLE OF CONTENTS

LIST OF FIGURES

LIST OF TABLES

NOMENCLATURE

a = long dimension of rectangular bearing

b = short dimension of rectangular bearing

k = shear stiffness

$(k_s)_\alpha$ = shear stiffness of skewed bearings for any given skew angle

$(k_t)_\alpha$ = shear stiffness of turned bearings for any given turn angle

t = thickness of one elastomeric layer

A = plan area of undeformed bearing

A_e = effective bearing area in shear

E = Young's modulus

G = shear modulus

H = total bearing height

I = moment of inertia of the bearing plan area taken about an axis perpendicular to the girder axis

L = length of skewed bearing parallel to girder axis

P = compressive force

S = shape factor

$T = \Sigma t_i$'s = sum of the internal elastomeric layer thicknesses

V = shear force

W = width of skewed bearing perpendicular to girder axis

α = skew or turn angle

Δ_c = compressive deflection

Δ_s = shear deformation

ε_c = compressive strain

τ = Poisson's ratio

σ_c = compressive stress

CHAPTER I

INTRODUCTION

1.1 Background

Expansion and contraction caused by temperature, deflection, relative support settlement, creep, etc., will produce longitudinal motion in a bridge. If this motion is constrained, the resulting forces may be very large. Moveable bearings at piers or abutments are commonly used to control the magnitude of these forces. The only horizontal force transmitted to the pier or abutment is then through fiction caused by the relative motion of the bearing parts or by shear deformation of a deformable bearing. In either case, the resulting force must be considered in the design of the supporting structure, if not, structural damage can occur.

Elastomeric bearings allow longitudinal motion to take place and transmit forces to the abutments or piers because of shear deformations. Current AASHTO specifications [1] are written for elastomeric bearings that are rectangular in shape with all movement perpendicular to a centerline of the bearing. If a bridge, however, spans a river or a highway that is not perpendicular to it, movement other than perpendicular to the centerline of the bearing may have to be allowed. Two methods of providing for movement when abutments or piers are "skewed" with respect to the bridge centerline are shown in Figures 1.1 and 1.2. Figure 1.1

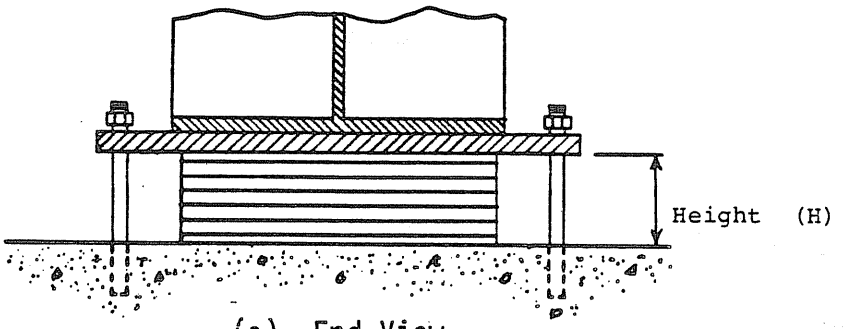

(a) End View

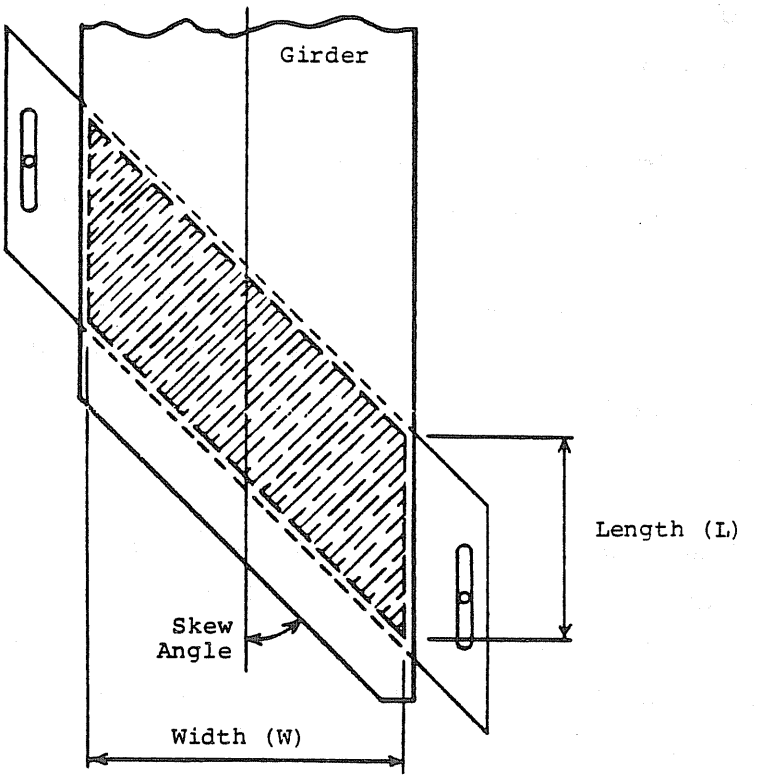

(b) Plan View

Figure 1.1 Typical Skewed Bearing

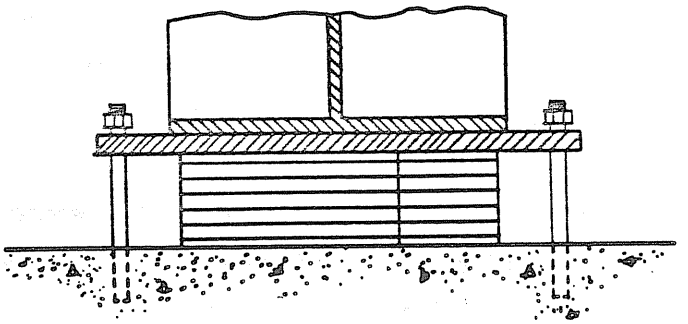

(a) End View

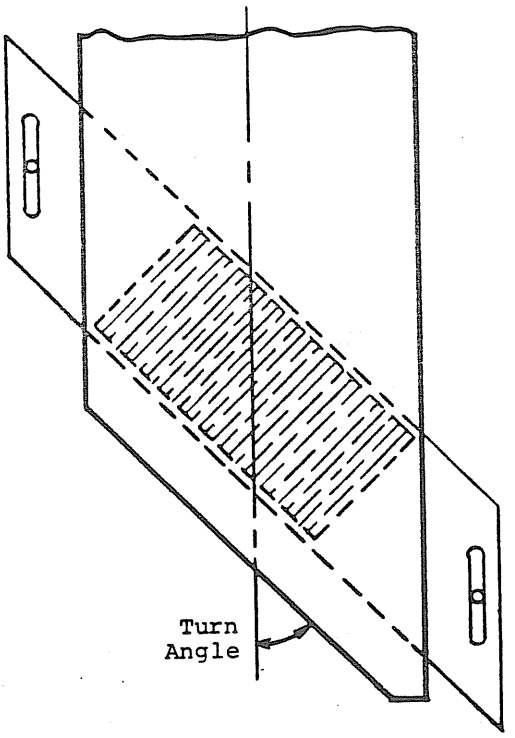

(b) Plan View

Figure 1.2 Typical Turned Bearing

shows what will be termed a "skewed bearing" in this report. Figure 1.2 illustrates what is termed here as a "turned bearing". Proper design of skewed or turned elastomeric bearings requires a knowledge of shear stiffness or the load-shear deformation relationship, compressive stiffness or the load-compression relationship, low temperature effects, and fatigue and out-of-plane rotation effects.

The first purpose of this study was to experimentally determine the effective shear stiffness and the behavior at low temperatures of twelve skewed elastomeric bearings. The second purpose was to investigate the effects of bridge girder end rotations and the performance of the bearings under fatigue loading. A typical skewed bearing used in the study is shown in Figure 1.1, and consists of a variable number of 1/2 inch layers of Neoprene bonded together by 14 gage steel laminates.

An outgrowth of the experimental work was the development of design expressions for determining the effective shear stiffnesses of both skewed and turned bearings.

1.2 Previous Research

A literature study was conducted and all of the findings are listed in the bibliography. Very few studies of full-scale elastomeric bridge bearings were found; none included skewed or turned bearings.

Long [11] has written a book about the properties and design of elastomeric bearings, but does not present any experimental work nor are skewed or turned bearings discussed.

Minor and Egen [13] conducted research including a survey of the literature and available test data, and an evaluation (testing) program of rectangular elastomeric bearings. The evaluation program investigated: 1) shear modulus and stress relaxation, 2) compressive behavior, 3) shear and compression of commercial bearings, and 4) cyclic shear under constant compression. Shape or orientation related elastomeric bearing research was not conducted nor was it reported in the literature survey presented.

Stanton and Roeder [18], in an extensive study of elastomeric bridge bearings, under the sponsorship of the National Cooperative Highway Research Program (NCHRP) published their findings for two tasks:

1) An extensive literature survey, which included a review of current domestic and foreign codes of practice, research findings, and performance data, and

2) Analysis and evaluation of the information generated in Task 1 to establish a rationale for the development of design, construction, and material specifications for unconfined, plain, and reinforced elastomeric bearings.

To reach the objectives of the above tasks, an advisory panel of specialists was selected by the researchers to assist in the investigation. These specialists assisted in the search for information, as well as contributing their expertise concerning elastomeric bearings. The acquisition of information was carried out in three areas: 1) A telephone survey of bridge engineers in the United States to determine the current practice trends and to find out what problems are occurring in elastomeric bearings. 2) An

extensive literature search providing information on materials, theoretical mechanics, experimentations in laboratories and in the field, and codes of practice. And 3), visits to manufacturers, researchers, and engineers in the United States, as well as abroad, in order to gain the unpublished knowledge that has been accumulated over many years of practical experience.

Since Stanton and Roeder's report is the state-of-the-art in the behavior and design of elastomeric bearings, a complete review is not presented here; however, some of their findings and related theoretical mechanics will be presented in Chapter II. Stanton suggests that shape related parameters do affect shear deformations and that there is an insufficient amount of research findings in this area to change current specifications. Skew and other shape-related effects, and effects of orientation, however, were not reported in their findings. It is the intent of this study to help further the technology in this area.

1.3 Provisions of the AASHTO Specifications

The major provisions of the 1985 Interim, Section 14, Elastomeric Bearings, of the AASHTO Specifications [1] for steel reinforced rectangular elastomeric bearings are summarized in Table 1.1. These provisions include the allowable shear and compressive displacements, shear and compressive displacement equations, the rotational capacity, and the limiting criteria for compressive loading. The nomenclature used in Table 1.1 is defined in Figures 1.3, 1.4 and 1.5.

This specification limits the average compressive stress, $\sigma_c = P/A$, of any layer to the smaller of 1000 psi or GS/β, where G = shear modulus, S = shape factor and β = a

Table 1.1

Summary of the Major Provisions
of the AASHTO Specifications [1]

Allowable Shear Deformation	Shear Force Equation	Allowable Compressive Displacement	Compressive Deflection Equation
$\Delta_s \leq 0.5T$ $T = \Sigma t_i$'s	$V = GA\Delta_s/T$ $A = LW$	*	$\Delta_c = \Sigma \varepsilon_{ci} t_i$
Limiting Criteria for Allowable Compressive Load, P		Allowable Rotational Capacity	
$\sigma_c = P/A \leq 1000$ psi $\leq GS/\beta$ $\geq 5V$		$L\alpha_l + W\alpha_w \leq 2\Delta_c$	

*In previous versions of AASHTO Specifications, but not included in 1985 Interim AASHTO Specification

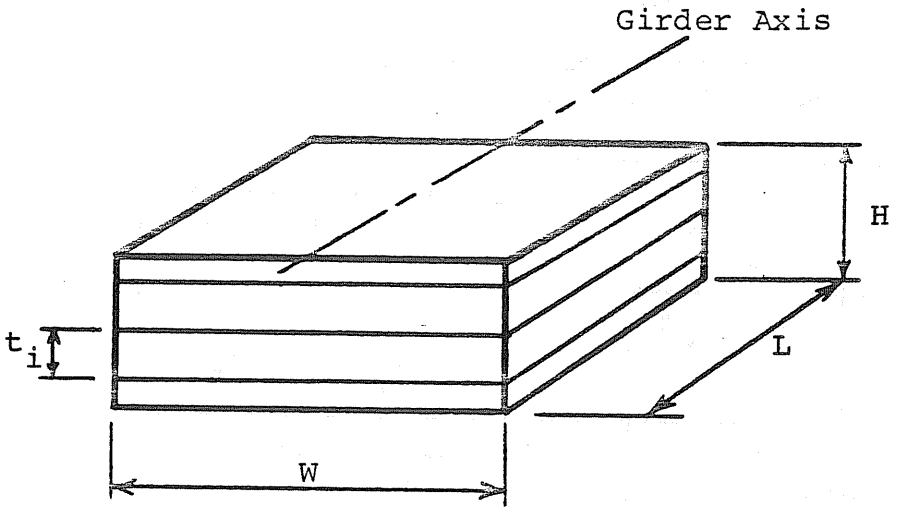

Figure 1.3 AASHTO Geometric Parameters

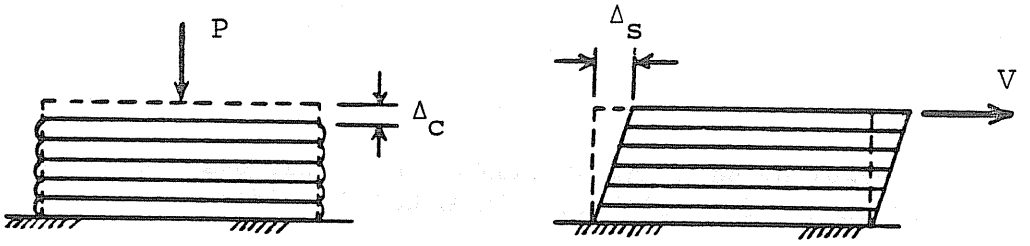

Figure 1.4 Compressive and Shear Displacements

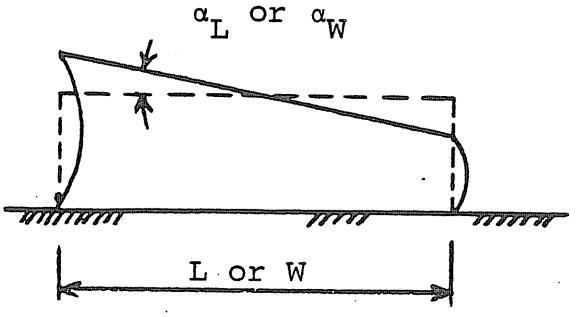

Figure 1.5 Rotational Displacements

modifying factor having a value of 1.0 for internal layers and 1.4 for the cover layers of a reinforced elastomeric bearing. However, the compressive stress must be greater than 200 psi to prevent slip of the bearing relative to its concrete support. The shape factor, S, is defined as

$$S = LW/[2t(L+W)] \tag{1.1}$$

where L = the length of bearing parallel to the shear deformation, W = the bearing width transverse to the shear deformation, and t = the thickness of one elastomer layer. If layer thicknesses vary, the value of S used is that for the thickest layer of elastomer. Equation 1.1 applies for rectangular bearings with the applied shear force perpendicular to one of its centerlines.

Compressive deflection, Δ_c, is calculated as the sum of the compressive strain, ε_{ci}, times the layer thickness for each layer. Values for ε_{ci} are obtained from design aids such as shown in Figure 1.6. The provisions state that Δ_c shall be less than 0.07 times the total elastomeric thickness, T, taken as the sum of the internal and cover layer thicknesses, Σt_i's.

Rotation of a reinforced elastomeric bearing, due to end girder rotation or construction tolerance, defined as $L\alpha_1 + W\alpha_w$, is limited to two times the compressive displacement. This rotation limitation is intended to prevent the development of tensile stresses in a bearing to minimize a delamination of the elastomer layer from the steel reinforcement [18].

The required shear deformation is the maximum bridge girder displacement caused by creep, shrinkage, post-tensioning and thermal expansion, computed between the

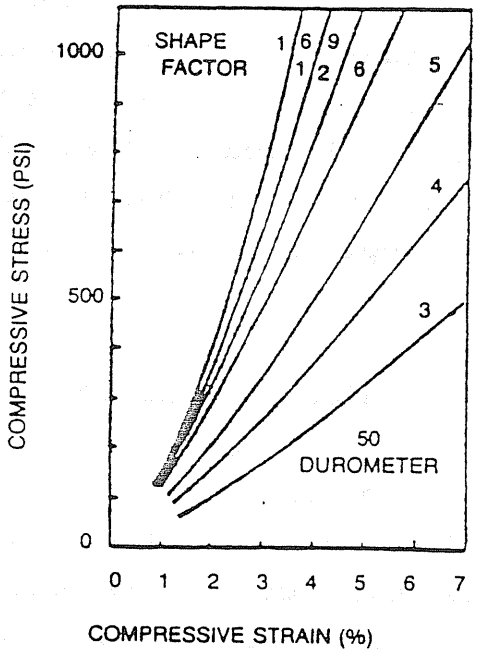

(a) 50 Durometer Rubber

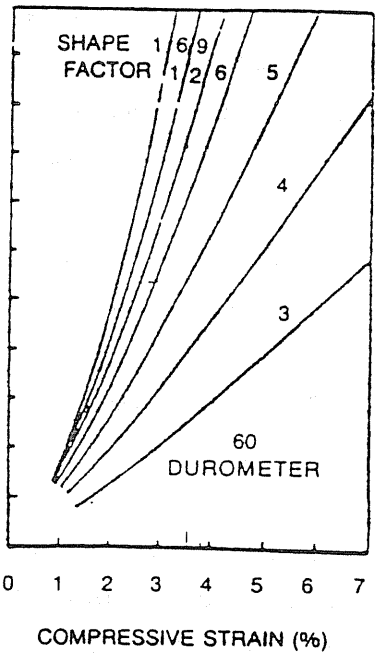

(b) 60 Durometer Rubber

Figure 1.6 Compressive Stress-Strain Curves as an AASHTO Design Aid (from reference 1)

bearing installation temperature and the least favorable extreme temperature. The AASHTO Specification states that the shear strain is to be limited to 50%, or $\Delta_s \leq 0.5\ T$, to insure bearing stability. The shear force caused by shear deformation, V, is to be approximated by

$$V = \frac{G\ L\ W}{T}\ \Delta_s \tag{1.2}$$

The variation of the shear modulus, G, due to low temperature is to be taken into account. Shear stiffness, k, is then defined as

$$k = V/\Delta_s = GA/T \tag{1.3}$$

and does not include any consideration of bearing geometry.

Among the foreign codes discussed by Stanton [18], all have the same major design provisions as the AASHTO Specifications. All have similar allowable design values and the design expressions seem to have come from the same theoretical basis even though they vary slightly. The only design criteria that differs between these foreign codes and the AASHTO Specification is that of the allowable compressive load. AASHTO bases its design criteria on the average compressive stress. The foreign codes, however, all base the allowable compressive load on the combined shear stress due to compressive loading, shear displacement and bearing rotation. Both the foreign codes and the AASHTO Specification estimate shear stiffness using Equation 1.3, which does not take into account any geometric effects.

1.4 Scope of Research

Since no published data was found on skewed bearings, a testing program was undertaken to investigate the

performance of bearings typically used by the Oklahoma Department of Transportation (ODOT).

The bearings were designed according to the current AASHTO Specification [1] by the ODOT Bridge Division. Three series of four bearings each were configured for different steel bridge spans; bearings type "A" were designed for a bridge span of approximately 200 feet, type "D" for approximately 400 feet spans, and the "E" series bearings for 100 feet span bridges. In all cases, the maximum change in temperature for design purposes was 90°F and the coefficient of thermal expansion for the steel girder was taken as 6.5 x 10-6 in/in/°F. The equation used to establish the maximum longitudinal expansion of the girder is

$$\Delta_s = \alpha L T \qquad (1.4)$$

where α = coefficient of thermal expansion, L = girder span, T = change in temperature in °F, and Δ_s = the longitudinal expansion of the girder.

Design parameters for the bearings included skew angle, height, width and length, as defined in Figure 1.1. The bearings are divided into three series, A, D, and E, depending on the design girder span, which resulted in heights of 3 7/16 in., 6 5/16 in. and 1 3/4 in., respectively. These heights were determined by adding the total rubber thicknesses and the steel laminate thicknesses of each bearing. The total rubber thickness was determined using the AASHTO 50% shear strain limitation. Each series included bearings having skew angles, as defined in Figure 1.1, of 90°, 60°, 45° and 30°, thus the designations A90, A60, etc. The bearing area of each bearing was such that under design dead loads, the contact pressure was at least 200 psi, as specified by AASHTO to insure no slippage.

Tables 1.2 and 1.3 are summaries of the bearing geometric parameters (skew angle, internal bearing details, height, width and length) and bearing test parameters (maximum design shear displacement, area, shape factor, neoprene hardness measured with a Shore A type durometer, shear modulus and design loads), respectfully. It is noted that the area, shape factor and Durometer reading for each bearing in a series are not equal. Since the plan areas differ, direct comparisons of the shear stiffnesses of bearings in a series are not possible. The shear stiffness per unit area for each bearing pad can be compared, but this comparison would mean very little since the elastomer hardness readings and thus the shear moduli are not the same.

To simulate actual bridge and environmental conditions, the bearings were placed in a test setup that simulated bridge girder movement with respect to an abutment. The test setup, instrumentation and testing procedures are discussed in Appendix A; Figure 1.7 is a photograph showing an overall view of the test setup.

Each bearing was subjected to six phases of testing. Phase I consisted of a series of shear and compressive stiffness tests. In this phase, the two contact surfaces of the bearing was parallel, and there was no intentional rotation of the elastomeric bearing. In Phase II, each bearing was subjected to a fatigue loading program that simulated the effects of temperature changes throughout every year for an anticipated fifty year life span of a bridge. Phase III is a repeat of Phase I to establish the effects of the fatigue cycles of Phase II. Any changes in the shear and compressive stiffness detected were contributed solely to fatigue effects.

Table 1.2

Skewed Bearing Geometric Parameters

Bearing Pad Series	Internal Bearing Details	Skew Angle (deg)	H Height (in)	W Width (in)	L Length (in)
A	7 ply Neoprene 5 inner plies of 1/2 in. 2 cover plies of 1/4 in. 6-14 Ga. laminates	90 60 45 30	3 7/16	18	9 9 5/8 10 1/2 12
D	12 ply Neoprene 10 inner plies of 1/2 in. 2 cover plies of 1/4 in. 11-14 Ga. laminates	90 60 45 30	6 5/16	16 1/2	16 1/2 17 1/4 18 1/2 21
E	4 ply Neoprene 2 inner plies of 1/2 in. 2 cover plies of 1/4 in. 3-14 Ga. laminates	90 60 45 30	1 3/4	18	17 17 1/4 18 1/2 21

Table 1.3

Additional Skewed Bearing Parameters

Bearing	Max. Design Displacement (in)	Area (in^2)	Shape Factor	Durometer Reading* (hardness)	Shear Modulus (psi)	Design Loading (kips)
A90	1 1/2	162.0	6.0	55	105	RDL = 75
A60		173.3	5.7	60	128	RLL = 40
A45		189.0	5.3	57	111	
A30		216.0	4.5	58	114	TL = 115
D90	2 3/4	272.3	8.3	55	105	RDL = 190
D60		284.6	7.9	62	128	RLL = 40
D45		305.3	7.3	60	120	
D30		346.5	6.4	59	117	TL = 265
E90	3/4	306.0	8.7	55	105	RDL = 215
E60		310.5	8.2	61	124	RLL = 85
E45		333.0	7.6	56	108	
E30		378.0	6.6	58	114	TL = 300

Note: RDL = Dead Load Reaction
RLL = Live Load Reaction
TL = Total Load

*Measured

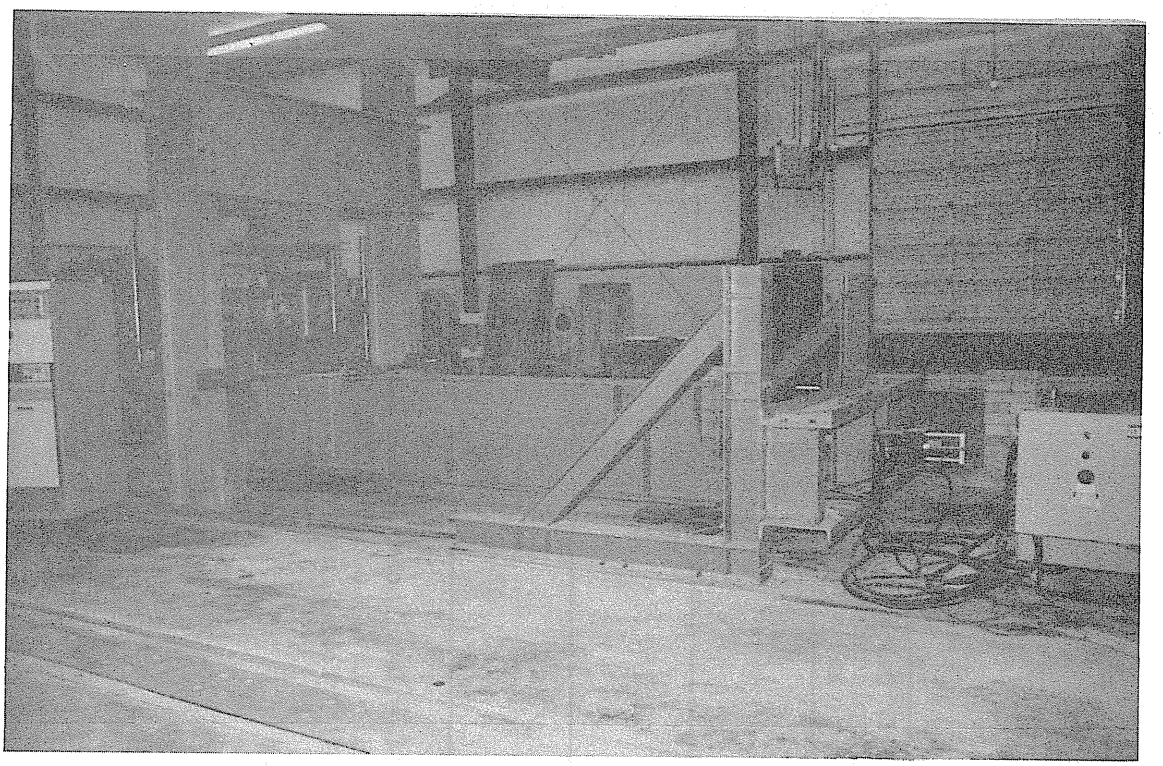

Figure 1.7 Photograph of Test Setup

In Phase IV, each bearing was placed for 72 hours in a deep freeze unit set at a nominal temperature of -20°F. Immediately upon removal, a shear stiffness test was conducted with a compressive force equal to the design dead loading. The shear stiffness of each bearing found in this phase was compared to the values of Phase III and any increase in the stiffnesses was attributed to the effects of low temperature.

The tests of Phases V and VI were repeats of those of in Phases II and III, respectively, except that the test setup was altered so that one of the contact surfaces of the bearing was at a 2% slope with respect to the other surface. This slope accounts for end rotations of the bridge girder due either to loading or construction misalignment. The results of Phase VI were compared with those of Phase III to assess the performance of each bearing after it had been subjected to a "rotated" fatigue program.

After the six test phases were completed on the original twelve bearings, the bearings of the "A series" were twice cut to form additional test specimens. The purpose was twofold: 1) To compare the shear stiffnesses of skewed bearings with different skew angles and the same shear modulus, and 2) To establish the effects of turning a rectangular bearing. Table 1.4 shows the parameters for these additional test bearings. The bearings are designated by the original bearing designation followed by the new skew angle; i.e. A30-M45 for bearing A30 "modified" to a 45° skewed bearing. After the shear stiffness tests of bearing A30-M90A, this bearing was recut to form A30-M90B, which was also tested.

As background for interpreting the results of the testing program the theoretical aspects of the mechanics of elastomeric bearings are first given in the next chapter.

Table 1.4

Parameters for the Additional Test Specimens

Bearing	Skew Angle (deg)	W Width (in)	L Length (in)	Shape Factor
A30-M45	45	20.0	9.00	4.8
A30-M60	60	20.0	7.50	4.9
A30-M90A	90	19.0	6.50	4.8
A30-M90B	90	12.5	6.50	4.3
A45-M90	90	18.0	7.50	5.3
A60-M90	90	15.5	8.75	5.6

CHAPTER II

MECHANICS OF ELASTOMERIC BEARINGS

2.1 General Behavior

To establish a basis of comparison of the test results and to help assess skew effects, if any, the general behavior and theoretical mechanics of elastomeric bearings are first presented. The principles of mechanics are used to provide a theoretical relationship between the forces and deformations of an elastomeric pad. These principles combine the constitutive equations and equilibrium with the boundary conditions to obtain a solution. The mechanical behavior of rubber is very complex, but in some cases may be considered as linearly elastic, as will be discussed later. Elastomeric behavior is unlike that of other more conventional material in that it is very flexible in shear and yet it is nearly incompressible [18]. Also, compressive loads have little effect on the shear stiffness of a bearing.

An elastomeric pad compressed between two perfectly lubricated surfaces will deform as shown in Figures 2.1(a) and 2.1(b). The deformation will occur such that a constant volume is maintained. If the compressing surfaces are bonded to the elastomeric pad, the bulge shape shown in Figure 2.1(c) will result. If a number of internal laminates are added to restrain the bulging, the elastomeric pad will deform as shown in Figure 2.1(d). The addition of

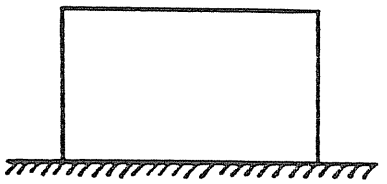

(a) Undeformed Pad

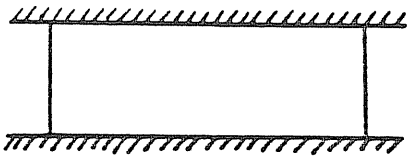

(b) Perfectly Lubricated Pad

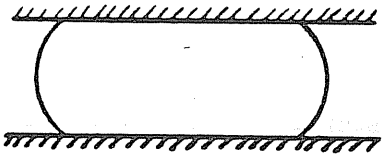

(c) Confined Bearing Surfaces

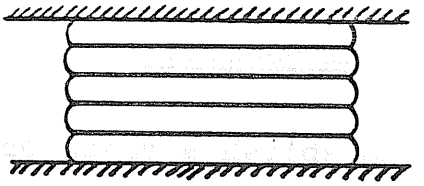

(d) Laminated Bearing with Confined Bearing Surfaces

Figure 2.1 Compressive Behavior of Elastomeric Pads

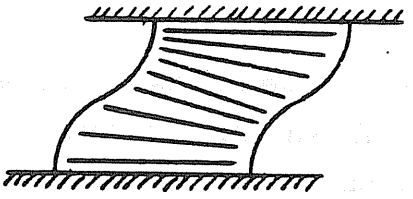

(a) Bending

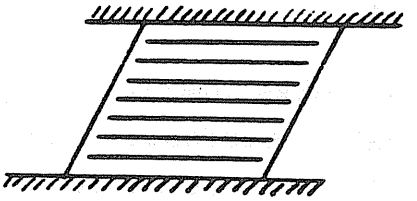

(b) Shear

Figure 2.2 Shear Behavior of Elastomeric Pads

internal laminates significantly increases the compressive stiffness [18].

When horizontal shear is applied, lateral displacement of one surface relative to the other is a combination of both bending and shear, as shown in Figure 2.2. The flexural component of this lateral movement is generally small, even when second order effects of the compressive load (P-δ effect) and lateral bulging is taken into account. Boundary conditions may also have an effect on the shear component of the lateral deformation. Part of the purpose of this investigation is to determine how skew affects shear deformations.

2.2 Compressive Behavior

A non-dimensional, boundary condition type parameter for a single layer of rubber is called the shape factor and is a good indication of the compressive stiffness of a layer [18]. Shape factor, S, for an elastomeric layer is defined as

$$S = \frac{\text{area of one loaded surface}}{\text{area free to bulge}} \qquad (2.1)$$

$$= \frac{a\,b}{2t\,(a+b)}$$

where a = width of bearing, b = length of bearing, and t = thickness of one elastomeric layer.

Bearings with high shape factors have relatively higher compressive stiffnesses than those with small shape factors. Laminated, or reinforced bridge bearings typically have shape factors from 4 to 12 [18].

An elastomeric pad in compression shows a nonlinear,

stiffening force-deformation curve as shown in Figure 2.3. Since the compressive behavior in this study is qualitative and not quantitative, no further discussion is included.

2.3 Shear Behavior

2.3.1 Simple Shear

Even though there are contributions to lateral deformations of a bearing other than shear deformations, such as the P-δ effect and lateral bulging of the rubber layers, these contributions are very small as compared to simple shear deformations [18]. For practical design purposes, the lateral movement is assumed to be a linear elastic, e.g. simple shear deformation. The shear stiffness is then given by

$$k = \frac{G\,A}{\Sigma t_i} \tag{2.2}$$

where G = shear modulus, A = plan area of undeformed bearing, and Σt_i = sum of the internal elastomeric layer thicknesses. Since the shear deformation is assumed to be linear elastic, Hooke's Law applies, that is,

$$G = \frac{E}{2(1 + \tau)} \tag{2.3}$$

where E = Young's modulus and τ = Poisson's ratio. Poisson's ratio for the elastomeric pads used in this study is taken as 0.5; according to Stanton values for τ range from 0.4985 to 0.4999 [18]. Where as the value of τ is rather stable for this type of rubber, the shear modulus can vary substantially.

The compounding and vulcanization process of making

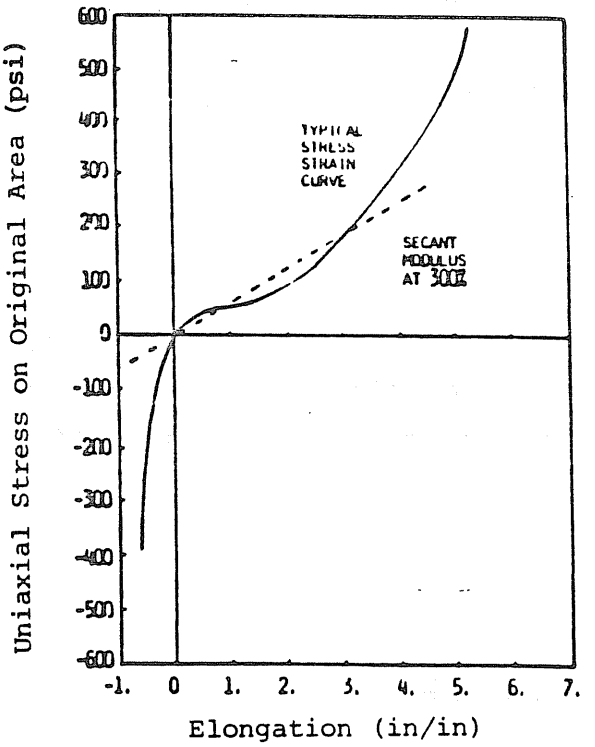

Figure 2.3 Typical Stress/Strain Curve for Neoprene (18)

reinforced elastomeric bearings effect the properties of the rubber [18]. The most easily measured property of the completed bearing is the International Degrees of Hardness measured with a Shore A durometer. Hardness is in turn used to define other properties of a completed bearing. Since the fabrication processes significantly affect hardness, there is a wide scatter in relating hardness to shear modulus. For the purposes of this study, the following values were used: 90 to 120 psi at 50 hardness, 120 to 180 psi at 60 hardness, and 180 to 240 psi at 70 hardness as the shear moduli [18]. Figure 2.4 shows the elastic modulus as a function of rubber hardness.

According to Stanton [3], the effect of shape factors on the shear stiffness can be accommodated by substituting for G an apparent shear modulus, G_a. Stanton gives the variation of G_a with shape factor as shown in Figure 2.5. As seen in this figure, for shape factors greater than 3 the ratio of G_a to G approaches 1.0. The effects of shape factor values on shear stiffness were not taken into account for the skewed bearings tested because their shape factors were larger than 3.0.

2.3.2 Combined Shear and Bending

Although it is often assumed that shape effects can be ignored in simple shear theory, when rubber is "sheared" in the conventional manner, both shearing and bending occur and the total displacement, Δ_s, is the sum of the displacements due to both effects. Using Southwell's [17] equation for the displacement and using E = 3G [18], the resulting shear stiffness including bending effects is

$$k = \frac{V}{\Delta_s} = \frac{G / T}{(1/A + T^2/36I)} \qquad (2.4)$$

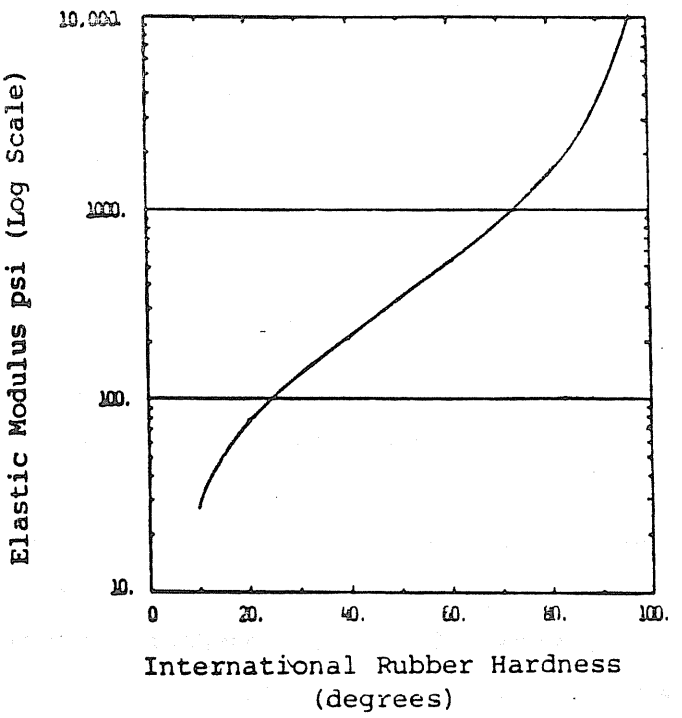

Figure 2.4 Elastic Modulus as a Function of Rubber Hardness (18)

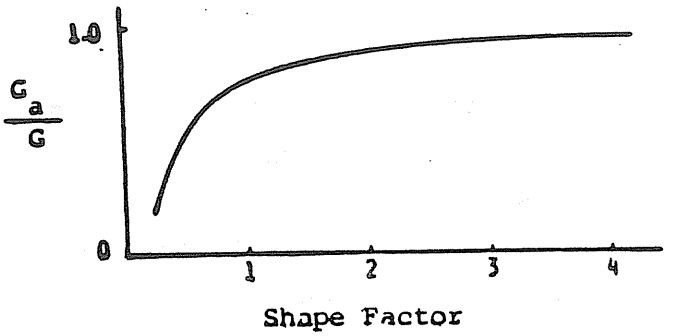

Figure 2.5 Apparent Shear Modulus as a Function of Shape Factor (18)

where I = the moment of inertia of the bearing plan area taken about an axis perpendicular to the girder axis. The first term in the denominator is the pure shear term. The second term is the pure bending contribution which reduces the horizontal stiffness of the bearing. The bending contribution is included in the development of design equations for skewed and turned bearings which are presented in Chapter III.

2.4 Rotational Effects

Elastomeric bearings may develop a hydrostatic tensile stress within a rubber layer due to a rotation of one bearing contact surface with respect to another, see Figure 2.6. Laminated bearings with relatively large shape factors will develop large hydrostatic tensile stresses with relatively small strains [18]. An initial crack or a flaw in the rubber may grow and cause bearing failure due to this tensile stress when the bearing is subjected to fatigue loading.

The distribution of stresses due to bearing rotation caused by the supported girder is shown in Figure 2.7 for a rectangular bearing. The shear stress due to rotation is distributed along the entire width of a rectangular bearing transverse to the girder line. Similarly, the compressive stresses due to rotation and direct normal loading are distributed along the bearing width for rectangular bearings. For skewed bearings, however, these stresses must be distributed around the relatively small area near the "point" of the skewed bearing, see Figure 2.8. Similarly, hydrostatic tensile stresses will be distributed around the diagonally opposite point of skew. Since these stresses concentrate in the skew points, which is unlike rectangular bearings, the fatigue effects on rotated skewed bearings were investigated in this study.

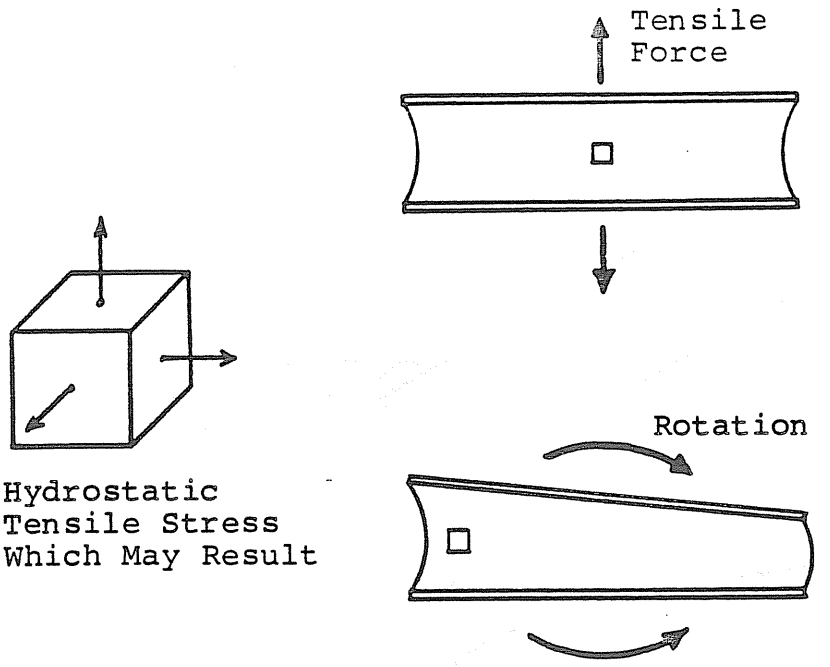

Figure 2.6 Hydrostatic Tensile Stresses

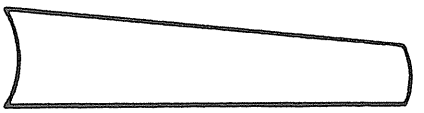

(a) Rotation

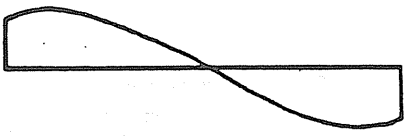

(b) Direct Stress

(c) Shear Stress

Figure 2.7 Stresses Caused by Bearing Rotation

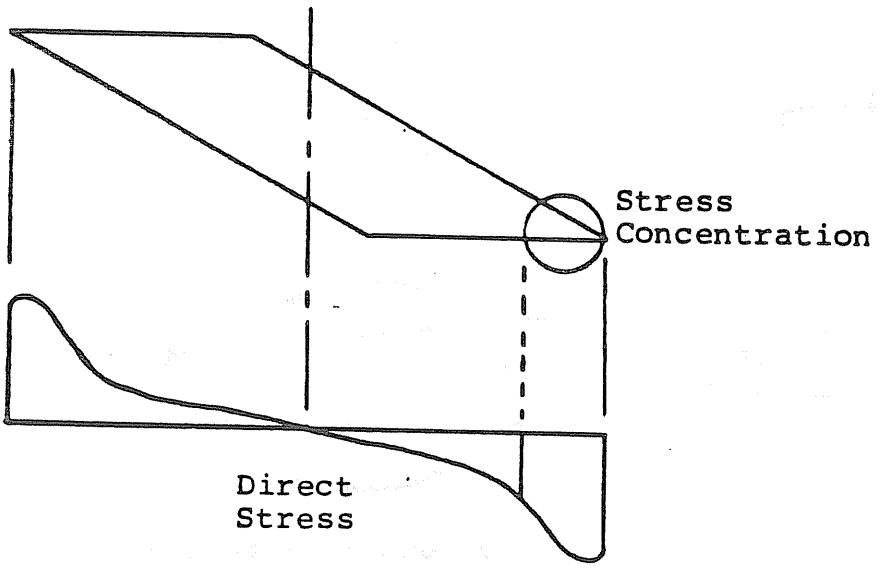

Figure 2.8 Direct Stress Caused by Skewed Bearing Rotations

Table 2.1

Shear Modulus Ratio of Low-to-Normal Temperatures

(From Reference 13)

Durometer Reading (Hardness)	Ratio for Temperatures Of:				
	40°F	20°F	0°F	-20°F	-40°F
50	1.00	1.00	1.10	1.25	1.55
60	1.05	1.25	1.65	1.90	2.05
70	1.05	1.15	1.50	1.85	2.15

2.5 Low Temperature Effects

The effects of temperature on the shear modulus of rubber are best described as a thermal stiffening at lower temperatures. Low temperatures induce a phenomenon called crystallization which locks the elastomer fibers together resulting in a much stiffer material. Table 2.1 shows the shear modulus ratio of low-to-normal temperatures, as published by Minor and Egen [13]. The effect of low temperatures on the shear modulus is not linear and the rate of crystallization is most rapid at approximately 10°F.

The intent of the low temperature tests in this study was to determine how low temperatures effect the shear stiffness of skewed bearings.

CHAPTER III

SHEAR PERFORMANCE OF TEST BEARINGS

3.1 Skewed Bearing Test Results and Simple Shear Comparisons

To evaluate skew effects on shear stiffness each of the twelve original bearings were tested using the setup and procedures described in Appendix A. In addition, three of the A-series bearings were modified and retested to verify that differences in material properties between the original bearings would not effect the conclusions. Bearing shear stiffnesses obtained for each 10 kips compressive load increment between the design dead and total loads are shown in Tables 3.1, 3.2 and 3.3. Results for the original twelve bearings are from tests conducted prior to fatigue loading.

Average measured shear stiffnesses and the corresponding simple shear predictions are shown in Table 3.4. All of the modified bearings were tested after both the parallel and rotated fatigue sequences had been conducted. The A90, D90, E90 and Axx-M90 bearings are rectangular bearings and the applied shear force was parallel to one of the bearing centerlines. To obtain predicted simple shear stiffness, a value for the theoretical shear modulus was determined using the durometer reading and assuming for 50, 60, and 70 hardness, the shear modulus is 90, 120, and 160 psi, respectfully. These values are given in Table 3.4. Using this theoretical shear modulus, the total rubber thickness, and the bearing area, the shear stiffnesses were estimated

Table 3.1

Shear Stiffness Test Results of "A Series" Bearings

Bearing	Normal Compressive Load (kips)	Experimental Shear Stiffness (kips/in)
A90	75 85 95 105 115	3.56 3.72 3.63 3.54 3.63
A60	75 85 95 105 115	6.36 6.35 6.36 6.35 6.38
A45	75 85 95 105 115	5.73 5.68 5.72 5.57 5.46
A30	75 85 95 105 115	7.37 7.33 7.30 7.27 7.26

Table 3.2

Shear Stiffness Test Results of "D Series" Bearings

Bearing	Normal Compressive Load (kips)	Experimental Shear Stiffness (kips/in)
D90	190 200 210 220 230 240 250 265	3.59 3.64 3.64 3.62 3.64 3.66 3.74 3.82
D60	190 200 210 220 230 240 250 265	5.29 5.26 5.18 5.20 5.21 5.23 5.21 5.20
D45	190 200 210 220 230 240 250 265	5.44 5.43 5.46 5.49 5.52 5.61 5.33 5.38
D30	190 200 210 220 230 240 250 265	6.76 6.64 6.67 6.73 6.78 6.81 6.86 6.93

Table 3.3

Shear Stiffness Test Results of "E Series" Bearings

Bearing	Nominal Compressive Load (kips)	Experimental Shear Stiffness (kips/in)
E90	215 225 235 245 255 265 275 285 300	16.12 16.28 16.50 16.71 16.89 17.93 17.33 17.54 17.93
E60	215 225 235 245 255 265 275 285 300	20.30 19.87 20.19 20.43 20.76 20.83 21.15 --- ---
E45	215 225 235 245 255 265 275 285 300	17.87 17.85 17.92 17.95 18.12 18.29 18.53 18.80 19.14
E30	215 225 235 245 255 265 275 285 300	24.00 24.08 24.40 24.39 24.59 24.79 25.09 25.21 25.64

Table 3.4

Average Experimental Shear Stiffness
and Simple Shear Comparisons for Skewed Bearings

Bearing	Shear Stiffness (kips/in)		Ratio: Predicted to Measured	Measured Durometer Hardness
	Measured	Simple Shear		
A90	3.62	5.67	1.57	55
A60	6.36	7.39	1.16	60
A45	5.63	6.99	1.24	57
A30	7.31	8.21	1.12	58
D90	3.68	5.20	1.41	55
D60	5.22	6.62	1.27	62
D45	5.46	6.66	1.22	60
D30	6.77	7.37	1.09	59
E90	16.91	21.42	1.27	55
E60	20.50	25.67	1.25	61
E45	18.26	23.98	1.31	56
E30	24.69	28.73	1.16	58
A30-M90A	2.99	4.69	1.57	58
A30-M90B	2.05	3.09	1.51	58
A30-M60	3.96	5.70	1.44	58
A30-M45	5.16	6.84	1.33	58
A45-M90	3.49	5.00	1.43	57
A60-M90	4.37	5.79	1.32	60

Notes: 1) The measured shear stiffness of the original twelve bearings are from test Phase I.

2) The measured shear stiffnesses of the "modified" bearings were determined after Test Phase IV.

for each bearing, using Equation 2.2.

The ratio of estimated-to-experimental shear stiffness ranged from 1.09 to 1.57, meaning that in all cases, the simple shear stiffness was greater than the measured stiffness. For each of the original series, the 30° bearing was the most stiff and the 90° bearing the least stiff. Since all of the second order effects discussed in Section 2.3 tend to reduce shear stiffness, these effects may explain the fact the measured stiffness of the 90° bearings was less than the predicted stiffness. A second possibility is that the shear moduli which were estimated from durometer readings are too high. Since virgin rubber was not available, tests to determine the actual shear moduli could not be conducted. However, even without accurate values for the shear modulus of each layer of each bearing, it is obvious from the data in Table 3.4 that an increase in shear angle results in an increase in effective shear stiffness. For this reason, procedures to estimate the shear stiffness of skewed bearings were developed, as explained in Section 3.3.

3.2 Turned Bearing Test Results and Simple Shear Comparisons

To investigate possible shear stiffness effects due to orientation of rectangular bearings, tests were conducted using the original A90 rectangular bearing and four other rectangular bearings that were cut from the remaining A-series bearings. (See Appendix A for testing details.) Tests were conducted at orientations of 90°, 60°, 45°, 30° and 0° (see Figure 3.1). Bearing dimensions and test results, along with simple shear estimations and the ratios of simple shear-to-experimentally found stiffnesses are given in Table 3.5. Simple shear theory stiffnesses were calculated in the same manner as discussed in the previous

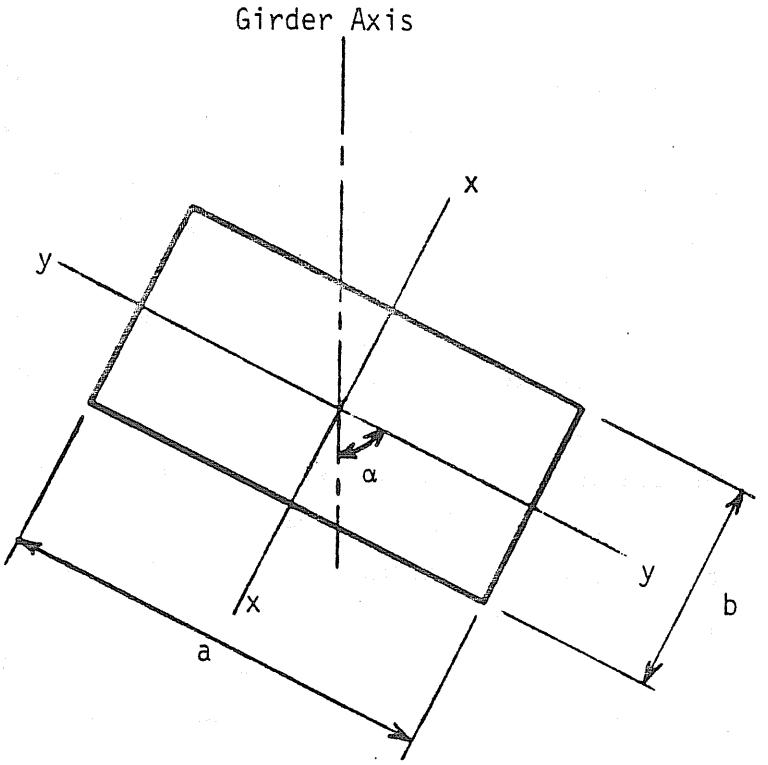

Figure 3.1 Bearing Parameters for the Turned Shear Axis Tests

Table 3.5

Averaged Experimental Shear Stiffness
and Simple Shear Comparisions for Turned Bearings

Test Parameters				Shear Stiffness (kips/in)		Ratio: Predicted to Measured
Bearing	a (in)	b (in)	Angle of Turn, Tα	Measured	Simple Shear Prediction	
A30-M90A	19	6.5	T90 T60 T45 T30 T00	2.99 3.28 3.42 3.56 3.77	4.69	1.57 1.43 1.37 1.32 1.24
A30-M90B	12.5	6.5	T90 T60 T45 T30 T00	2.05 2.13 2.24 2.36 2.44	3.09	1.51 1.45 1.38 1.37 1.27
A45-M90	18	7.5	T90 T60 T45 T30 T00	3.49 3.57 3.65 3.97 4.14	5.00	1.43 1.40 1.37 1.26 1.21
A60-M90	15.5	8.7	T90 T60 T45 T30 T00	4.37 4.47 4.59 4.72 4.58	5.79	1.32 1.30 1.26 1.23 1.26
A90	18	9	T90 T60 T45 T30 T00	3.48 3.70 3.75 3.88 3.94	5.67	1.63 1.53 1.51 1.48 1.44

Note: All measured shear stiffness values were determined after the six test phases were conducted.

section.

The ratio of estimated-to-experimental shear stiffness ranged from 1.21 to 1.63. As with the skewed bearing results, the general trend is that the shear stiffnesses increased with a decrease in the angle of turn. Simple shear theory suggests that this should not occur since each bearing had the same plan area regardless of the angle of turn. Further, the T90 and T00 tests are for rectangular bearings loaded parallel to centerline axes meaning that turn effects are not present, yet an increase in stiffness was found for the T00 orientation.

From the data in Table 3.5, it is evident that orientation of a rectangular bearing effects shear stiffness. Design equations which predict this increase in stiffness are developed in Section 3.5.

3.3 General Development of Proposed Design Expressions for Skewed and Turned Bearings

From the experimental data obtained for the T90 and T00 turned bearings tests, it is evident that the length of the bearing in the direction of shear loading and subsequent movement effects the shear stiffness of the bearing. The data shows that as this length increases, the bearing stiffness increases. Two reasons were found to explain this phenomena. The first concerns stress discontinuity and resulting rollover at two edges of the bearing, as shown in Figures 3.2 and 3.3. The second concerns the increase in bending stiffness as the length of the bearing increases.

By careful measurement of the length of the rollover for several of the modified bearings in the T90 and T00 orientation, it was found that the length of the rollover is approximately equal to the shear displacement as shown in

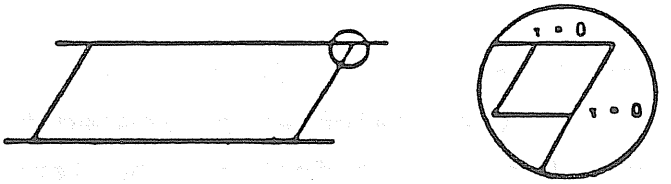

Figure 3.2 Shear Stress Singularity at Edge of Bearing

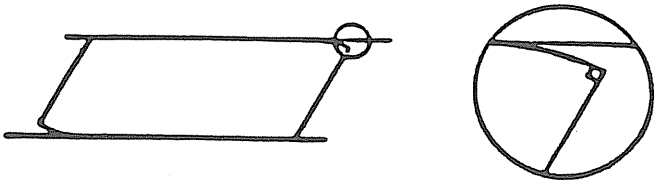

Figure 3.3 Rollover of Bearing

Figure 3.4. Since shear stiffness is directly related to area, rollover has the effect of reducing the area and thus the shear stiffness. The effective bearing area, A_e, at a shear displacement, Δ_s, is defined as

$$A_e = (L - \Delta_s)W \tag{3.1}$$

where L and W equal the length parallel and the width perpendicular to the loaded axis, respectfully. It is noted that rollover has less effect as the length of the bearing in the loaded direction increases, which reflects the experimental data in Table 3.5. (This reduced effective area is not new to bearing technology. Many foreign codes use effective areas of compression [18] when bearings are loaded with combined shear and compression.)

The simple shear equation now becomes

$$k = \frac{G\,A_e}{T} \tag{3.2}$$

When bending effects are included (see Section 2.3.2), shear stiffness is given by

$$k = \frac{G / T}{1/A_e + T^2/36I} \tag{3.3}$$

The accuracy of this equation for the prediction of shear stiffness of rectangular bearings oriented with one centerline parallel to the direction of loading will be demonstrated in subsequent sections. Further modification of the effective area and bending stiffness terms are needed to predict shear stiffness of skewed and arbitrarily turned bearings.

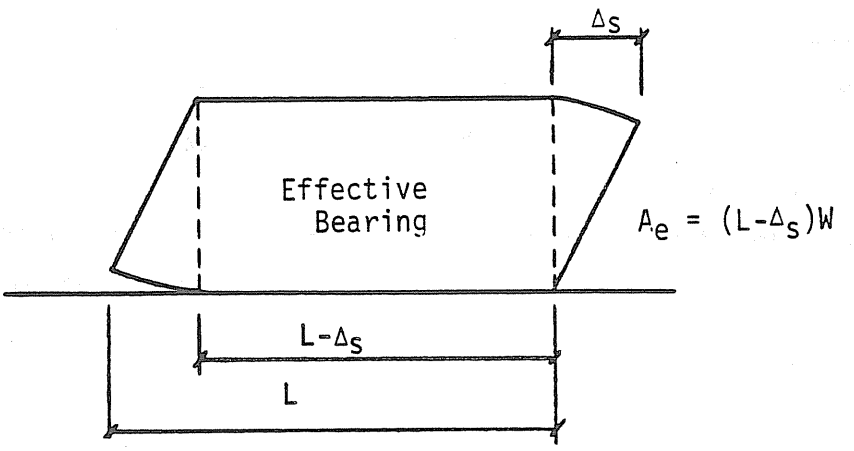

Figure 3.4 Reduced Effective Area For Bearings in Shear

3.4 Proposed Shear Stiffness Prediction Equations for Skewed Bearings

From observation of tests, the effective shear area for a skewed bearing is shown in Figure 3.5. In the figure, W is the width of the bearing transverse to the girder axis and L is the length of bearing parallel to the girder axis. Alpha (α) is defined as the angle of skew, in which a value of 90° denotes a rectangular bearing. The effective area, A_e, for a skewed bearing is independent of skew angle and is

$$A_e = W(L - \Delta_s) \tag{3.4}$$

The moment of inertia of the plan area of a skewed bearing is

$$I_y = 1/12\ W\ L\ (L^2 + W^2\ \mathrm{Cot}^2\ \alpha) \tag{3.5}$$

When Equation 3.4 and 3.5 are substituted into Equation 3.3, the resulting shear stiffness, k_α, of a skewed bearing is

$$k_\alpha = \frac{G\ /\ T}{\dfrac{1}{W(L - \Delta_s)} + \dfrac{T^2}{3WL(L^2 + W^2\ \mathrm{Cot}^2\ \alpha)}} \tag{3.6}$$

Rearranging terms yields

$$k_\alpha = \frac{GA\ /\ T}{\dfrac{L}{(L - \Delta_s)} + \dfrac{(T\ \mathrm{Sin}\ \alpha)^2}{3[(L\ \mathrm{Sin}\ \alpha)^2 + (W\ \mathrm{Cos}\ \alpha)^2]}} \tag{3.7}$$

where the numerator is the simple shear stiffness term and the denominator is the simple shear stiffness modifier.

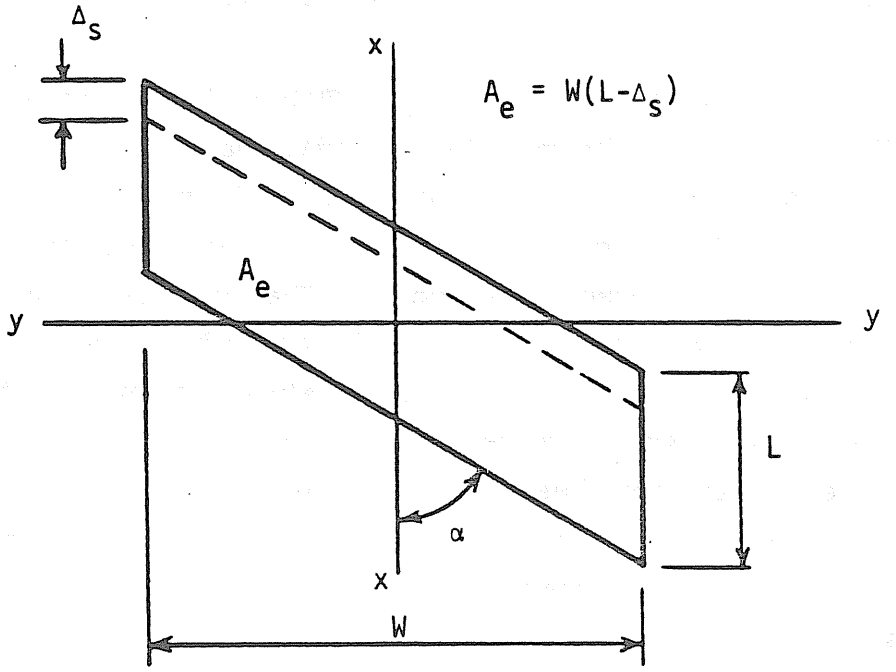

Figure 3.5 Skewed Bearing Parameters

Equation 3.7 was used to calculate the predicted shear stiffnesses shown in Table 3.6 The shear moduli values shown in Table 1.3 were used in the calculations. Table 3.6 also shows the experimentally determined shear stiffnesses and the ratios of predicted-to-measured shear stiffnesses. The range of the ratios is 0.94 to 1.27. A ratio greater than unity indicates that the predicted value is greater than the measured value, that is, conservative.

Comparison of the ratios shown in Table 3.6 with those found in Table 3.4 (where the predicted values were calculated using the simple shear stiffness equation) clearly shows that Equation 3.7 is a superior predictor of shear stiffness for skewed bearings. The scatter in the ratios in Table 3.6 are attributed to the previously discussed difficulties in determining shear modulus from durometer readings. An examination of the A30-M results further verifies this conclusion. All of these tests were conducted using material from the same bearing, and almost identical ratio values were obtained for the three orientations.

3.5 Proposed Shear Stiffness Prediction Equations for Turned Bearings

Figures 3.6(a) and (b) show the effective areas and moments of inertia for a rectangular bearing in the two primary orientations. Figure 3.6(c) shows the effective area and moment of inertia for the same bearing turned an angle α from the line of load application.

To develop a prediction equation for the shear stiffness of a turned bearing, it was first assumed that the stiffness for any orientation, k_α, is a function of the stiffnesses for the two primary orientations, k_0 and k_{90}, i.e.,

Table 3.6

Comparison of the Experimental and Proposed Prediction Equation Results for Skewed Bearings

Bearing	Shear Stiffness (kips/in)		Ratio: Predicted to Measured
	Measured	Predicted	
A90	3.62	4.58	1.27
A60	6.36	6.16	0.97
A45	5.63	5.96	1.05
A30	7.31	7.17	0.98
D90	3.68	4.20	1.14
D60	5.22	5.45	1.04
D45	5.46	5.59	0.98
D30	6.77	6.36	0.94
E90	16.91	20.42	1.21
E60	20.50	24.51	1.20
E45	18.26	22.98	1.26
E30	24.69	27.69	1.12
A45-M90	3.49	3.83	1.10
A60-M90	4.37	4.64	1.06
A30-M60	3.96	4.50	1.14
A30-M45	5.16	5.67	1.10
A30-M90A	2.99	3.42	1.14
A30-M90B	2.05	2.25	1.10

Note: All measured shear stiffness values were determined after the six test phases.

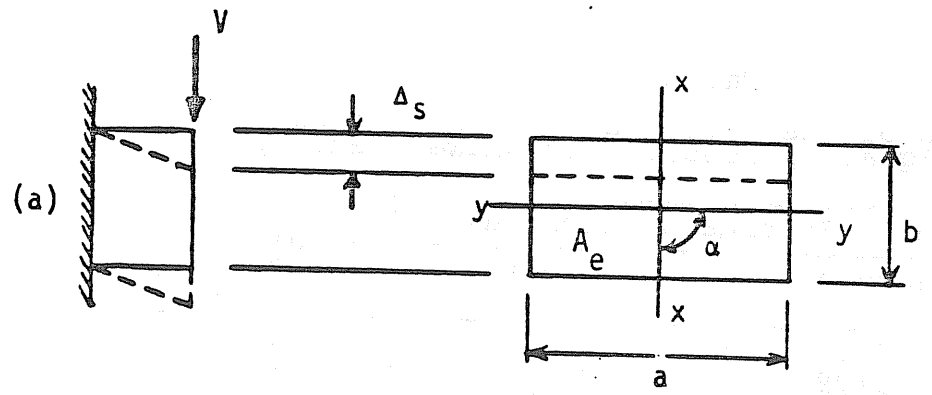

(a)

$$(A_e)_{90} = a(b - \Delta_s)$$

$$(I_y)_{90} = \frac{ab^3}{12}$$

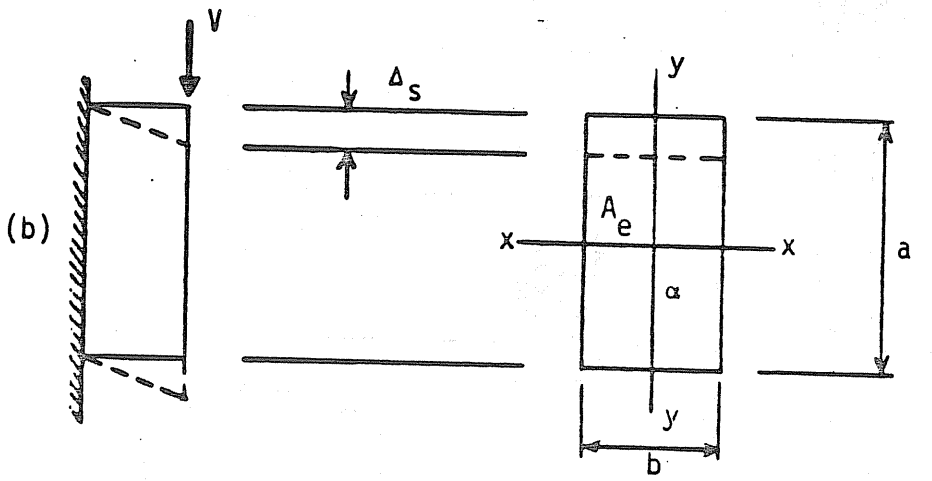

(b)

$$(A_e)_0 = b(a - \Delta_s)$$

$$(I_x)_0 = \frac{ba^3}{12}$$

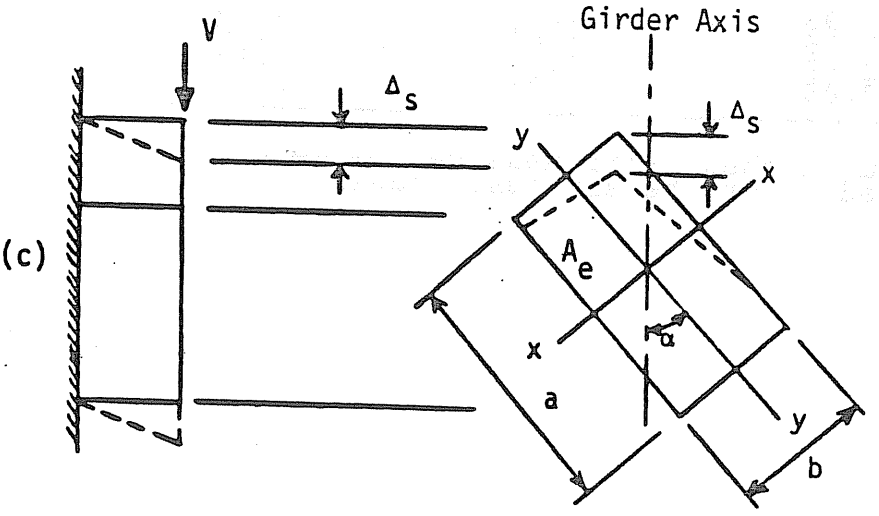

(c)

$$A_e = A_0 \cos^2\alpha + A_{90} \sin^2\alpha$$

$$I_\alpha = I_x \cos^2\alpha + I_y \sin^2\alpha$$

Figure 3.6 Effective Area and Moment of Inertia Distribution for Turned Bearings

$$k_\alpha = f(\alpha)\ k_{0^\circ} + g(\alpha)\ k_{90^\circ} \qquad (3.8)$$

Using orientations a) and b) of Figure 3.6 and $k\alpha$ from Equations 3.6, Equation 3.8 becomes

$$k_\alpha = \frac{G}{T}\left[\frac{f(\alpha)}{\frac{1}{b(a-\Delta_s)} + \frac{T^2}{3ba^3}} + \frac{g(\alpha)}{\frac{1}{(a(b-\Delta_s)} + \frac{T^2}{3ab^3}}\right] \qquad (3.9)$$

Further it was assumed that the effective area for any orientation varies in the same manner as the moments of inertia, that is,

$$I_\alpha = I_x \cos^2\alpha + I_y \sin^2\alpha \qquad (3.10)$$

and

$$\begin{aligned}(A_e)_\alpha &= (A_e)_o \cos^2\alpha + (A_e)_{90} \sin^2\alpha \\ &= b(a - \Delta_s)\cos^2\alpha + a(b - \Delta_s) \sin^2\alpha \end{aligned} \qquad (3.11)$$

Thus, Equation 3.9 can be written as follows, which in turn defines $f(\alpha)$ and $g(\alpha)$

$$k_\alpha = \frac{G}{T}\left[\frac{\cos^2\alpha}{\frac{1}{b(a-\Delta_s)} + \frac{T^2}{3ba^3}} + \frac{\sin^2\alpha}{\frac{1}{a(b-\Delta_s)} + \frac{T^2}{3ab^3}}\right] \qquad (3.12)$$

Or, on rearranging terms

$$k_\alpha = \frac{GA}{T}\left[\frac{\cos^2\alpha}{\frac{a}{a-\Delta_s} + \frac{T^2}{3a^2}} + \frac{\sin^2\alpha}{\frac{b}{b-\Delta_s} + \frac{T^2}{3b^2}}\right] \qquad (3.13)$$

which is the final form of the shear stiffness prediction equation for rectangular bearings turned at any angle, α. The dimensions a, b, and α used in Equation 3.3 must be the

long dimension, the short dimension, and the angle between the weak axis of bending and the girder axis, of the bearing pad, respectively.

Measured shear stiffnesses, predicted shear stiffnesses using Equation 3.13, and the ratios of predicted-to-measured stiffnesses for the turned bearing tests are found in Table 3.7. The range of these ratios is from 1.06 to 1.31, which represents a very favorable improvement over the ratios calculated using the simple shear equation for the predicted values, Table 3.5 (range from 1.21 to 1.63). Again, the scatter is attributed to the difficulty in determining shear modulus from durometer reading.

Table 3.7 also shows for each bearing the predicted-to-measured shear stiffness ratios for all angles of alpha normalized with respect to the values determined for the 90° turned angle (T90). This normalized stiffness ratio was calculated to show the accuracy of the predicted "turn" effects separate from the error due to shear modulus prediction from durometer readings. The normalized ratios of predicted-to-measured stiffnesses ranged from 0.97 to 1.05, which shows that Equation 3.13 adequately predicts the measured shear stiffness of turned bearings when the shear modulus is accurately predicted.

Figures 3.7 through 3.11 graphically compare the simple shear equation, the proposed prediction equation (Equation 3.13) and the measured results for the five turned bearing tests. In all cases, the proposed and experimental results are below the simple shear predictions. The proposed and experimental results follow the same trends, but with the experimental results slightly below the proposed equation predictions.

Table 3.7

Comparison of the Experimental and Proposed Equation Results for Turned Bearings

Bearing	Alpha (deg) (Tα)	Shear Stiffness (kips/in)		Ratio: Predicted to Measured	Ratio Normalized to T90
		Measured	Predicted		
A30-M90A	T90	2.99	3.42	1.14	1.00
	T60	3.28	3.64	1.11	0.97
	T45	3.42	3.86	1.13	0.99
	T30	3.56	4.07	1.14	1.00
	T00	3.77	4.29	1.14	1.00
A30-M90B	T90	2.05	2.25	1.10	1.00
	T60	2.13	2.36	1.11	1.01
	T45	2.24	2.46	1.10	1.00
	T30	2.36	2.57	1.09	0.99
	T00	2.44	2.67	1.09	0.99
A45-M90	T90	3.49	3.83	1.10	1.00
	T60	3.57	4.01	1.12	1.02
	T45	3.65	4.19	1.15	1.05
	T30	3.97	4.36	1.10	1.00
	T00	4.14	4.54	1.10	1.00
A60-M90	T90	4.37	4.64	1.06	1.00
	T60	4.47	4.78	1.07	1.01
	T45	4.59	4.91	1.07	1.01
	T30	4.72	5.04	1.07	1.01
	T00	4.59	5.17	1.13	1.07
A90	T90	3.48	4.58	1.32	1.00
	T60	3.70	4.73	1.28	0.97
	T45	3.75	4.87	1.30	0.98
	T30	3.88	5.01	1.29	0.98
	T00	3.94	5.15	1.31	0.99

Note: All measured shear stiffness values were determined after the six test phases were conducted.

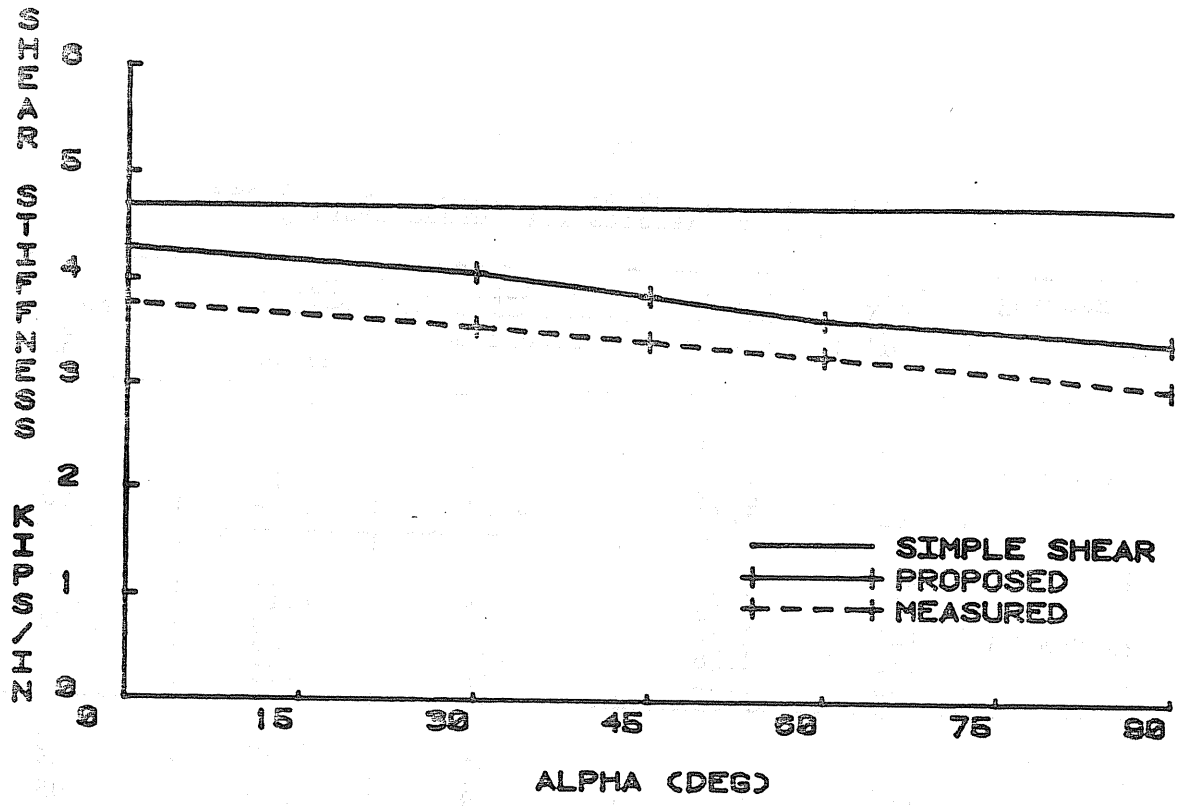

Figure 3.7 Shear Stiffness versus Turn Angle for Bearing A30-M90A

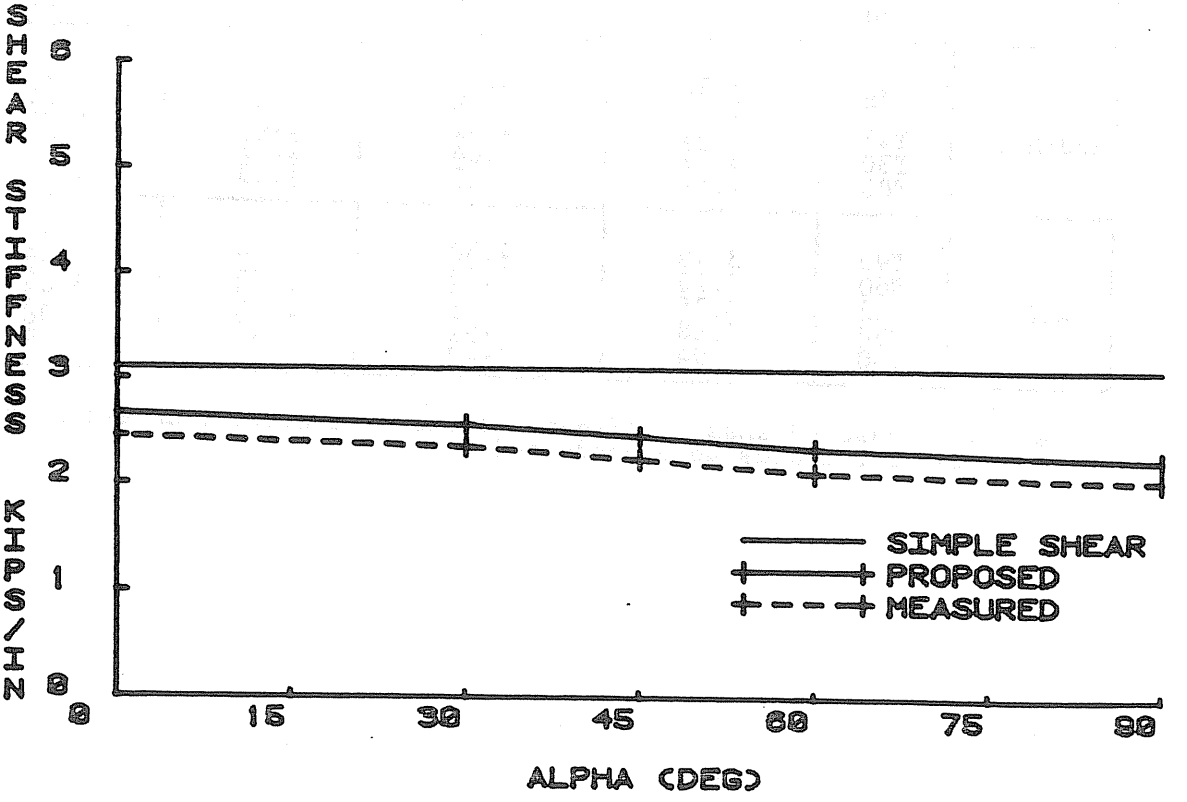

Figure 3.8 Shear Stiffness versus Turn Angle for Bearing A30-M90B

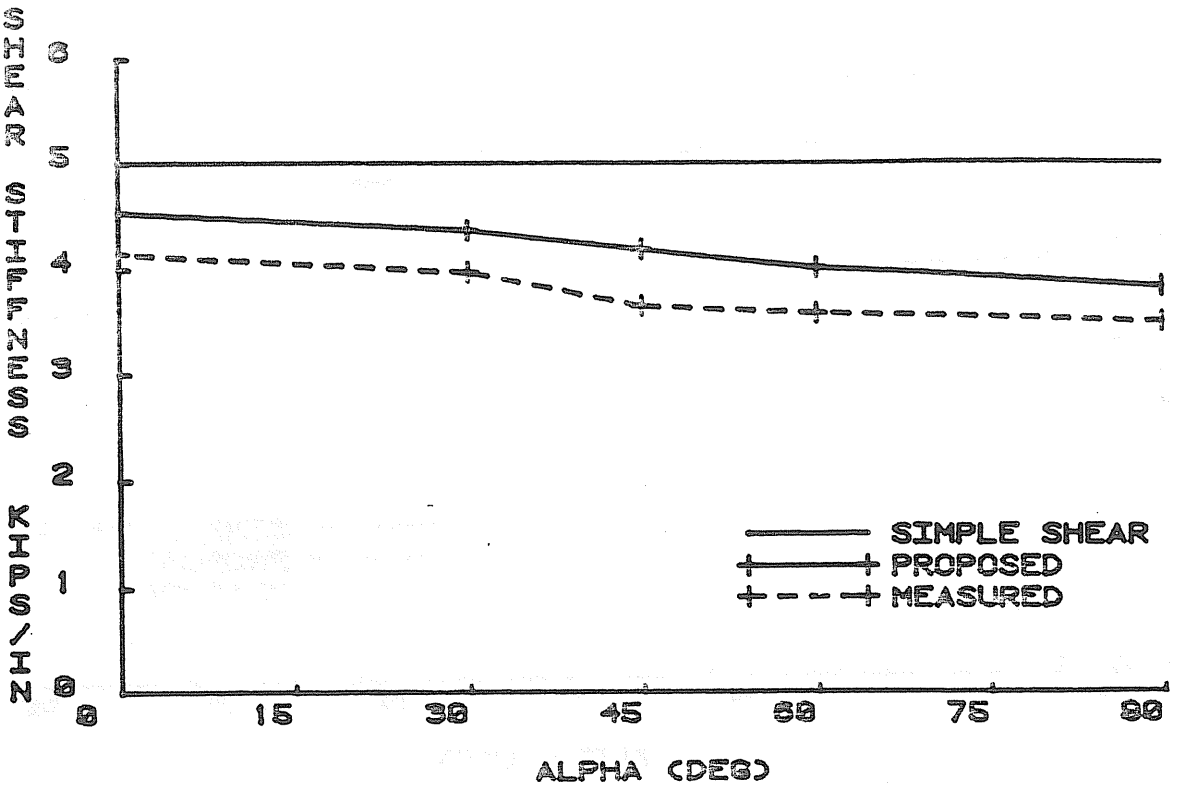

Figure 3.9 Shear Stiffness versus Turn Angle for Bearing A45-M90

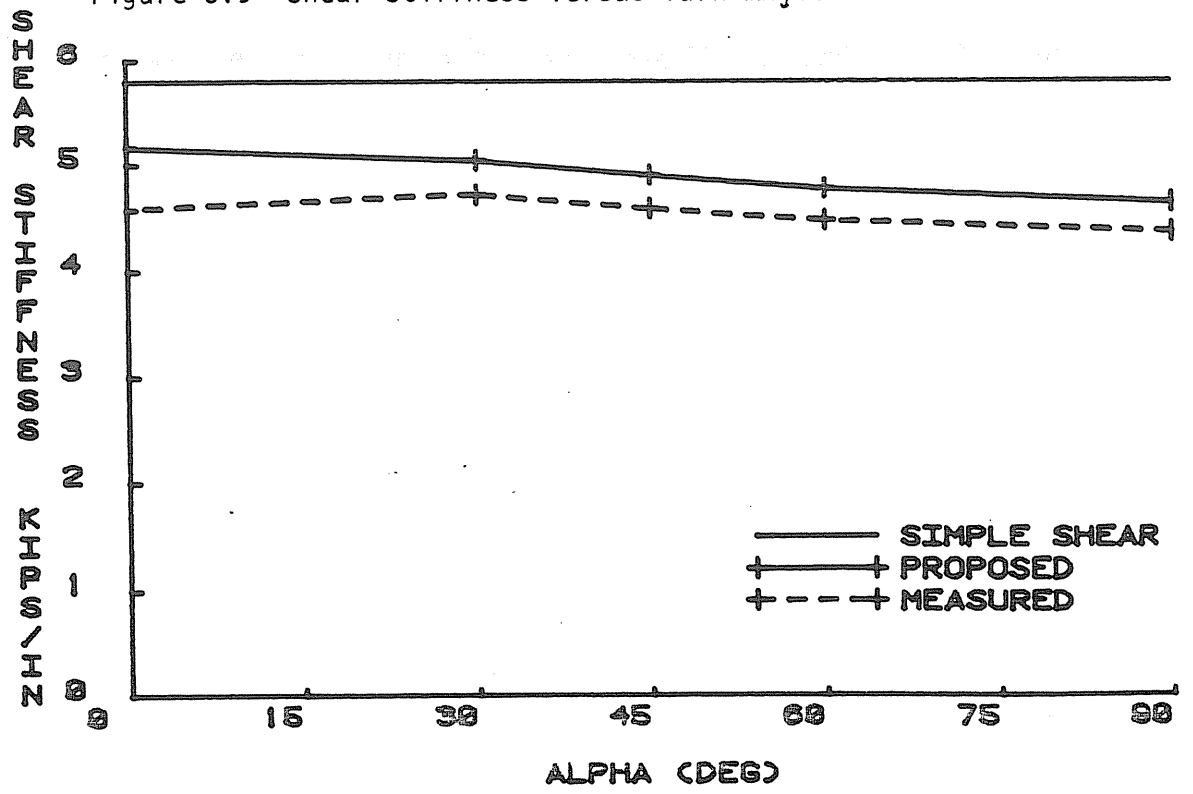

Figure 3.10 Shear Stiffness versus Turn Angle for Bearing A60-M90

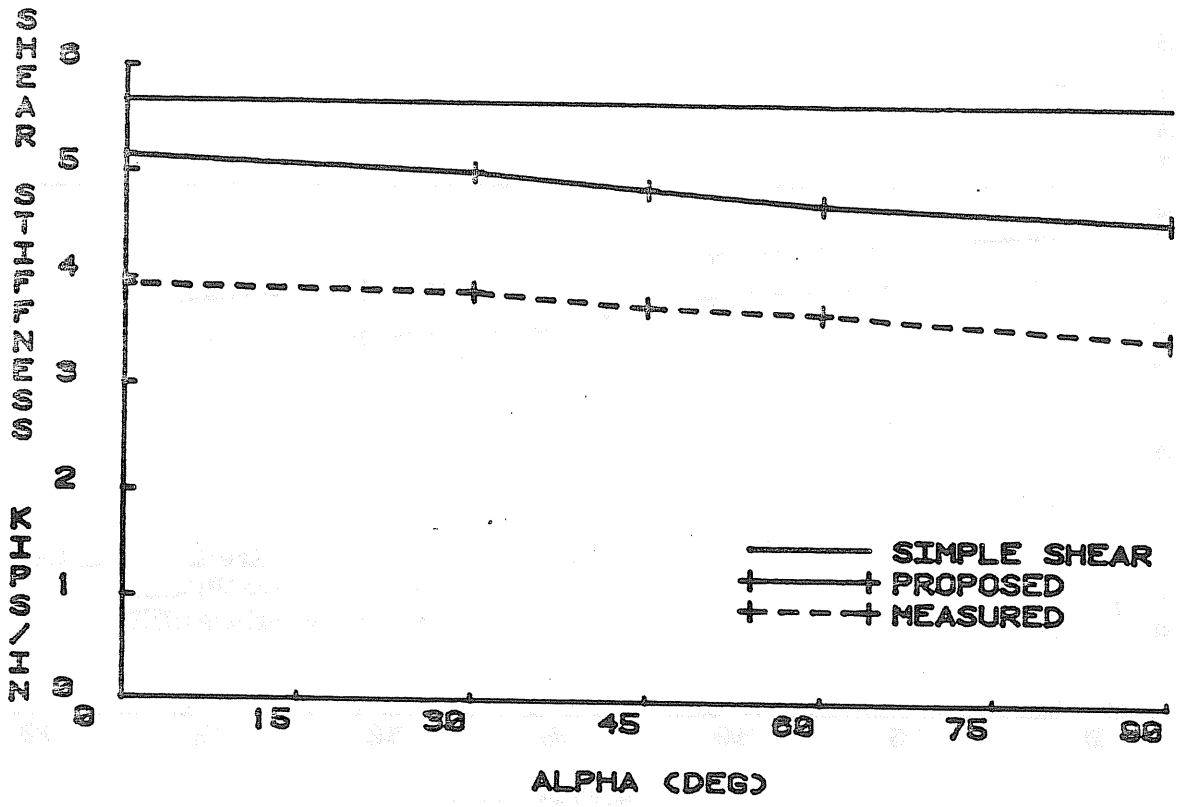

Figure 3.11 Shear Stiffness versus Turn Angle for Bearing A90

In summary, Figures 3.7 through 3.11 show that the proposed shear stiffness equation, Equation 3.13, adequately predicts measured shear stiffness even when the shear modulus is interpolated from durometer readings.

3.6 Low Temperature Test Results

As described in Section 1.4, each bearing was placed in a -20°F environment and a shear stiffness test was conducted immediately upon removal. Each bearing was subjected to its design dead load for these tests. Ambient temperature and the temperature of the top steel plate at the time of testing, shear stiffnesses at low and normal temperatures, and low temperature-to-room temperature shear stiffnesses ratios are shown in Table 3.8.

The shear force versus deformation plots for all bearings are found in Appendix B. These plots show a substantial increase in hysterises, as shown in the typical plot, Figure 3.12. Since for the purposes of this study, the shear stiffness is calculated between the end points of curve, the increased hysterises does not effect shear stiffness values.

Theoretical values for the low-to-room temperature stiffness ratios, which were interpolated and extrapolated from Table 2.1, are also shown in Table 3.8. It is noted that the theoretical ratios are a function of durometer readings as well as temperature. The theoretical stiffness ratios are relatively near the experimental ratios but are conservative for all of the bearings except for A90 and D90. These bearings were the only ones where the steel plate temperature at the time of testing was below 0°F.

The steel temperatures, recorded at the time of the

Table 3.8

Low Temperature Test Results

Bearing Pad	Temp. at Time of Test (°F)		Shear Stiffness (kips/in)		Stiffness Ratio Low to Room Temp.	
	Steel	Room	Low Temp.	Room Temp.	Measured	Theoret.
A90	-3	72	5.77	3.56	1.62	1.41
A60	+5	72	8.17	6.36	1.28	1.52
A45	+3	72	7.90	5.73	1.38	1.44
A30	+5	72	9.48	7.37	1.29	1.46
D90	-3	64	5.91	3.59	1.65	1.41
D60	+3	64	7.30	5.29	1.38	1.56
D45	+4	64	7.61	5.44	1.40	1.56
D30	+6	64	9.19	6.76	1.36	1.47
E90	+5	65	20.07	16.12	1.25	1.32
E60	+6	64	26.42	20.30	1.30	1.52
E45	+8	66	22.16	17.87	1.24	1.32
E30	+5	66	30.70	24.00	1.28	1.46

Note: All tests with design dead load applied to the bearings.

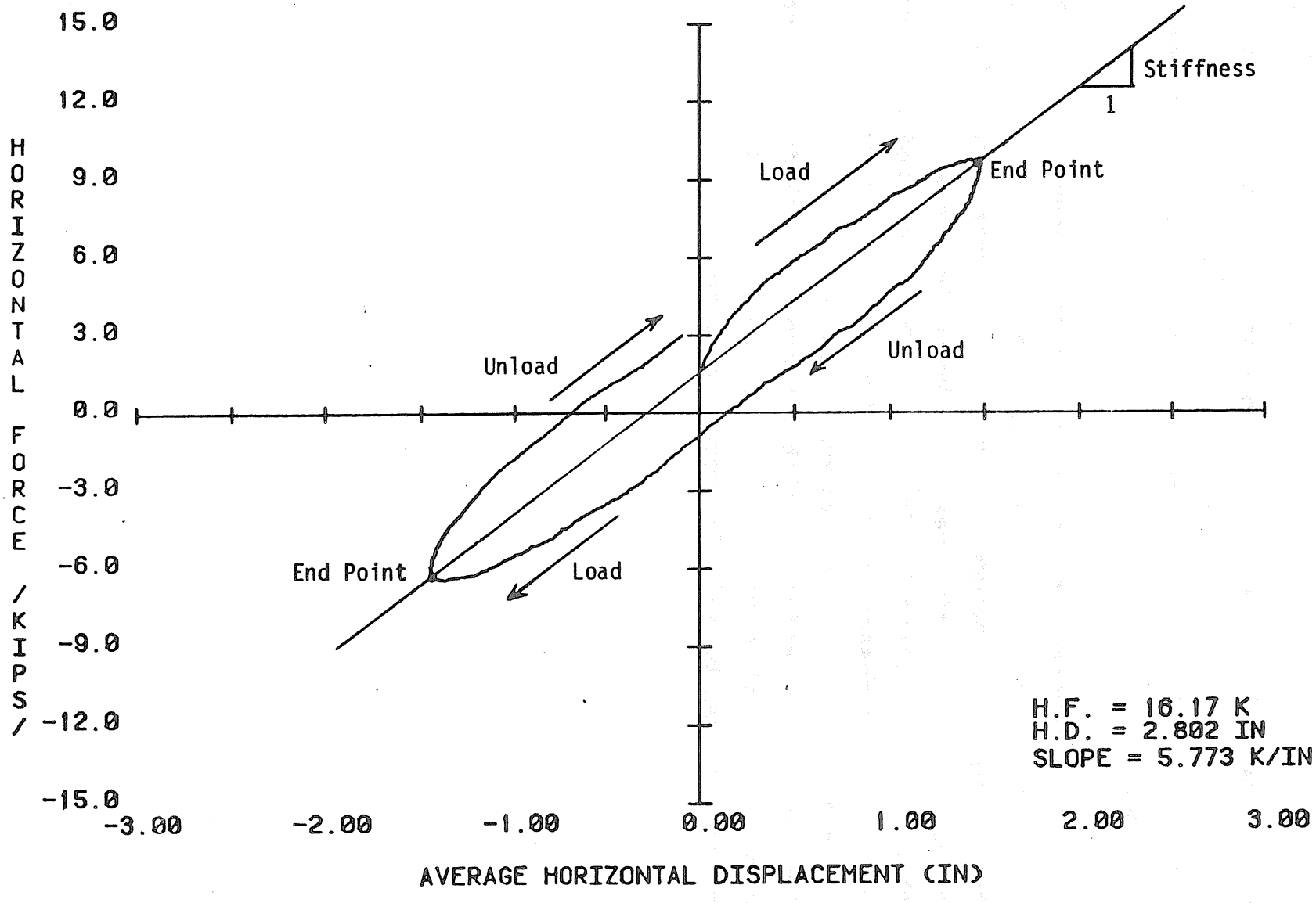

Figure 3.12 Typical Shear Force-Displacement Plot for a Bearing Subjected to Low Temperatures

shear stiffness tests, range from -3°F to +8°F. This slight variation in temperature substantially changed the stiffness ratios within each pad series. However, considering the normal variation in elastomeric bearing material properties, the results compare well with the values given in the literature for non-laminated, rectangular elastomeric bearings.

The increase in the shear force transmitted to the abutment, due to low temperature effects must be included in the design of a bridge. However, low temperatures do not effect the shear stiffness of skewed bearings differently than that of rectangular bearings. Thus, the predicted skew bearing stiffnesses given by Equation 3.7 need only be corrected by the values given in Table 2.1 to account for low temperature effects. Although experimental data was not developed in this research, it is believed that a similar correction can be made for turned bearings.

CHAPTER IV

FATIGUE PERFORMANCE OF SKEWED BEARINGS

4.1 Determination Of Fatigue Criterion

Changes of temperature from day-to-day, month-to-month, and year-to-year produce horizontal displacements in a bridge due to thermal expansion of the bridge material. To determine the magnitude of these displacements and the number of fatigue cycles to be used in the fatigue testing phase, a rational program had to be determined. From temperature data for the state of Oklahoma, three sets of temperature ranges were determined: daily variations, monthly variations, and yearly variations. Figure 4.1 shows a typical temperature variation chart for one year for Oklahoma.

To determine the necessary temperature ranges, the following steps were taken:

1) The average high and low temperatures of each month of the year for Oklahoma City, Oklahoma were found for the randomly picked years of 1936, 1945, 1962, 1974 and 1981.

2) The average highs and lows for each month were averaged over the same five years.

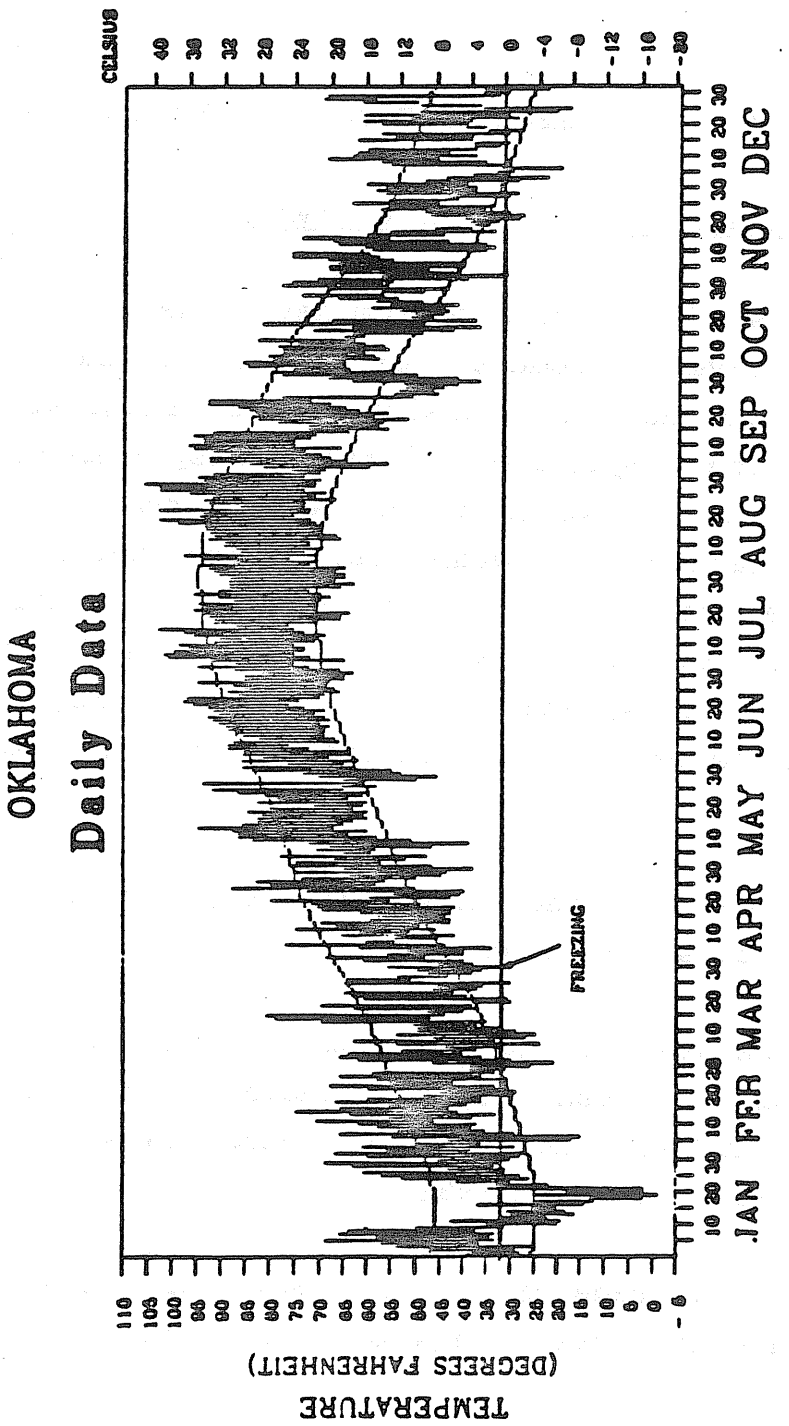

Figure 4.1 Typical Temperature Variations

3) The daily low-to-high temperature ranges for each day of the month, for all months of the year, were found and averaged so that an average daily range for each month was obtained.

4) The standard deviation of the daily ranges from the monthly average were calculated for each month. This standard deviation was added to the average daily range to obtain a conservative daily range for each month.

5) Steps 3) and 4) were repeated for each of the five years and averaged to obtain the final daily temperature range for each month of the year. These daily temperature ranges for each month were consistently close to 30°F, so this value was used for each month.

6) The absolute highs and lows for each month were recorded and averaged over the five years to obtain the monthly temperature range for each month of the year.

7) The absolute highs and lows of the five years were recorded and averaged to obtain the yearly temperature range.

The design life of a bridge built by ODOT is 50 years; therefore, the fatigue program was set up to simulate the number of environmental cyclic displacements that an elastomeric bearing might be required to deform over a 50 year period. The daily cycles occur 30 times a month for 50 years, or 1500 cycles. The monthly cycle occurs once a month for 50 years, or 50 cycles for each month. The total number of yearly cycles is, of course, 50.

At time of construction ODOT sets their bearings so that there is no elastomeric shear deformation at a nominal temperature of 60°F. Therefore, 60°F becomes the zero shear displacement reference point. The temperature ranges for the daily, monthly and yearly cycles with respect to the 60°F reference point are shown in Tables 4.1 and 4.2.

With design spans of approximately 200 ft., 300 ft., and 100 ft. for the A, D, and E series bearings, respectively, the coefficient of thermal expansion for steel, and these temperature variations, the corresponding girder displacements were calculated using Equation 1.4. The resulting displacements for the daily, monthly and yearly cycles for each bearing series are shown in Tables 4.3, 4.4, 4.5 and 4.6. In these tables all positive displacement values correspond to temperatures below 60°F.

For the daily fatigue cycle for a particular month, the girder was moved from the zero displacement reference point to a displacement corresponding to the average daily temperature for that month, from step 2 above. The girder was then forced to oscillate around this point a displacement corresponding to the final temperature range determined by step 5 above or a displacement corresponding to a temperature cycle of ±15°F. Similarly, the monthly and yearly cycles were conducted in a similar manner using the values in Tables 4.1 and 4.2.

4.2 Shear Stiffness Response to Fatigue for Skewed Bearings

Shear stiffness tests were conducted before and after the bearings were subjected to the fatigue programs of Phases II (horizontal surfaces) and Phase V (2% sloped surfaces). Tables 4.7, 4.8, and 4.9 show the results of these tests before and after the fatigue cycles for the A, D, and E series bearings, respectfully.

Table 4.1

Daily and Monthly Temperature Cycles

Month	Daily Cycles			Monthly Cycles		
	From 60°F move to (°F)	Range (°F)	Number of Cycles	From 60°F move to (°F)	Range (°F)	Number of Cycles
Jan	36.2	±15	1500	39.3	±30.5	50
Feb	41.3	±15	1500	42.0	±34.8	50
Mar	52.6	±15	1500	52.3	±30.3	50
Apr	60.4	±15	1500	58.3	±28.3	50
May	70.5	±15	1500	67.3	±22.1	50
Jun	76.8	±15	1500	76.8	±21.6	50
Jul	83.2	±15	1500	84.7	±19.5	50
Aug	82.1	±15	1500	81.3	±21.9	50
Sep	72.3	±15	1500	70.5	±26.7	50
Oct	63.3	±15	1500	60.1	±25.9	50
Nov	50.3	±15	1500	51.3	±26.7	50
Dec	40.2	±15	1500	40.5	±27.1	50

Table 4.2

Yearly Temperature Cycles

From 60°F move to	Range	Number of Cycles
55.7°F	±48.5°F	50

Table 4.3

Daily and Monthly Reference Displacements for "A Series" Bearings, Fatigue Tests

Month	Daily Cycles			Monthly Cycles		
	From Zero move to (in)	Range (in)	Number of Cycles	From Zero move to (in)	Range (in)	Number of Cycles
Jan	+0.397	±0.250	1500	+0.346	±0.509	50
Feb	+0.312	±0.250	1500	+0.300	±0.581	50
Mar	+0.124	±0.250	1500	+0.129	±0.506	50
Apr	-0.007	±0.250	1500	+0.028	±0.472	50
May	-0.175	±0.250	1500	-0.122	±0.369	50
Jun	-0.280	±0.250	1500	-0.280	±0.361	50
Jul	-0.387	±0.250	1500	-0.412	±0.325	50
Aug	-0.364	±0.250	1500	-0.356	±0.366	50
Sep	-0.205	±0.250	1500	-0.175	±0.446	50
Oct	-0.038	±0.250	1500	-0.002	±0.432	50
Nov	+0.162	±0.250	1500	+0.145	±0.446	50
Dec	+0.331	±0.250	1500	+0.325	±0.452	50

Note: "A Series" bearings were designed for a bridge span of 214 feet.

Table 4.4

Daily and Monthly Reference Displacements for "D Series" Bearings, Fatigue Tests

Month	Daily Cycles			Monthly Cycles		
	From Zero move to (in)	Range (in)	Number of Cycles	From Zero move to (in)	Range (in)	Number of Cycles
Jan	+0.728	±0.459	1500	+0.633	±0.933	50
Feb	+0.572	±0.459	1500	+0.550	±1.064	50
Mar	+0.196	±0.459	1500	+0.235	±0.929	50
Apr	-0.012	±0.459	1500	+0.052	±0.865	50
May	-0.321	±0.459	1500	-0.223	±0.676	50
Jun	-0.514	±0.459	1500	-0.514	±0.660	50
Jul	-0.709	±0.459	1500	-0.755	±0.596	50
Aug	-0.676	±0.459	1500	-0.651	±0.670	50
Sep	-0.376	±0.459	1500	-0.321	±0.816	50
Oct	-0.070	±0.459	1500	-0.003	±0.792	50
Nov	+0.297	±0.459	1500	+0.266	±0.816	50
Dec	+0.605	±0.459	1500	+0.596	±0.829	50

Note: "D Series" bearings were designed for a bridge span of 392 feet.

Table 4.5

Daily and Monthly Reference Displacements for "E Series" Bearings, Fatigue Tests

Month	Daily Cycles			Monthly Cycles		
	From Zero move to (in)	Range (in)	Number of Cycles	From Zero move to (in)	Range (in)	Number of Cycles
Jan	+0.199	±0.125	1500	+0.173	±0.255	50
Feb	+0.156	±0.125	1500	+0.150	±0.291	50
Mar	+0.062	±0.125	1500	+0.065	±0.253	50
Apr	-0.004	±0.125	1500	+0.014	±0.236	50
May	-0.088	±0.125	1500	-0.061	±0.185	50
Jun	-0.140	±0.125	1500	-0.140	±0.181	50
Jul	-0.194	±0.125	1500	-0.206	±0.163	50
Aug	-0.185	±0.125	1500	-0.178	±0.183	50
Sep	-0.103	±0.125	1500	-0.088	±0.223	50
Oct	-0.019	±0.125	1500	-0.001	±0.216	50
Nov	+0.081	±0.125	1500	+0.073	±0.223	50
Dec	+0.166	±0.125	1500	+0.163	±0.226	50

Note: "E Series" bearings were designed for a bridge span of 107 feet.

Table 4.6

Yearly Reference Displacements
for Fatigue Cycles

Bearing Series	From Zero move to (in)	Range (in)	Number of Cycles
A	+0.072	±0.810	50
D	+0.132	±1.483	50
E	+0.036	±0.405	50

Table 4.7

Evaluation of Fatigue Performance of Bearings in the "A" Series

Bearing Pad	Normal Load (kips)	Pre-Fatigue Shear Stiffness (kips/in)	Post Parallel Fatigue		Post Rotated Fatigue	
			Shear Stiffness (kips/in)	Average % Degradation	Shear Stiffness (kips/in)	Average % Degradation
A90	75 85 95 105 115	3.56 3.72 3.63 3.54 3.63	3.72 3.76 3.77 3.82 3.87	-4.8%	3.36 3.38 3.38 3.32 3.28	11.7%
A60	75 85 95 105 115	6.36 6.35 6.36 6.35 6.38	6.24 6.27 6.22 6.18 6.20	2.2%	5.65 5.66 5.71 5.71 5.75	8.5%
A45	75 85 95 105 115	5.73 5.68 5.72 5.57 5.46	5.48 5.50 5.51 5.50 5.49	2.4%	5.69 5.75 5.79 5.83 5.86	---
A30	75 85 95 105 115	7.37 7.33 7.30 7.27 7.26	7.22 7.22 7.23 7.29 7.31	0.7%	7.04 7.03 7.07 7.10 7.12	2.5%

Table 4.8

Evaluation of Fatigue Performance of Bearings in the "D" Series

Bearing Pad	Normal Load (kips)	Pre-Fatigue Shear Stiffness (kips/in)	Post Parallel Fatigue		Post Rotated Fatigue	
			Shear Stiffness (kips/in)	Average % Degredation	Shear Stiffness (kips/in)	Average % Degredation
D90	190	3.59	3.69	1.5	3.25	8.3
	200	3.64	3.62		3.25	
	210	3.64	3.60		3.28	
	220	3.62	3.59		3.25	
	230	3.64	3.56		3.31	
	240	3.66	3.56		3.33	
	250	3.74	3.63		3.39	
	265	3.82	3.66		3.45	
D60	190	5.29	5.20	1.1	4.88	4.7
	200	5.26	5.16		4.87	
	210	5.18	5.15		4.88	
	220	5.20	5.15		4.91	
	230	5.21	5.16		4.91	
	240	5.23	5.14		4.95	
	250	5.21	5.16		4.98	
	265	5.20	5.22		5.02	
D45	190	5.44	5.42	1.1	4.97	8.4
	200	5.43	5.43		5.05	
	210	5.46	5.46		5.02	
	220	5.49	5.49		5.03	
	230	5.52	5.52		5.05	
	240	5.61	5.54		5.06	
	250	5.33	5.62		5.10	
	265	5.38	5.64		5.14	
D30	190	6.76	6.70	0.6	6.22	6.1
	200	6.64	6.64		6.28	
	210	6.67	6.68		6.30	
	220	6.73	6.71		6.31	
	230	6.78	6.75		6.33	
	240	6.81	6.77		6.33	
	250	6.86	6.78		6.37	
	265	6.93	6.82		6.45	

Table 4.9

Evaluation of Fatigue Performance of Bearings in the "E" Series

Bearing Pad	Normal Load (kips)	Pre-Fatigue Shear Stiffness (kips/in)	Post Parallel Fatigue		Post Rotated Fatigue	
			Shear Stiffness (kips/in)	Average % Degredation	Shear Stiffness (kips/in)	Average % Degradation
E90	215	16.12	15.90	2.0%	14.30	9.7%
	225	16.28	16.14		14.38	
	235	16.50	16.24		14.49	
	245	16.71	16.44		14.89	
	255	16.89	16.58		15.14	
	265	16.93	16.70		15.39	
	275	17.33	16.82		15.16	
	285	17.54	-----		15.31	
	300	17.93	17.19		15.50	
E60	215	20.30	20.17	0.2%	17.42	13.0%
	225	19.87	20.42		17.45	
	235	20.19	20.68		17.53	
	245	20.43	20.75		17.70	
	255	20.76	20.37		18.09	
	265	20.83	20.58		18.22	
	275	21.15	20.89		18.35	
	285	-----	21.18		18.51	
	300	-----	21.46		18.97	
E45	215	17.87	17.59	0.0%	14.67	14.8%
	225	17.75	17.80		14.92	
	235	17.92	17.90		15.13	
	245	17.95	18.11		15.41	
	255	18.12	18.31		15.61	
	265	18.29	18.41		15.72	
	275	18.53	18.55		15.81	
	285	18.80	18.81		16.13	
	300	19.14	18.92		16.73	
E30	215	24.00	22.47	7.1%	21.17	2.8%
	225	24.08	22.66		21.44	
	235	24.40	22.74		21.66	
	245	24.39	22.72		21.96	
	255	24.59	23.02		22.30	
	265	24.79	22.92		22.57	
	275	25.09	23.18		22.82	
	285	25.21	23.21		23.17	
	300	25.64	23.39		23.53	

In general, fatigue cycles applied with parallel bearing contact surfaces did not significantly effect the post-fatigue shear stiffness of the bearings. The degrees of degradation ranged from -4.8% (bearing A90) to 7.1% (bearing E30). The average deterioration, excluding these lowest and highest values, was 1.2%. In the case of bearing A90, the average shear stiffness after parallel fatigue was greater than the average pre-fatigue stiffness by 4.8%. This is accounted for by the fact that, prior to the pre-fatigue stiffness test, the polished steel plate supporting the roller-nest (see Figure A.1) became worn directly under the roller-nest causing its effective coefficient of friction to be larger than what was initially used in the microcomputer program to calculate the net horizontal force. The plate was subsequently repolished at regular intervals.

For the second series of fatigue tests, the bearings were rotated to a 2% slope (as described in Section 1.4). The values of shear stiffness after "rotated fatigue" when compared to the post-parallel fatigue values decreased 2.5% to 14.8%, with an average of 8.2%. The average shear stiffness after the rotated fatigue of bearing A45 was larger than the post-parallel fatigue stiffness again due to unnoticed wear of the roller-nest bearing plate.

The effects of fatigue on skewed bearings with a girder end rotation are slightly larger than these for bearings with parallel bearing surfaces. However, after 100 years of simulated, environmentally induced shear displacements, the degradation of shear stiffness was not substantial.

4.3 Compressive Stiffness Response to Fatigue for Skewed Bearings

Compressive stiffness tests were conducted before and

after the shear fatigue program of Phase II. Since the compressive load versus displacement plots are not linear, an effective compressive stiffness value, k_c, as defined in Figure 4.2, was used to evaluate the fatigue performance of each skewed bearings. The compressive stiffness, k_c, is the secant modulus defined at the design dead load level. Compressive load versus displacement plots for all tests are found in Appendix C.

Table 4.10 shows the pre-parallel (Phase I) and post-parallel fatigue (Phase III) values of the compressive stiffnesses and the percent degradation due to fatigue. Compressive stiffness deterioration ranged from +2.4% to -18.4%. A negative value means that the stiffness after fatigue was greater than the pre-fatigue stiffness. This phenomenon occurred for all but three bearings, thus, it is concluded that shear fatigue does not significantly effect the compressive stiffness of elastomeric bearings.

A possible explanation for the increase of compressive stiffness after fatigue is because of the sustained compressive loading during fatigue. This sustained loading causes the bearing to "creep" in the compressive direction and when the load is removed there is a very small compressive displacement that is not immediately recoverable, see Figure 4.3. Since the compressive stiffness tests were conducted immediately following the fatigue cycles, this creep displacement was not taken into account, which makes a substantial difference in the compressive stiffness as it is defined here.

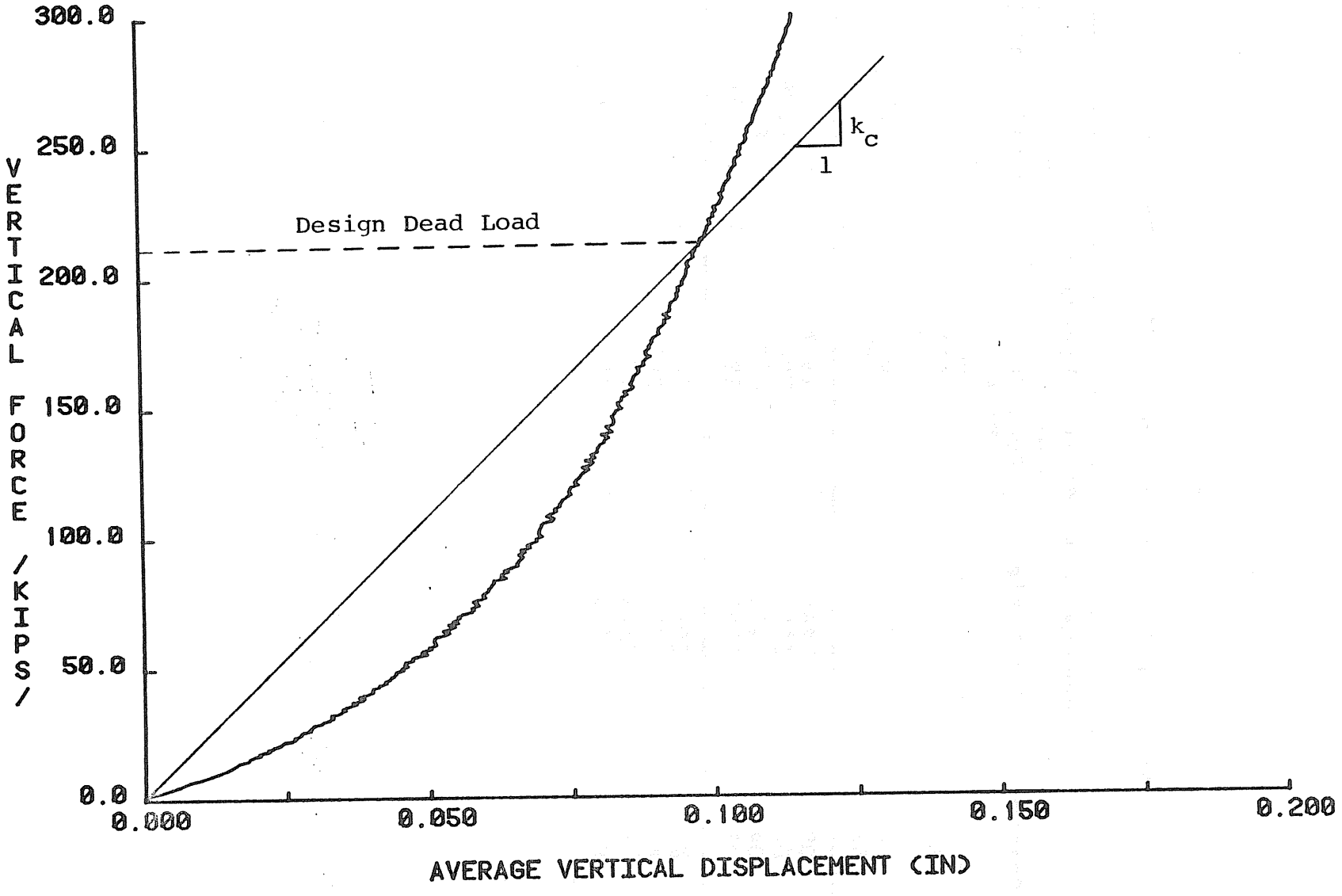

Figure 4.2 Typical Compressive Load verses Displacement Plot

Table 4.10

Experimental Compressive Stiffness Results

Bearing	Compressive Stiffness (kips/in)		Percent Degradation
	Pre-Fatigue	Post-Fatigue (Parallel)	
A90	----	811	----
A60	----	1250	----
A45	1034	1034	0.0%
A30	1091	1154	- 5.8%
D90	1448	1414	+ 2.4%
D60	1815	1900	- 4.7%
D45	1431	1689	-18.0%
D30	1993	1961	+ 1.6%
E90	2966	3071	- 3.5%
E60	3772	3805	- 0.9%
E45	3644	3945	- 8.3%
E30	3822	4526	-18.4%

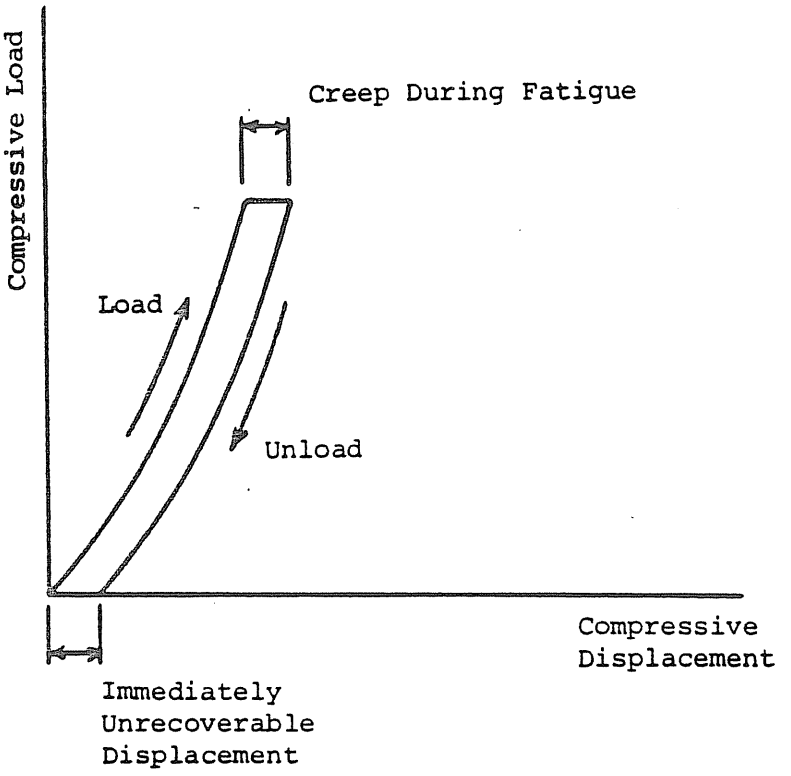

Figure 4.3 Compressive Creep Displacement

CHAPTER V

SUMMARY AND CONCLUSIONS

5.1 Summary of Shear Stiffness Tests and Proposed Design Equations

Twelve skewed elastomeric expansion bridge bearings were tested to determine the effects of skew on stiffness. It was found that the simple shear equation for estimating the shear stiffness of the bearings was very conservative and no direct correlation was evident between it and experimental results. In general, the change of shear stiffness increased more rapidly than the change in bearing area as the skew angle decreased from 90° (rectangular) to 30°. To partially account for this increase, an effective shear area for each bearing was defined. This effective area was used, in conjunction with bending effects, to establish a proposed design expression for the prediction of shear stiffness of skewed elastomeric bearings. The proposed shear stiffness expression for any practical skew angle ($\alpha > 0$) is

$$(k_s)_\alpha = \left[\frac{GA/T}{\frac{L}{L - \Delta_s} + \frac{(T \sin \alpha)^2}{3[(L \sin \alpha)^2 + (W \cos \alpha)^2]}} \right] \quad (5.1)$$

All variables are defined in the Nomenclature. This proposed design expression predicts the experimentally determined shear stiffnesses with good correlation.

An alternative solution to the skewed bridge bearing problem is to use a rectangular bearing oriented with two sides parallel to the centerline of the piers or abutments or a "turned" bearing. Tests were conducted using six turned elastomeric expansion bridge bearings to determine the effects of orientation on shear stiffness.

Using an effective shear area coupled with bending effects, similar to that used for the development of the skewed bearing prediction expression, a proposed design expression for the prediction of shear stiffness for rectangular bearings with turned shear axes was developed

$$(k_t)_\alpha = \frac{G\,A}{T}\left[\frac{\sin^2\alpha}{\frac{b}{b-\Delta_s}+\frac{T^2}{3b^2}}+\frac{\cos^2\alpha}{\frac{a}{a-\Delta_s}+\frac{T^2}{3a^2}}\right] \qquad (5.2)$$

Again good correlation between predicted and experimental results was found.

Equations 5.1 and 5.2 reduce to the same expression for rectangular bearings that are orientated perpendicular to the bridge girder axis.

5.2 Summary of Fatigue and Low Temperature Tests

To evaluate the in-situ performance of skewed elastomeric expansion bearings, the following six phases of testing were conducted on each of twelve bearings:

I. Shear and compressive stiffness tests using previously unloaded bearing.

II. Fatigue cycles representing 50 years of

service with parallel top and bottom bearing surfaces.

III. Shear and compressive stiffness tests immediately following Phase II.

IV. Shear stiffness tests with bearings at sub-freezing temperatures and after the bearings had been tested in Phase II.

V. Additional fatigue cycles representing 50 years of service with rotated bearing surfaces.

VI. Shear stiffness tests upon the completion of Phase V.

Phase I formed the basis of comparison with the post-fatigue results of Phases III and VI, and the low temperature test results of Phase IV.

In general, the fatigue loadings with parallel surfaces had very little effect on compressive and shear stiffnesses. The degrees of degradation in shear stiffness between Phases I and III ranged from 0.0% to 7.1%. When the bearing surfaces were rotated to a 2% slope and then fatigue loaded, additional degradation in shear stiffness occurred, but was not significant considering that 100 years of service life had been modeled.

In Phase IV, the average recorded bearing temperature at the time of the tests was 3.7°F. The average increases in shear stiffness between Phases IV and III for bearing type "A", "D" and "E" were found to be 39%, 45% and 27%, respectfully. These percent increases in shear stiffness are well within design values found in the literature for

rectangular, unturned bearings. Hence, the proposed shear stiffness prediction equations need only be corrected using the published values to account for the increase in shear stiffness of elastomeric bearings when at low temperatures.

BIBLIOGRAPHY

1. AASHTO, "Standard Specifications for Highway Bridges", 13th Edition, 1985 Interim Section 14, Washington, D.C., 1985.

2. ASTM, "Standard Specification for Plain and Steel-laminated Elastomeric Bearings for Bridges", ASTM, Vol 04.03, D4014, pp. 676-684.

3. Burton, W.E. Engineering with Rubber, McGraw-Hill, New York, New York, 1949.

4. Gent, A.N., Henry, R.L., and Roxbury, M.L., "Interfacial Stresses of Bonded Rubber Blocks in Compression and Shear", Transactions of the ASME, Journal of Applied Mechanics, Vol. 96 (1974).

5. Gent, A.N., and Lindley, P.B., "The Compression of Bonded Rubber Blocks", Institution of Mechanical Engineering Proceedings, Vol. 173, 1959, pp. 111-122.

6. Gent. A.N., and Meinecke, E.A., "Compression, Bending and Shear of Bonded Rubber Blocks", Polymer Engineering and Science, Vol. 10, No. 1, Jan. 1970, pp. 48-53.

7. Hall, M.M., "Pressure Distribution over the Flat End Surfaces of Compressed Rubber Cylinders", Journal of Strain Analysis, Vol. 6, No. 1 (1971).

8. Harper, C.A. Handbook of Plastics and Elastomers, McGraw-Hill, New York, New York, 1975.

9. Iverson, J.K. and Pfeifer, D.W., "Criteria for Design of Bearing Pads", PCI Technical Report No. 4, 1985.

10. Lindley, P.B., "Plane-Stress Analysis of Rubber at High Strains Using Finite Elements", Journal of Strain Analysis, Vol. 6, No. 1 (1971).

11. Long, J.E., Bearings in Structural Engineering, John Wiley and Sons, New York, New York, 1974.

12. McPherson, A.T., Engineering Uses of Rubber, Reinhold Pub. Corp., New York, New York, 1956.

13. Minor, J.C., and R.A. Egen, "Elastomeric Bearings Research", Transportation Research Board NCHRP Report No. 109, Washington, D.C., 1970.

14. Naunton, William, The Applied Science of Rubber, London Press, London, England, 1961.

15. Payne, A.R. and Scott S.R., Engineering Design With Rubber, Interscience Publishers, Inc., New York, New York, 1960.

16. Sestak, J.J., Jr., Aldridge, W.W., and Fears, F.K., "A Comparitive Study of Elastomeric Materials for Bridge Bearing Pads", University of Oklahoma Research Institute, Norman, Oklahoma, March 1967.

17. Southwell, R.V., Introduction to the Theory of Elasticity, 2nd Edition, Oxford University Press, 1944.

18. Stanton, J.F., and C.W. Roeder, "Elastomeric Bearings Design, Construction, and Materials", Transporation Research Board NCHRP Report No. 248, Washington, D.C., 1982.

19. Stanton, J.F. and Roeder, C.W., "Elastomeric Bridge Bearings Specifications: Review of the Present and Proposals for the Future", Journal of the American Concrete Institute, No. 6, Proceedings Vol. 80, Nov/Dec, 1983.

20. Stanton, J.F. and Roeder, C.w., "Elastomeric Bearings: State-of-the-Art", Journal of Structural Engineering, Vol. 109, No. 12, Dec. 1983.

21. Vinje, Leidulv, "Behavior and Design of Plain Elastomeric Bearing Pads in Precast Structures", PCI Journal, Vol. 30, No. 6, Nov/Dec. 1985.

APPENDIX A

TESTING DETAILS

APPENDIX A

TESTING DETAILS

A.1 Test Setup

In an actual bridge, the expansion and contraction of a bridge girder due to temperature changes causes a longitudinal displacement at the girder ends. This displacement is achieved through the shear deformation of the elastomeric bearing. The dead and live loads of the bridge are transferred through the girders causing the bearings to compress. A test setup was needed to allow the bearing to compress freely and to force the bearing to shear to the design displacement as if the bearing was part of an actual bridge system.

To determine the experimental compressive behavior and the shear stiffnesses of elastomeric bearings, a test setup which simulates an actual bridge was built; details are shown in Figures A.1 and A.2. The normal force was applied with a 400,000 lb. capacity hydraulic ram and the horizontal force with a 55,000 lb. capacity closed-loop hydraulic testing system.

The test setup was erected inside Fears Structural Engineering Laboratory on the laboratory reaction floor. The floor is a concrete slab 30 ft. by 60 ft. by 3 ft. 6 in. deep with four W36x150 steel beams embedded in the concrete.

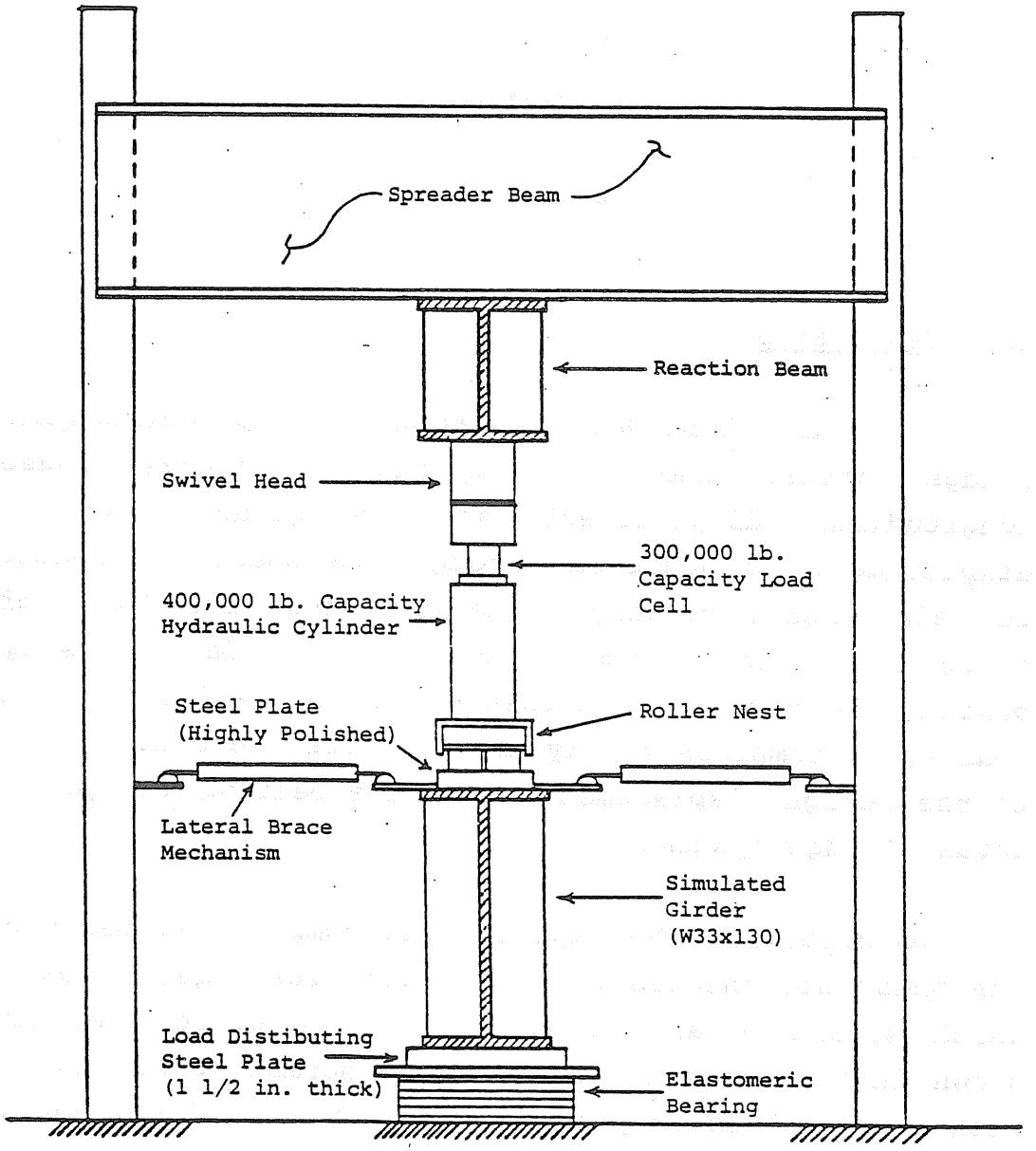

Figure A.1 Vertical Load Chain

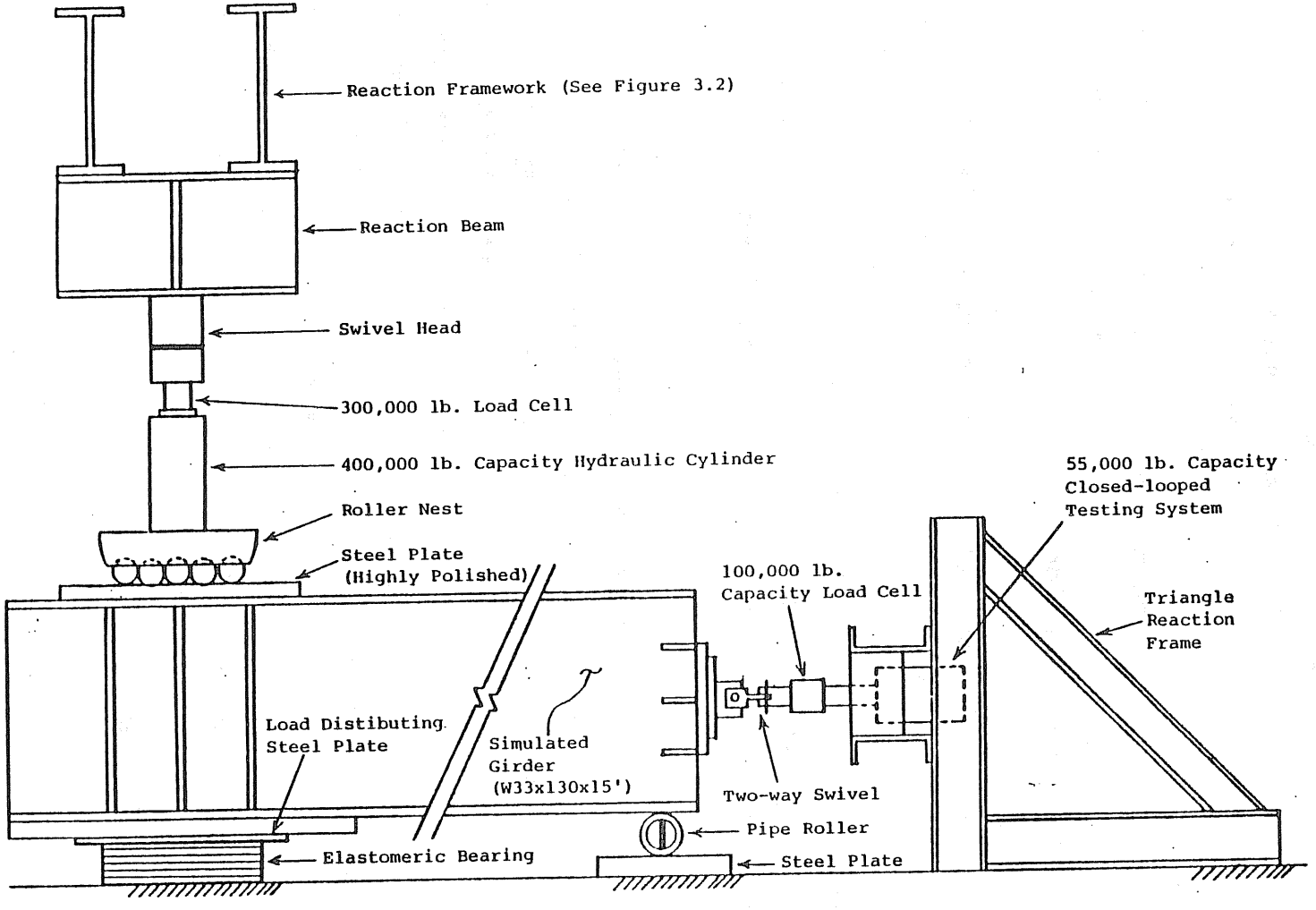

Figure A.2 Horizontal Load Chain

The slab weighs one million pounds and is capable of reacting 320,000 lbs. at any one location. The setup was erected directly over two of the embedded W36 beams spaced 8 ft. apart. The setup consisted of three parts: 1) An H-frame (Figure A.1) which was designed for 350,000 lbs. maximum vertical reaction, 2) A triangle frame (Figure A.2) which was designed for 55,000 lbs. maximum horizontal reaction and which supported the closed-loop hydraulic testing system, and 3) A W33 x 130 x 15 ft. girder which simulated the actual bridge girder.

The vertical load chain consisted of the H-frame, a reaction beam, a swivel, a load cell, a hydraulic ram, a roller nest with a known coefficient of friction, a highly polished steel plate, the simulated bridge girder, a load distributing steel plate (1.5 x 18 x 62 in.), the elastomeric bearing, and the reaction floor, as shown in Figure A.1.

The horizontal load chain consisted of the triangle frame, the actuator of the closed-loop hydraulic testing system, a load cell, a loading linkage (two-way swivel) to prevent out-of-plane forces, and the simulated bridge girder as shown in Figure A.2. A stiffened pipe roller was used to support the unloaded end of the girder, which allowed free horizontal movement of the girder. Lateral brace mechanisms, which prevent lateral movement without restraining longitudinal movement, were used to stabilize the girder against out-of-plane rotations and translations.

A.2 Instrumentation

Instrumentation consisted of two calibrated load cells, two horizontal displacement transducers, four vertical displacement transducers, an analog to digital signal converter, and a micro-computer.

The applied normal force was measured using a calibrated 300,000 lb. capacity load cell; the horizontal force was measured with a calibrated 100,000 lb. capacity load cell.

The horizontal displacements of the girder and, thus, the top fibers of elastomeric bearings in the shear stiffness tests were measured using two calibrated wire-type transducers, as shown in Figure A.3. The vertical displacements of the elastomeric bearing in the compressive stiffness tests were measured using four calibrated LVDT transducers, also shown in Figure A.3.

The analog signals for the eight instruments were digitized using a 16 channel differential input A/D converter with direct interface to the micro-computer. The micro-computer was used to reduce and plot the data in real time. The sample rate was approximately 950 samples per minute. In this manner, the instantaneous relationship of the two force and two displacement quantities of the shear stiffness tests, and the force and four displacement quantities of the compressive stiffness tests were determined.

The micro-computer was programmed to account for the coefficient of friction of the roller nest, the effects of the weight of the girder and other test setup parts not accounted for by the load cell in the vertical load chain, and for uplift effects caused by the horizontal force couple. This force-couple results because the applied horizontal force and the resisting force at the bearing/ reaction floor interface surfaces are not colinear. The couple tends to reduce the applied normal force at the bearing.

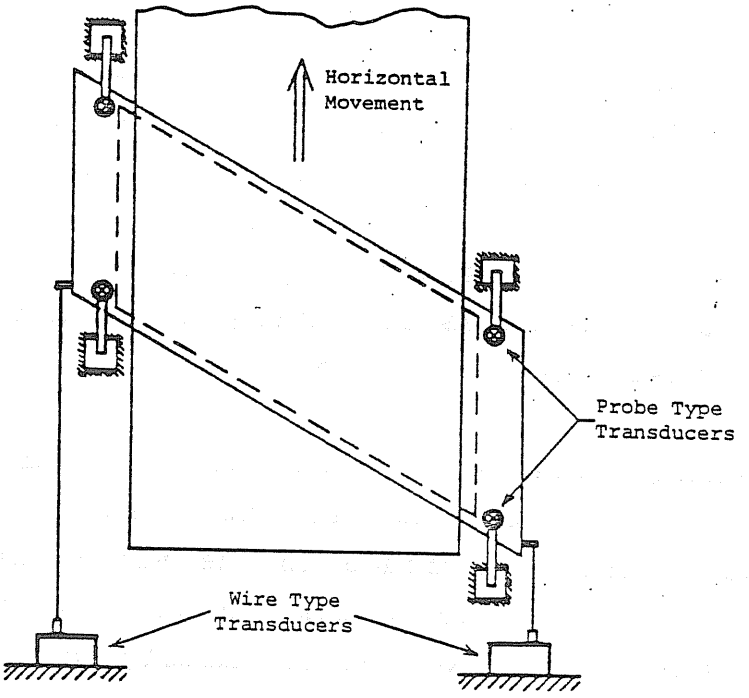

(a) Plan View

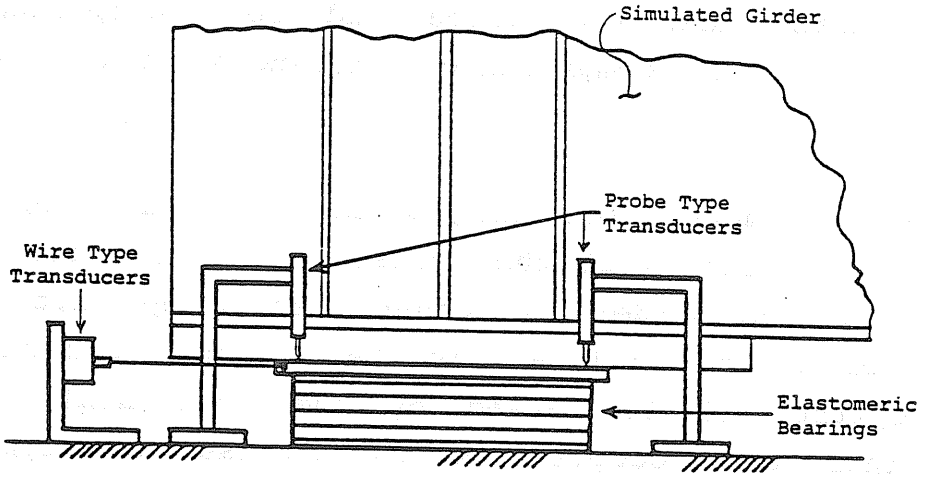

(b) Elevation

Figure A.3 Instrument Configuration

A.3 Test Procedures

Parallel and rotated shear stiffness tests of the skewed bearings were conducted at nominal compressive load increments of 10 kips (1 kip = 1000 lbs.) starting at the design dead load and increasing to dead plus live load (total working load) for that particular bearing type. All loading magnitudes were supplied by ODOT. For these tests, the bearing was positioned directly in line with the load chain and then the normal load was applied. The girder was then pulled the maximum design displacement (a shear strain of 50%), pushed back to zero, pushed in the opposite direction to the maximum displacement, and again pulled back to zero.

Approximately 1000 data sets, each set consisted of two force and two displacement readings, were recorded for each shear stiffness test. The slope of the horizontal force versus horizontal displacement curves was found to be generally linear and for the purposes of this study was calculated between the two end points of the curve as shown in Figure A.4. This slope is the shear stiffness and was calculated automatically by the micro-computer taking into account the initial force on the bearing due to the weight of the system, the horizontal force-couple effect, and the effective coefficient of friction of the roller nest. The graphics capabilities of the micro-computer system were used to plot the results in real time. Typical plots for various bearings are shown in Figures A.4, A.5, and A.6.

Compressive stiffness tests were also conducted for each bearing. The bearings were loaded in compression to the total working load of the bearing. Approximately 500 data sets, each set consisted of a normal load and four displacement readings were recorded for each test. Since

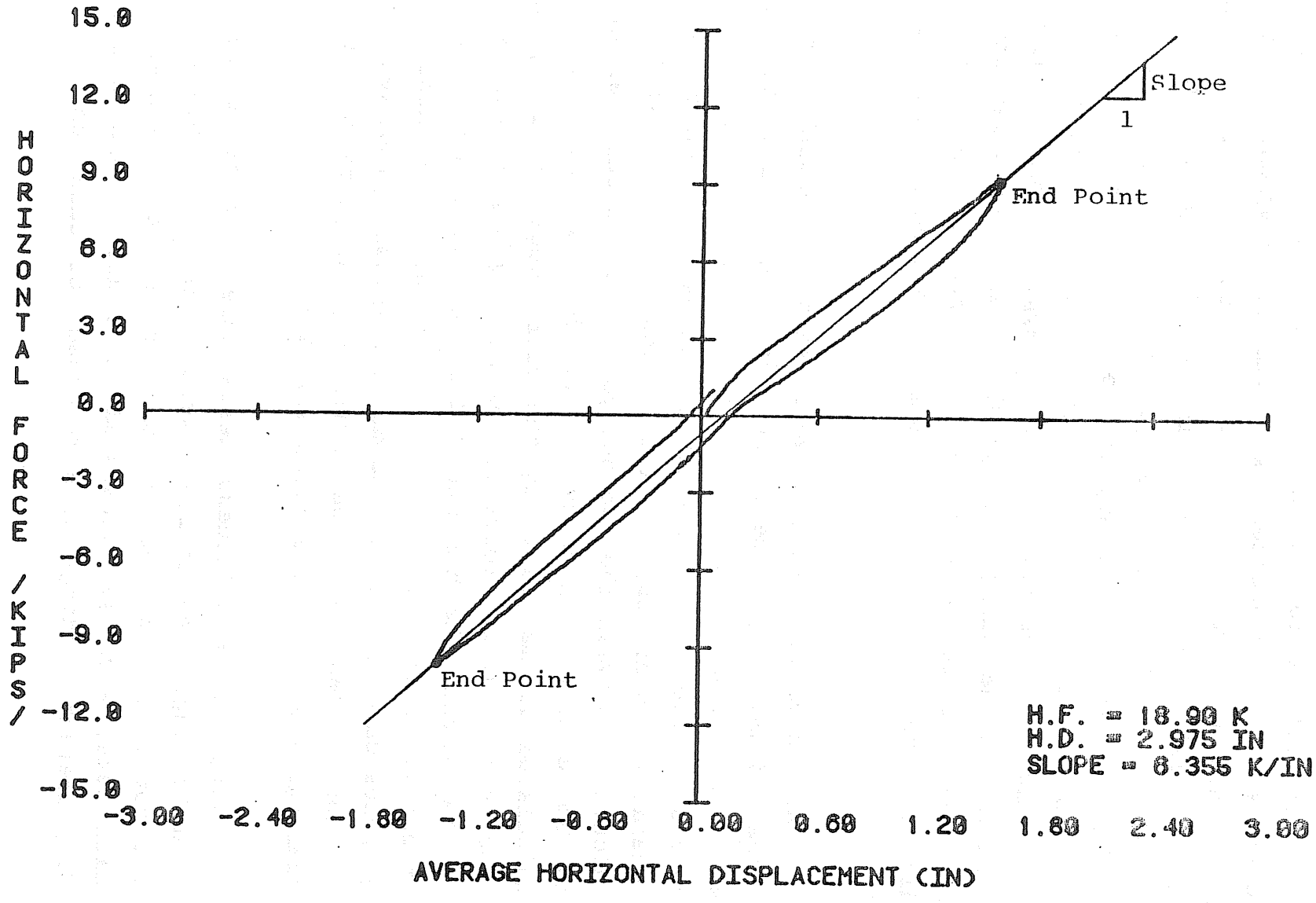

Figure A.4 Typical Shear Stiffness of "A Series" Bearings

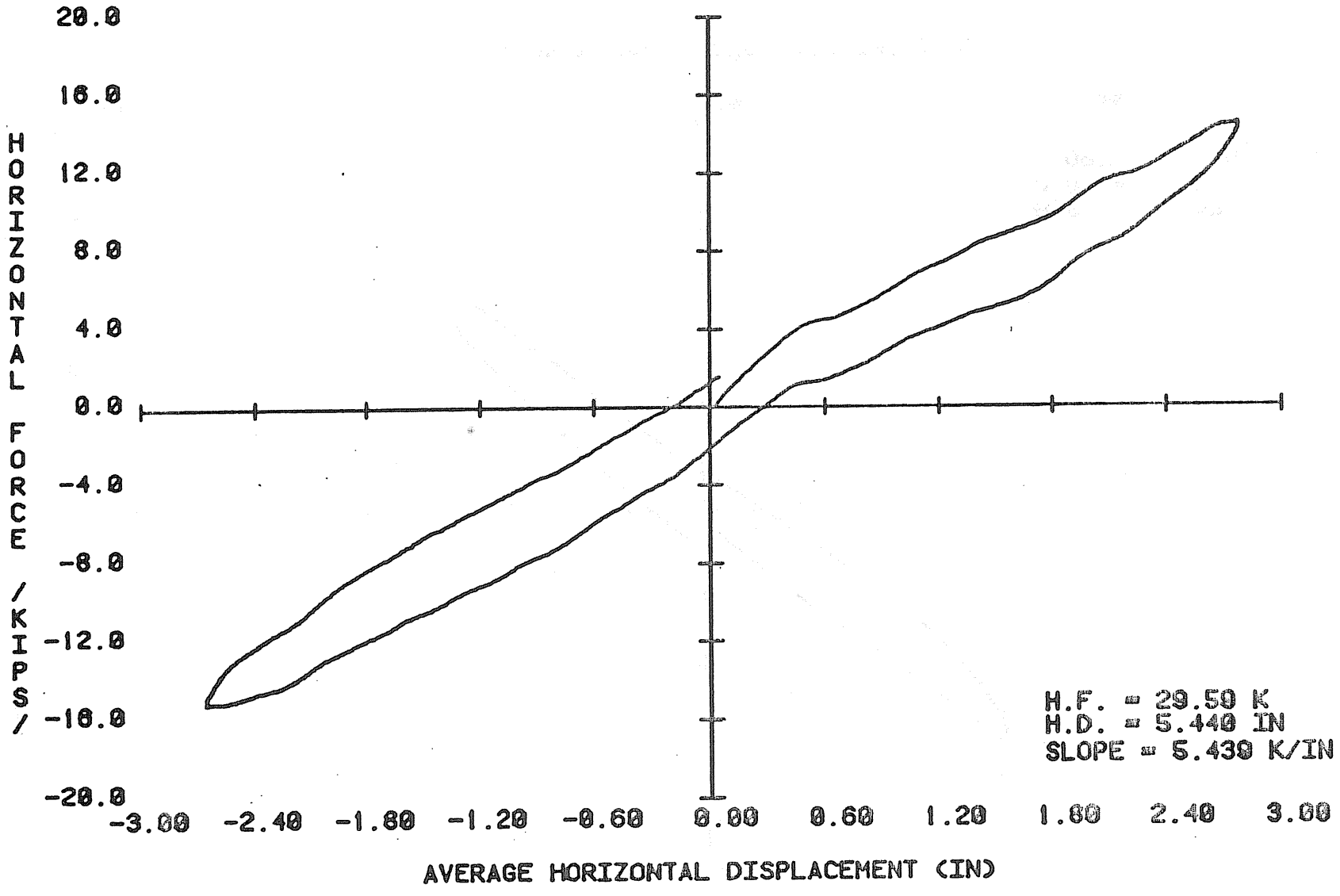

Figure A.5 Typical Shear Stiffness of "D Series" Bearings

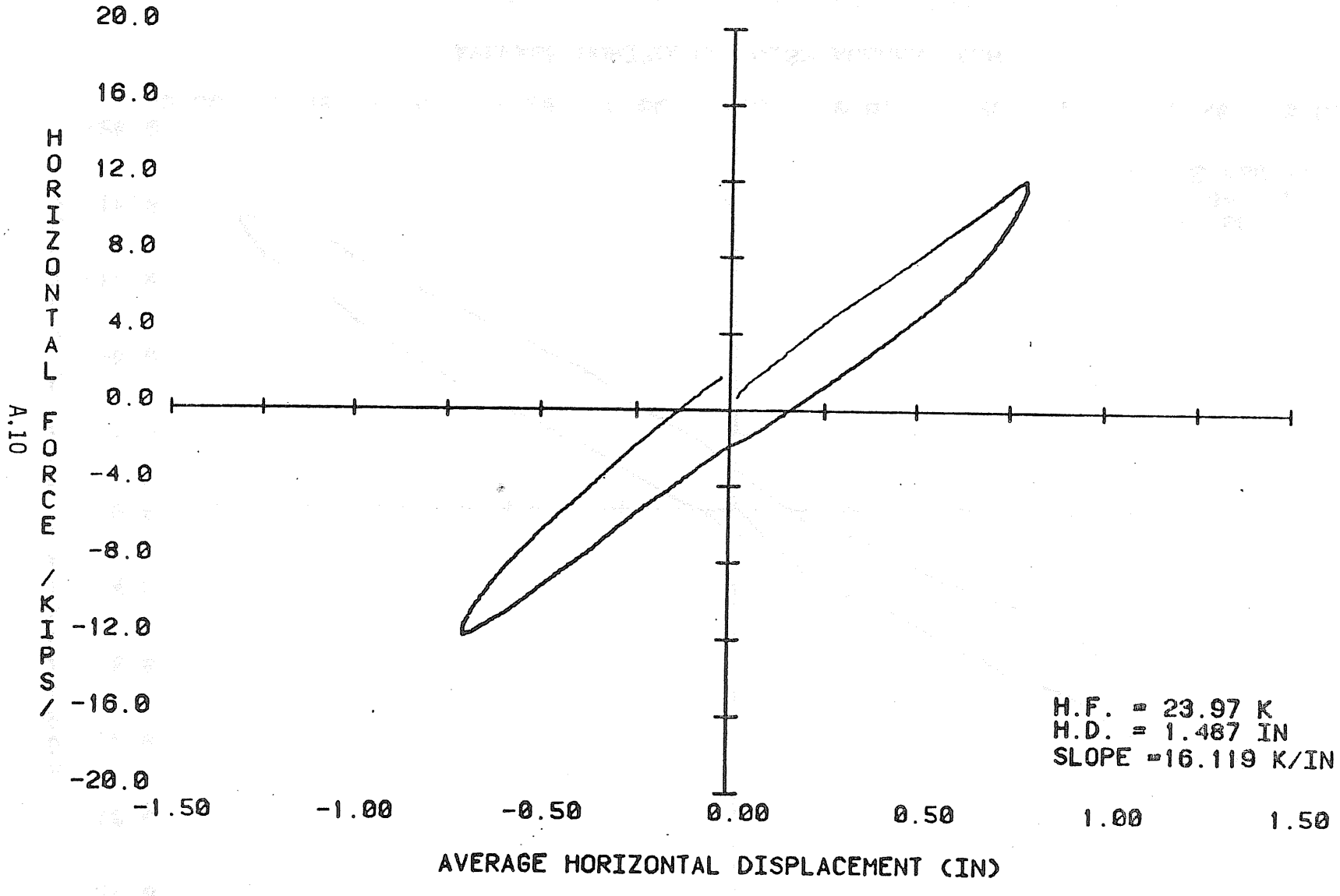

Figure A.6 Typical Shear Stiffness of "F Series" Bearings

the compressive stiffness of rubber and other rubber-like materials is non-linear, no effective value was calculated. A typical vertical load verses vertical displacement plot is shown in Figure A.7 and results from all compressive stiffness tests are found in Appendix C.

In test Phase IV, each bearing was placed in a deep freeze unit at a nominal temperature of -20°F for approximately 72 hours. Each bearing was taken from the freezer and placed in the test setup as quickly as possible to insure only a small rise in bearing temperature. Immediately upon bearing placement in the test setup, a shear stiffness test was conducted on the "frozen" bearing with the compressive force equal to the design dead loading. A temperature probe was embedded in the steel plate of each bearing and the temperature of the plate was measured and recorded at the time of the shear stiffness test. In this manner, the shear stiffness tests were conducted on the bearings subjected to low temperatures. The shear force verses displacement for all bearings subjected to low temperatures are found in Appendix B.

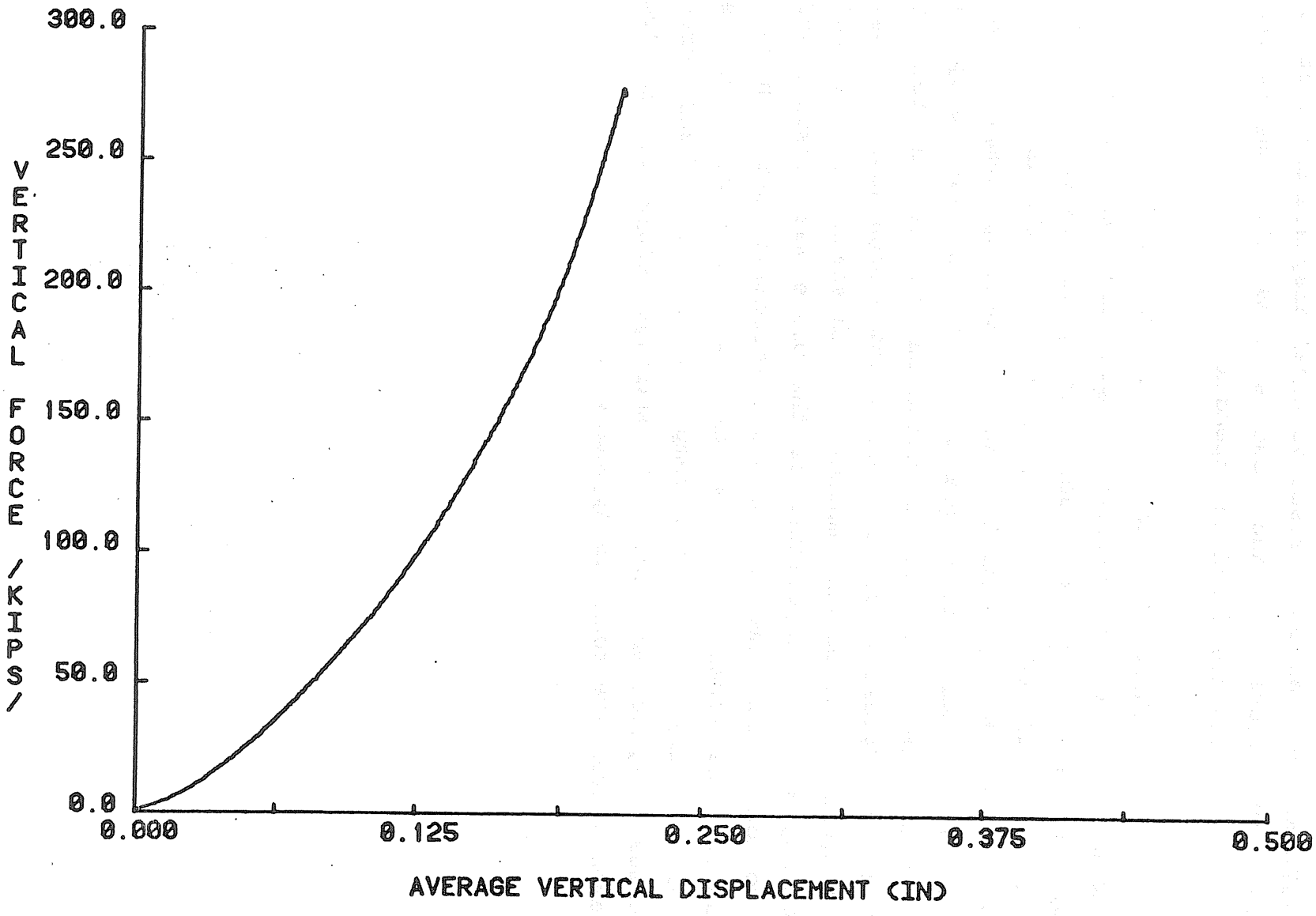

Figure A.7 Typical Compressive Load verses Displacement Plot

APPENDIX B

LOW TEMPERATURE TEST RESULTS

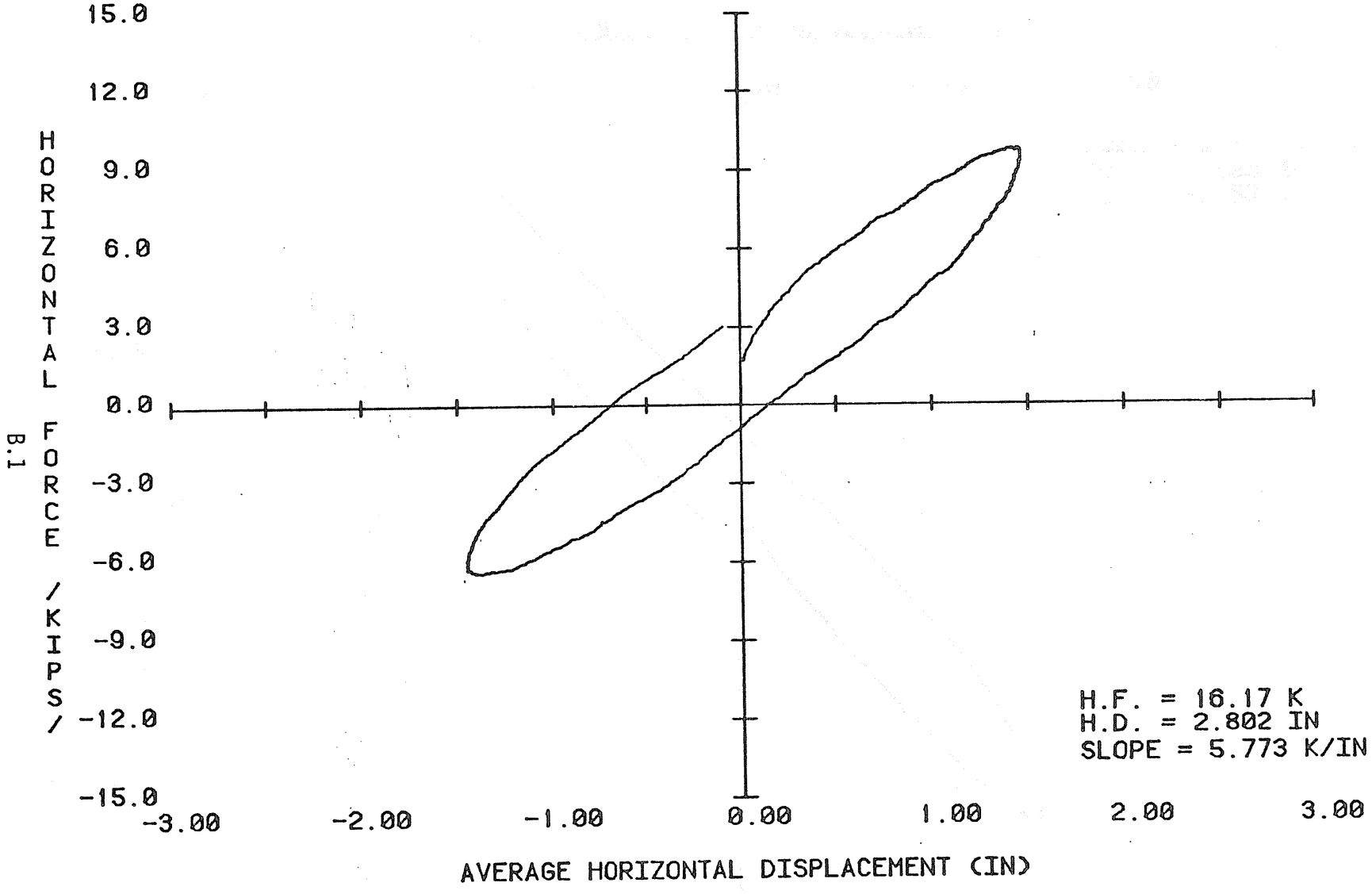

Figure B.1 Shear Force vs. Displacement for Bearing A90 at -3°F

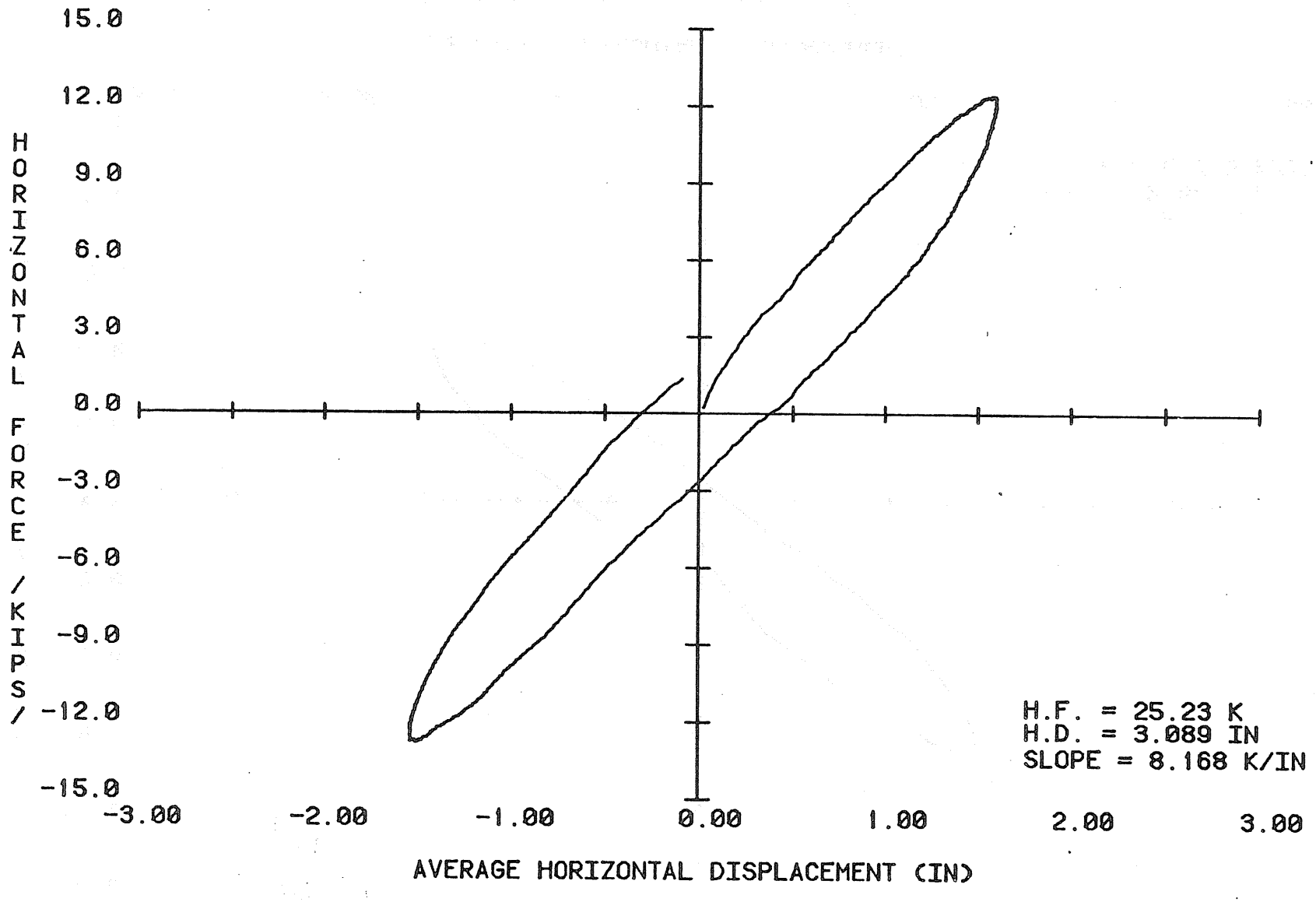

Figure B.2 Shear Force vs. Displacement for Bearing A60 at +5°F

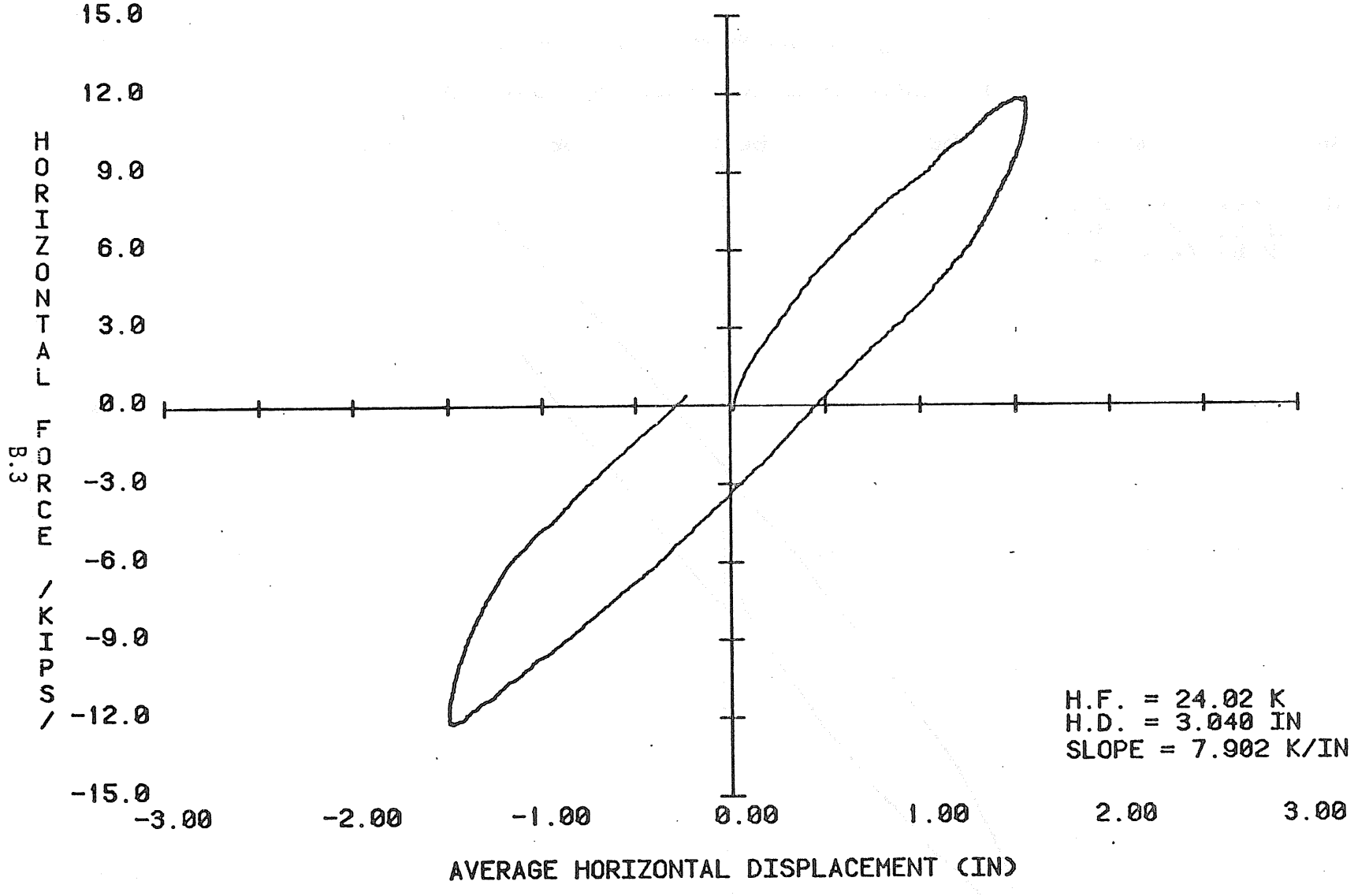

Figure B.3 Shear Force vs. Displacement for Bearing A45 at +3°F

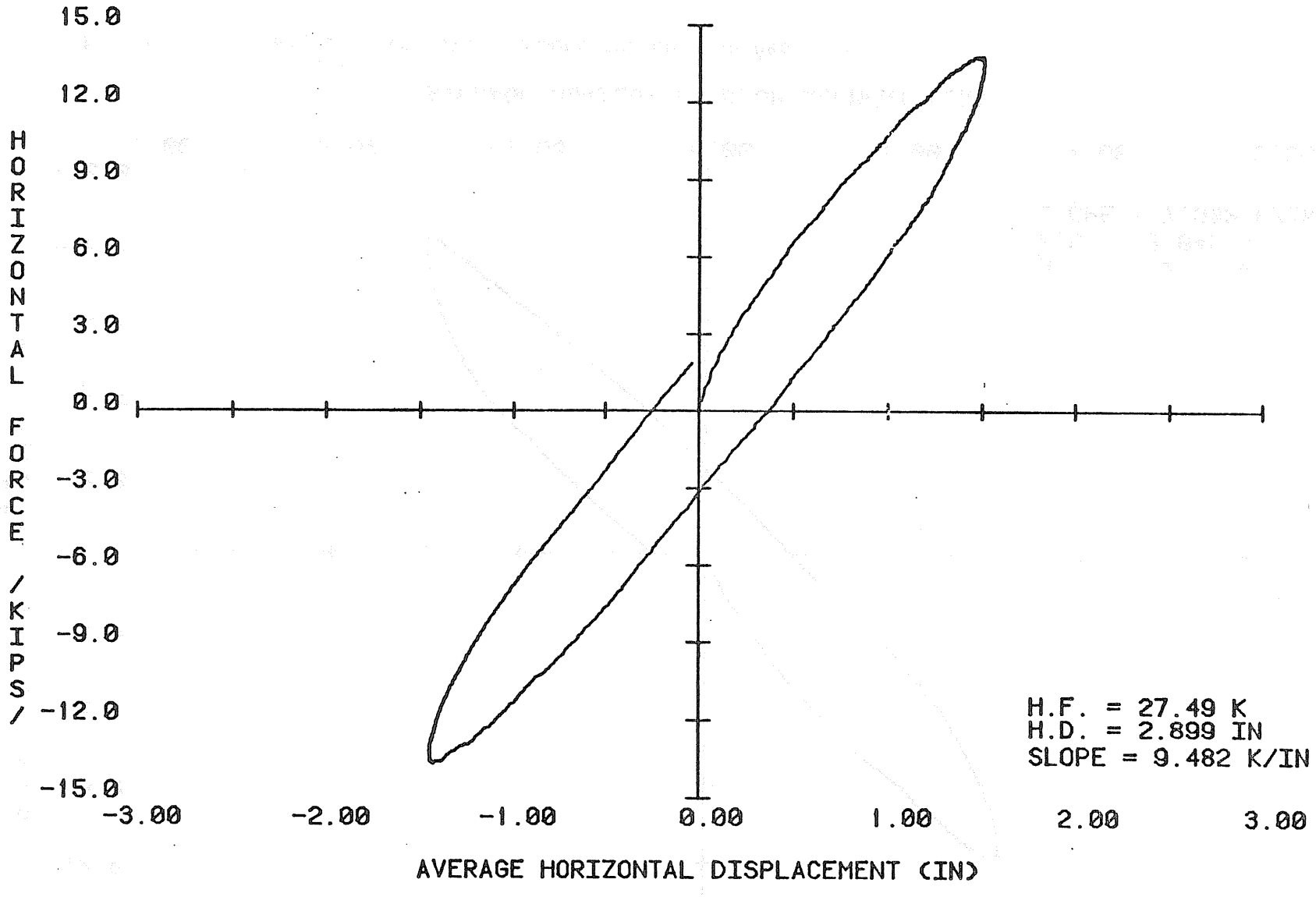

Figure B.4 Shear Force vs. Displacement for Bearing A30 at +5°F

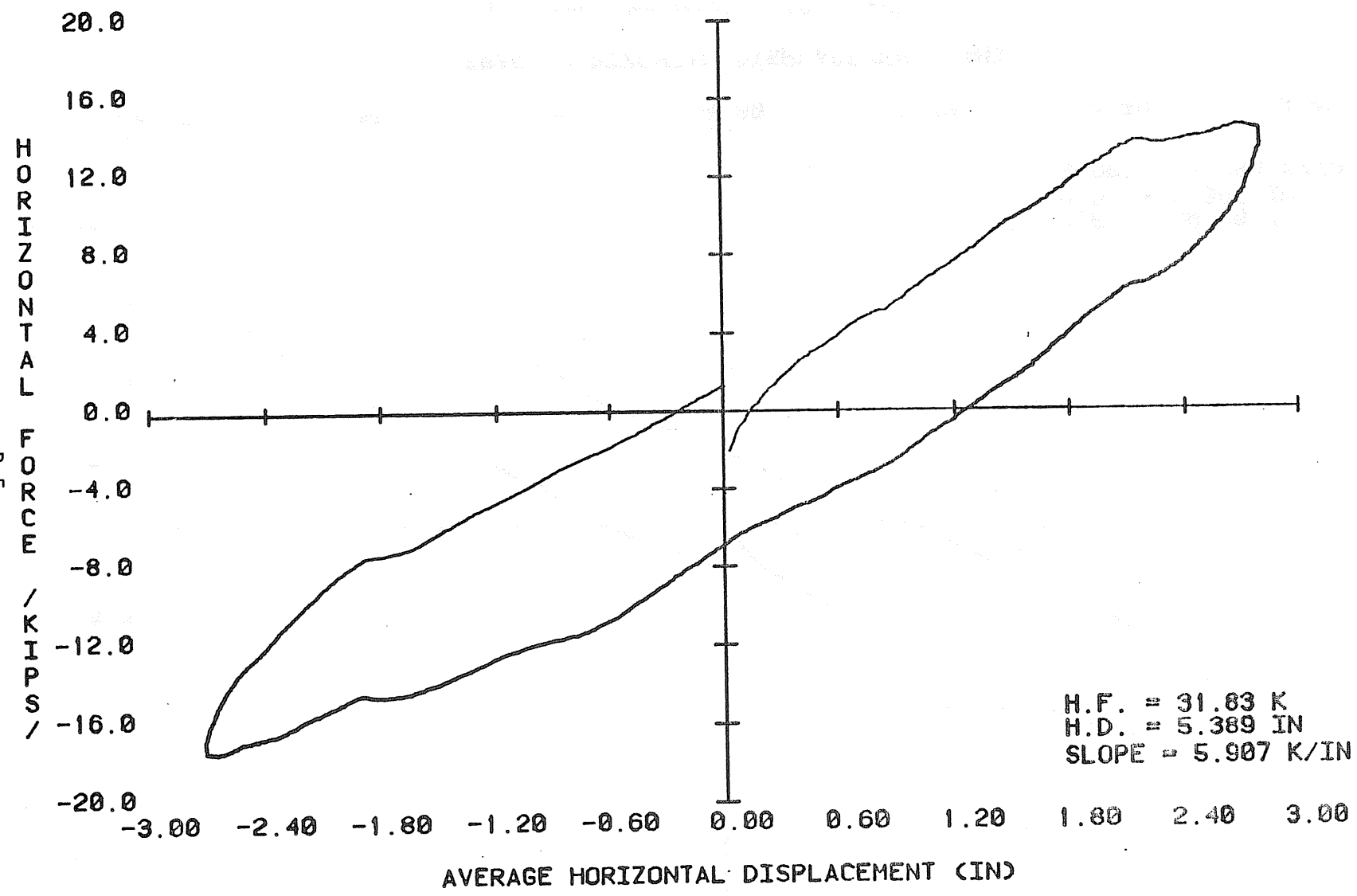

Figure B.5 Shear Force vs. Displacement for Bearing D90 at -3°F

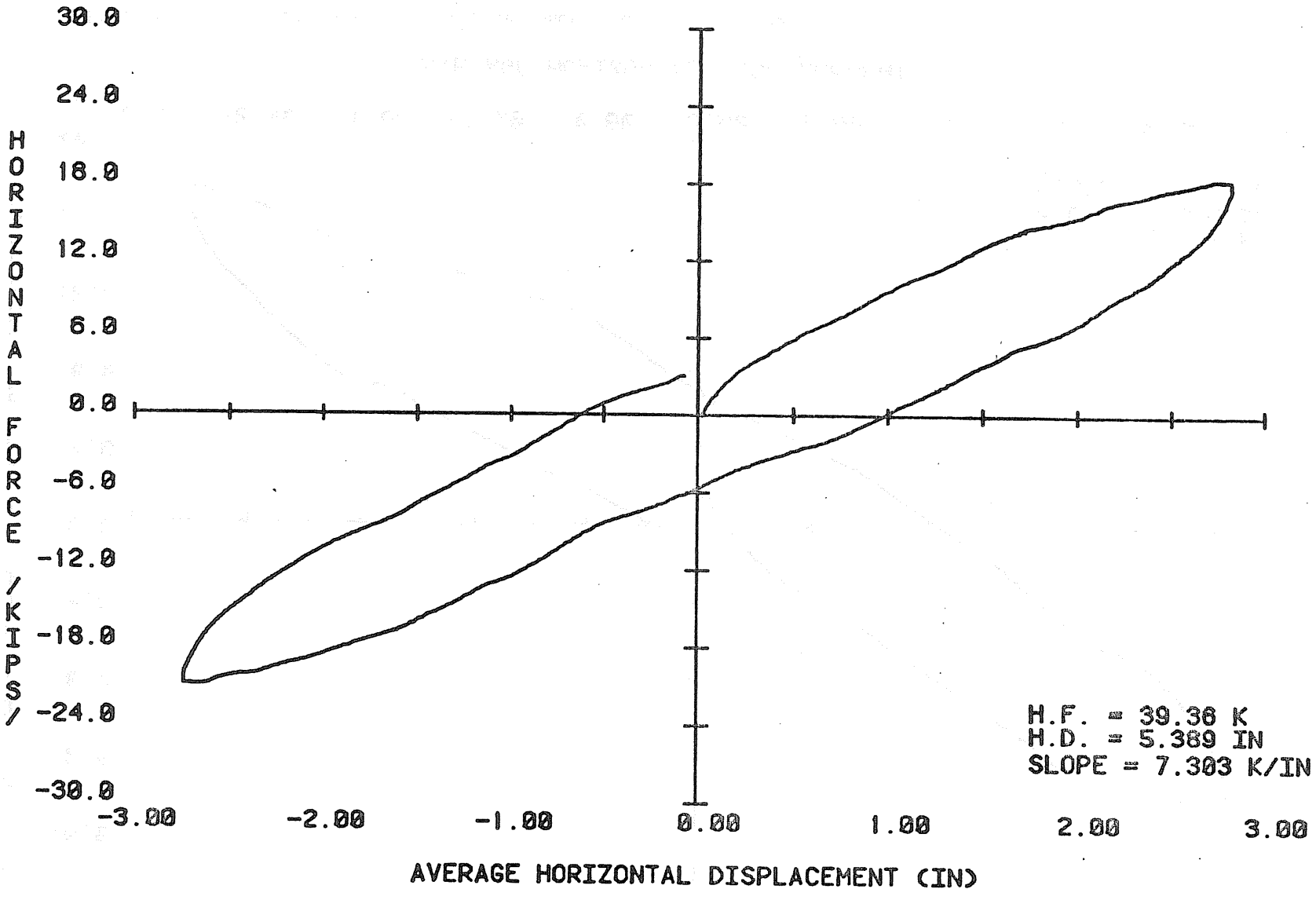

Figure B.6 Shear Force vs. Displacement for Bearing D60 at +3°F

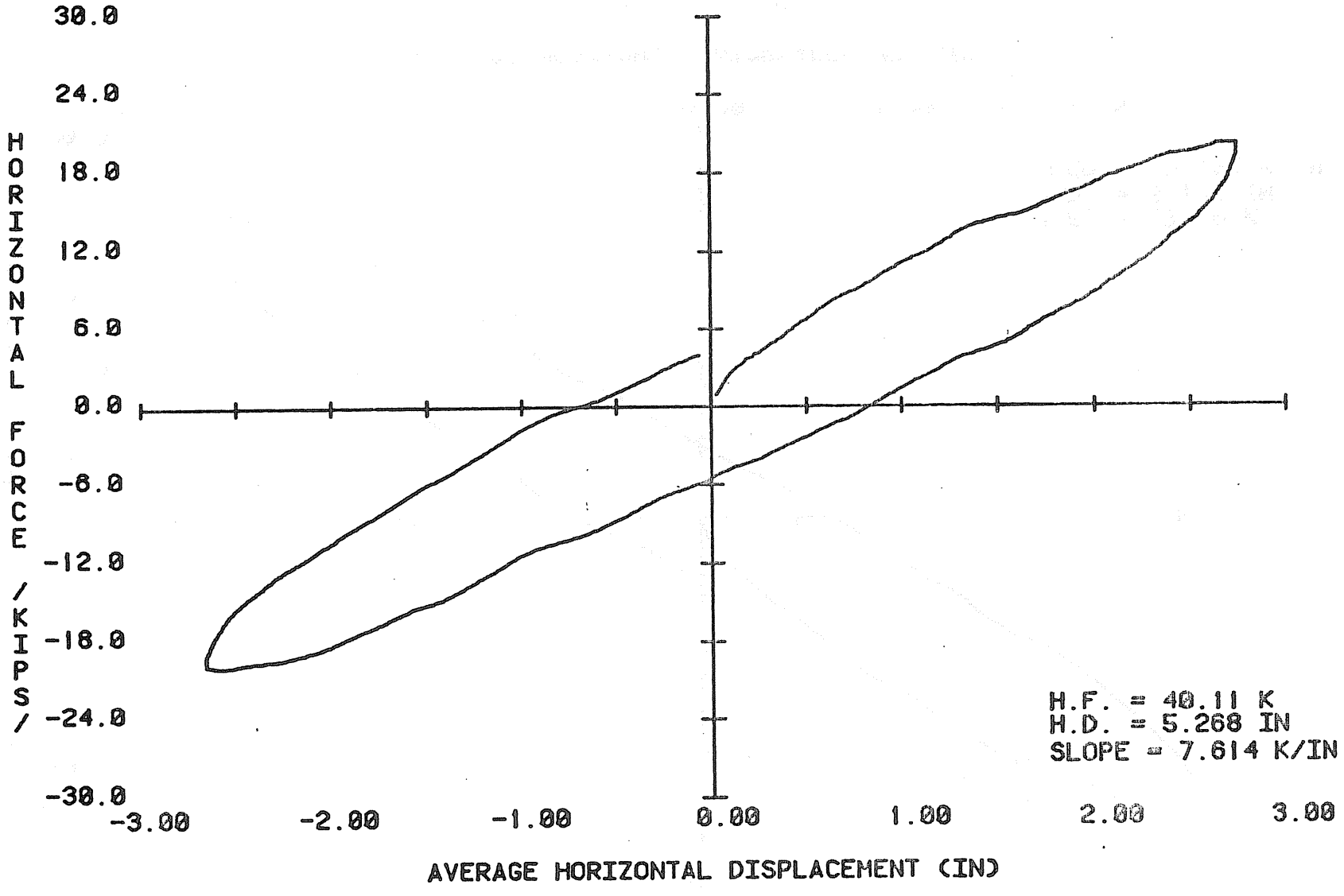

Figure B.7 Shear Force vs. Displacement for Bearing D45 at +4°F

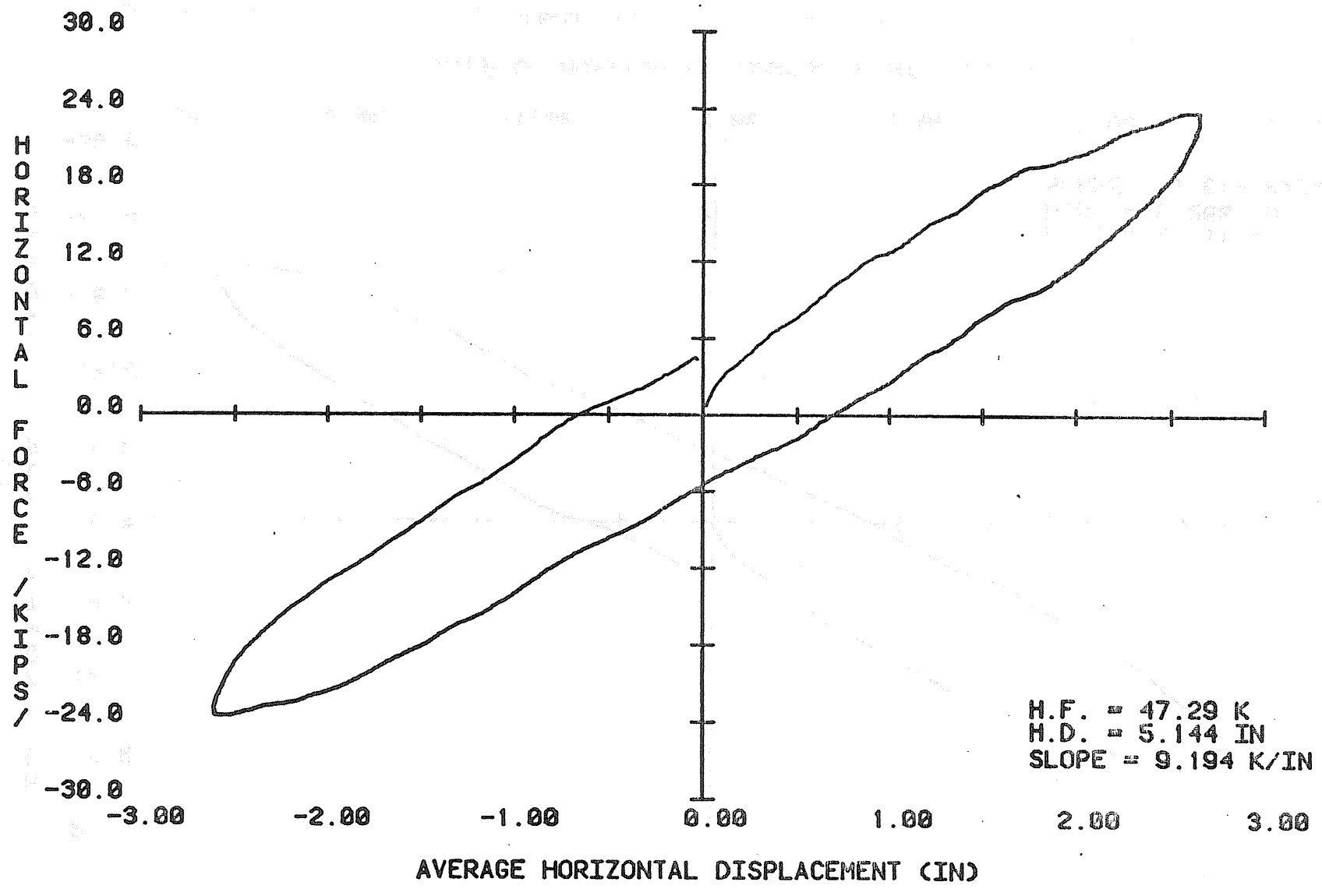

Figure B.8 Shear Force vs. Displacement for Bearing D30 at +6°F

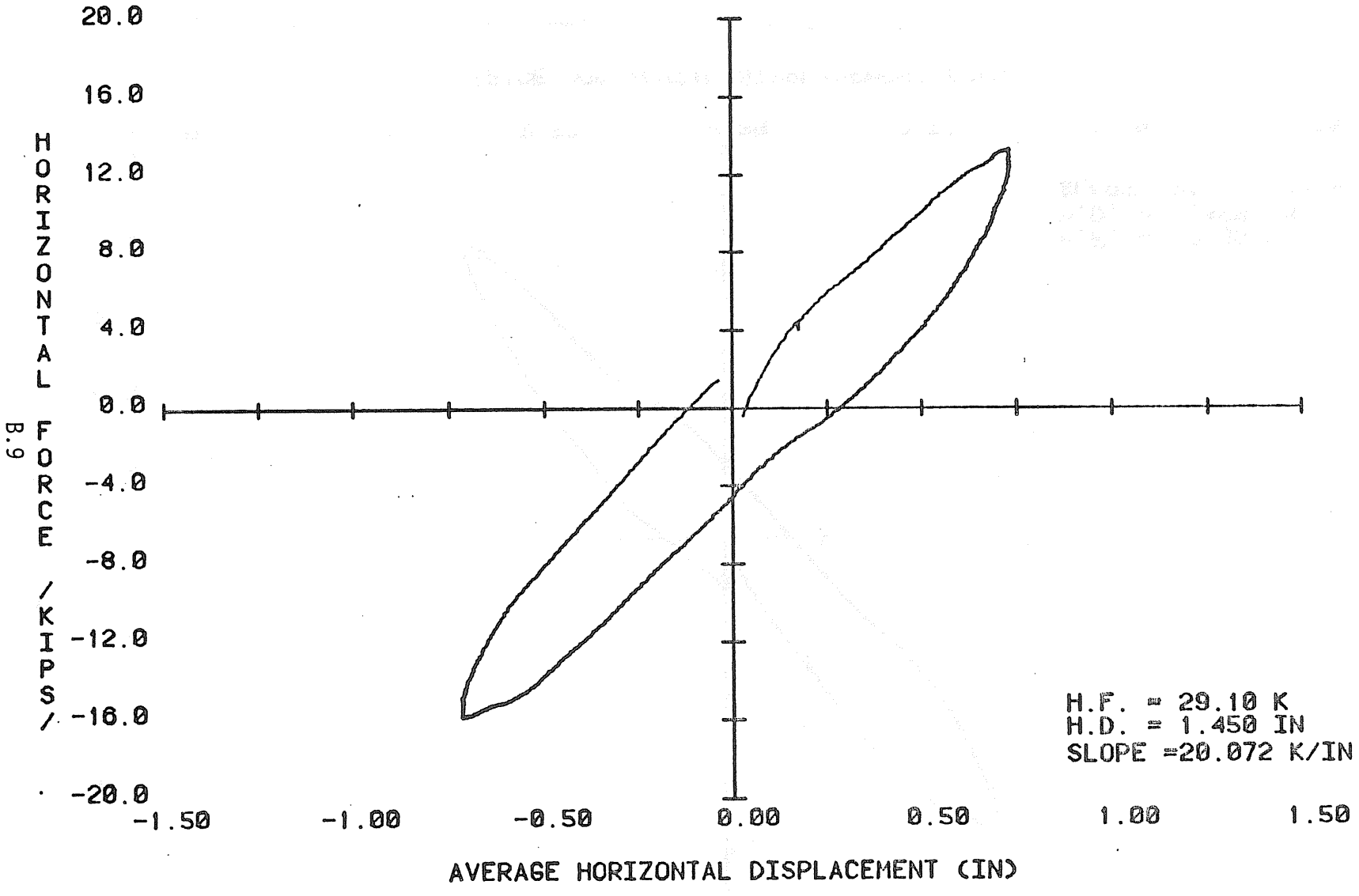

Figure B.9 Shear Force vs. Displacement for Bearing E90 at +5°F

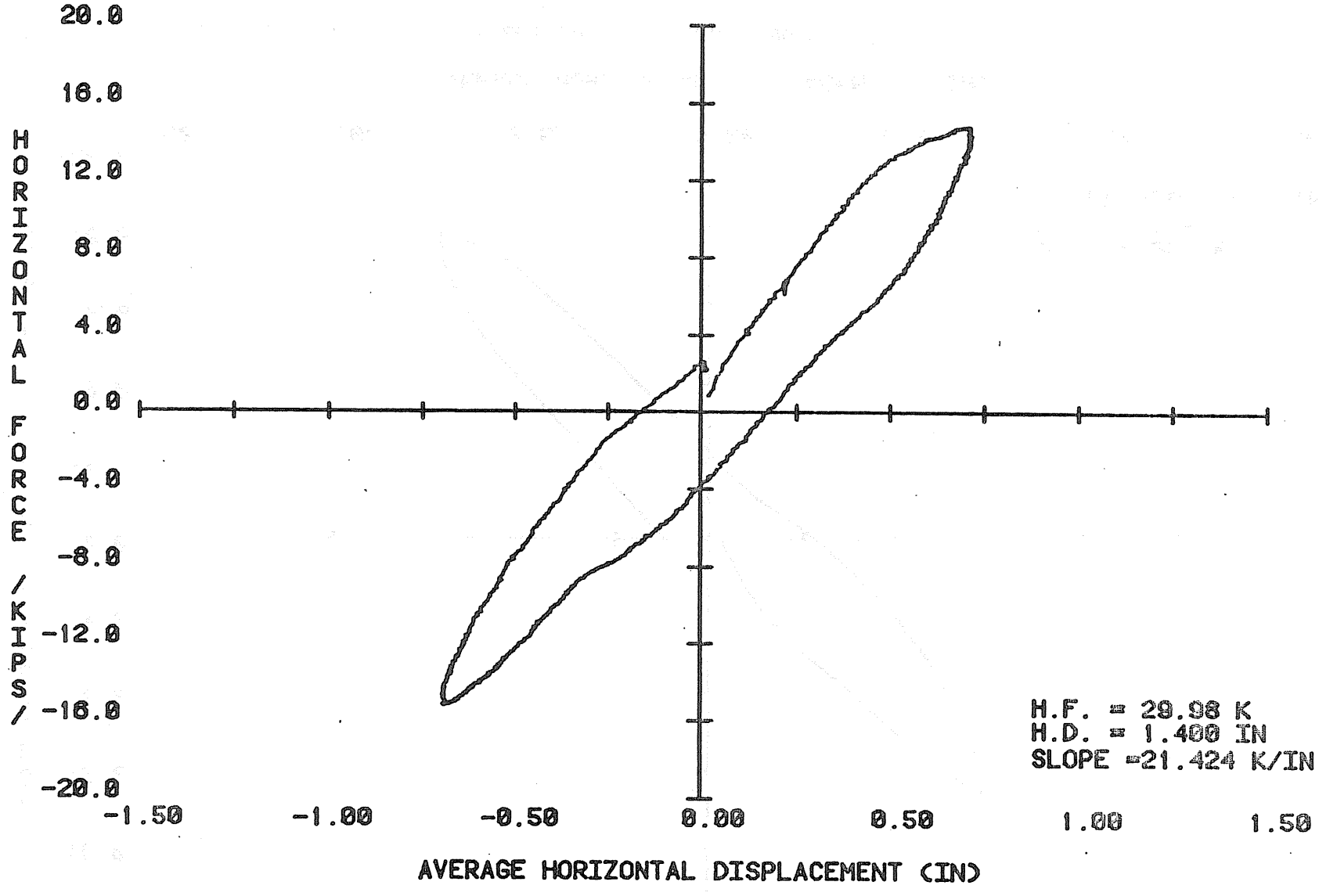

Figure B.10 Shear Force vs. Displacement for Bearing E60 at +6°F

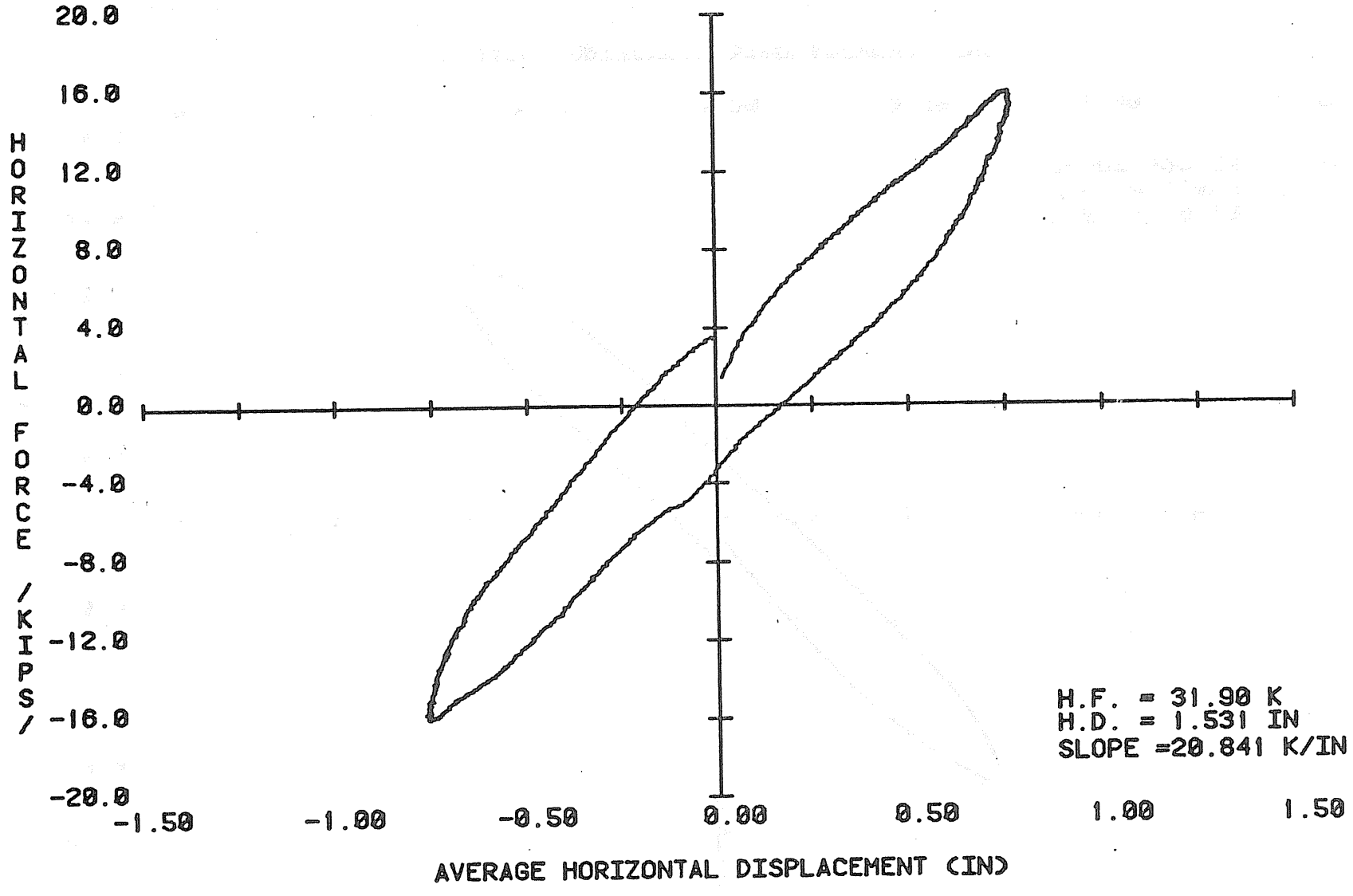

Figure B.11 Shear Force vs. Displacement for Bearing E45 at +8°F

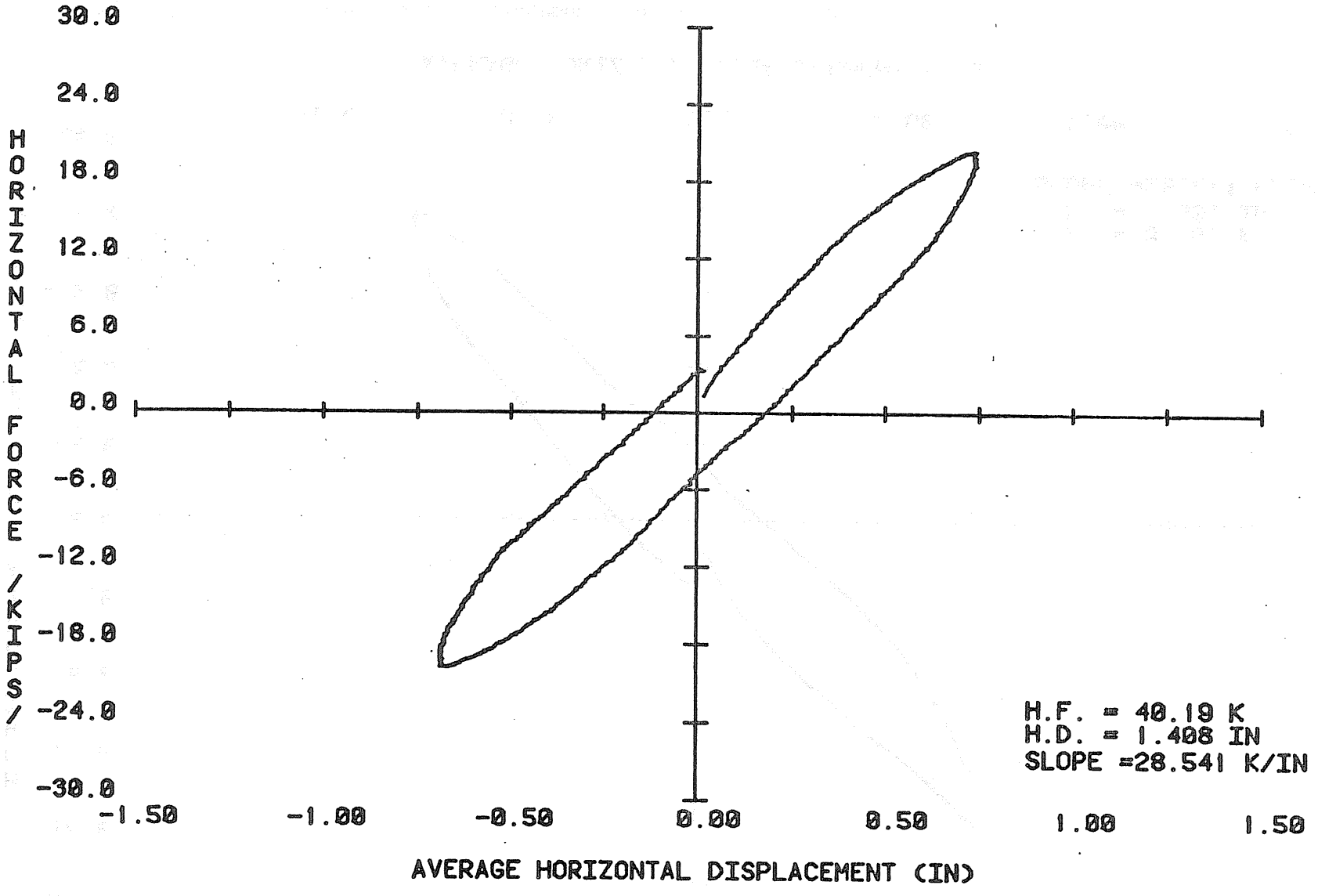

Figure B.12 Shear Force vs. Displacement for Bearing E30 at +5°F

APPENDIX C

COMPRESSIVE STIFFNESS TEST RESULTS

APPENDIX C.1

PRE-FATIGUE COMPRESSIVE STIFFNESS TESTS

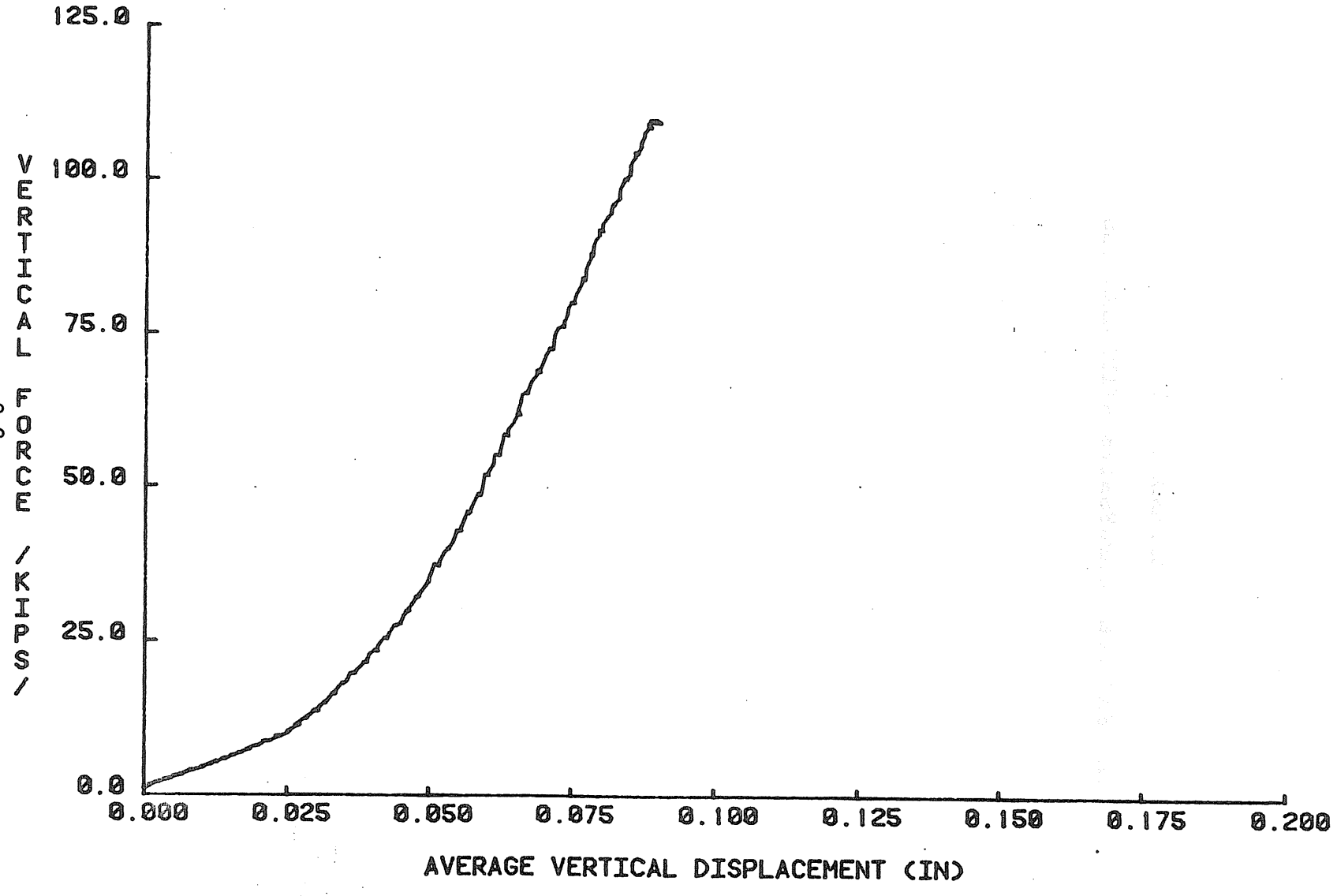

Figure C.1 Bearing A45, Pre-Fatigue Compressive Stiffness Test

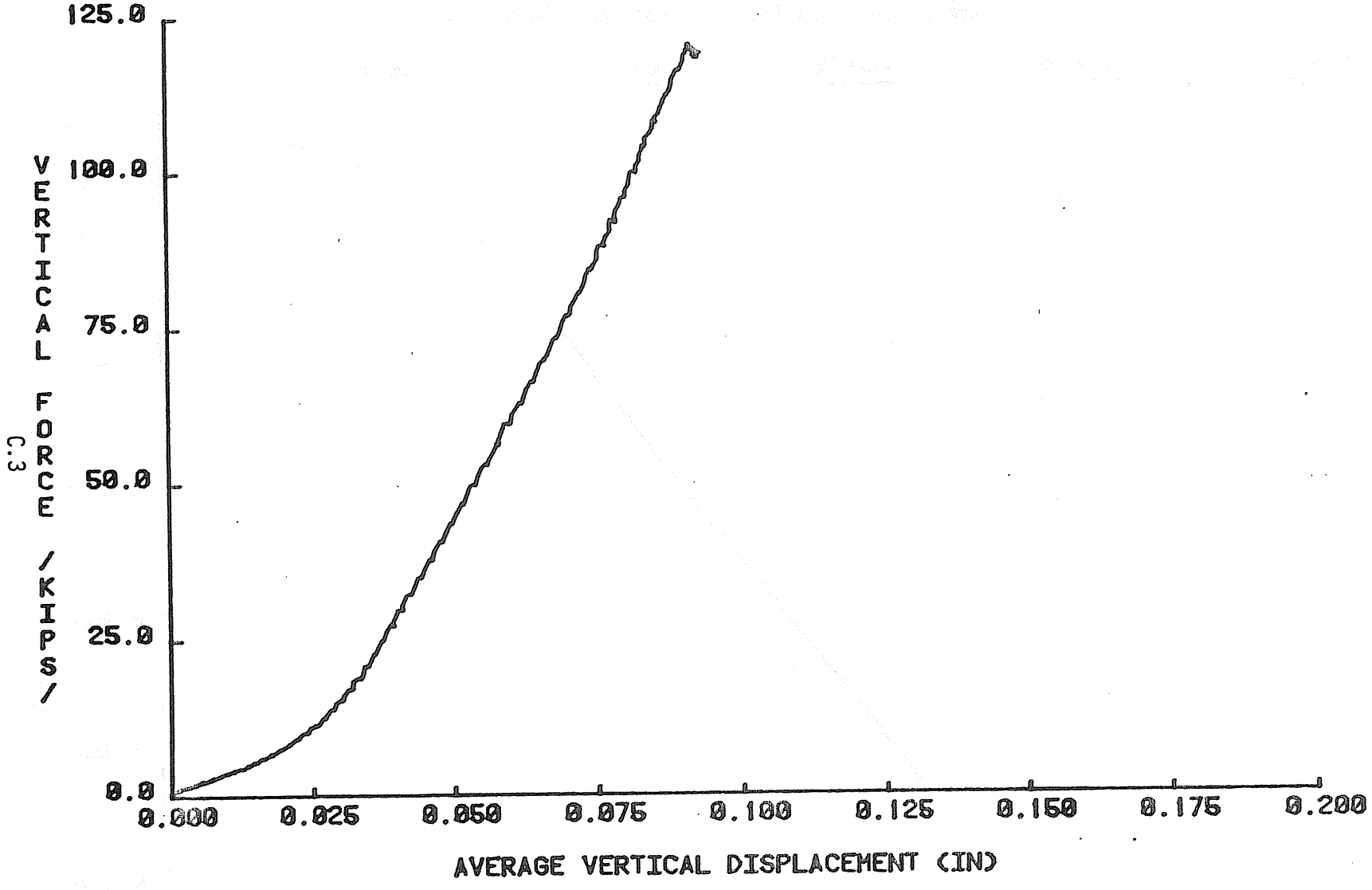

Figure C.2 Bearing A30, Pre-Fatique Compressive Stiffness Test

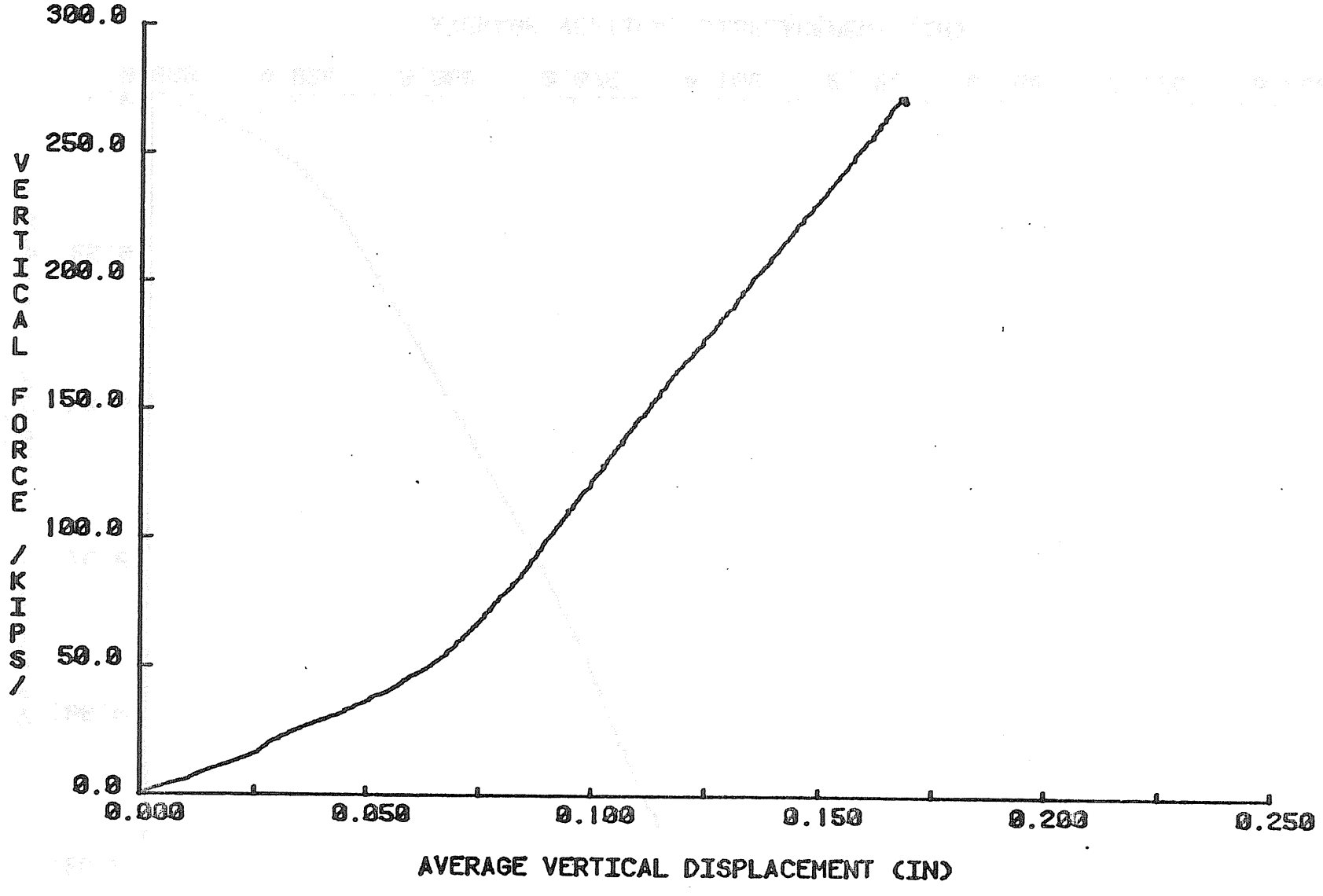

Figure C.3 Bearing D90, Pre-Fatigue Compressive Stiffness Test

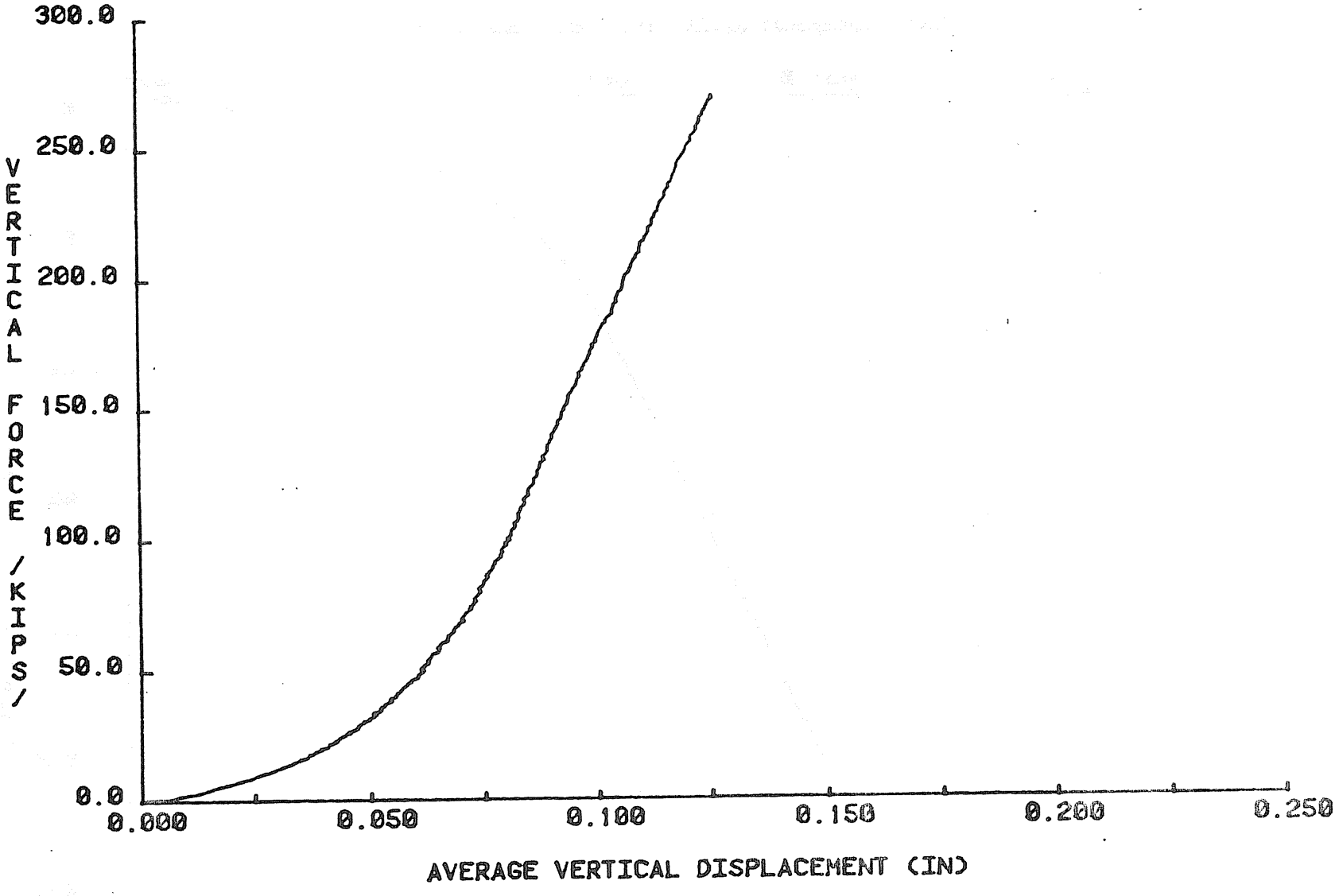

Figure C.4 Bearing D60, Pre-Fatigue Compressive Stiffness Test

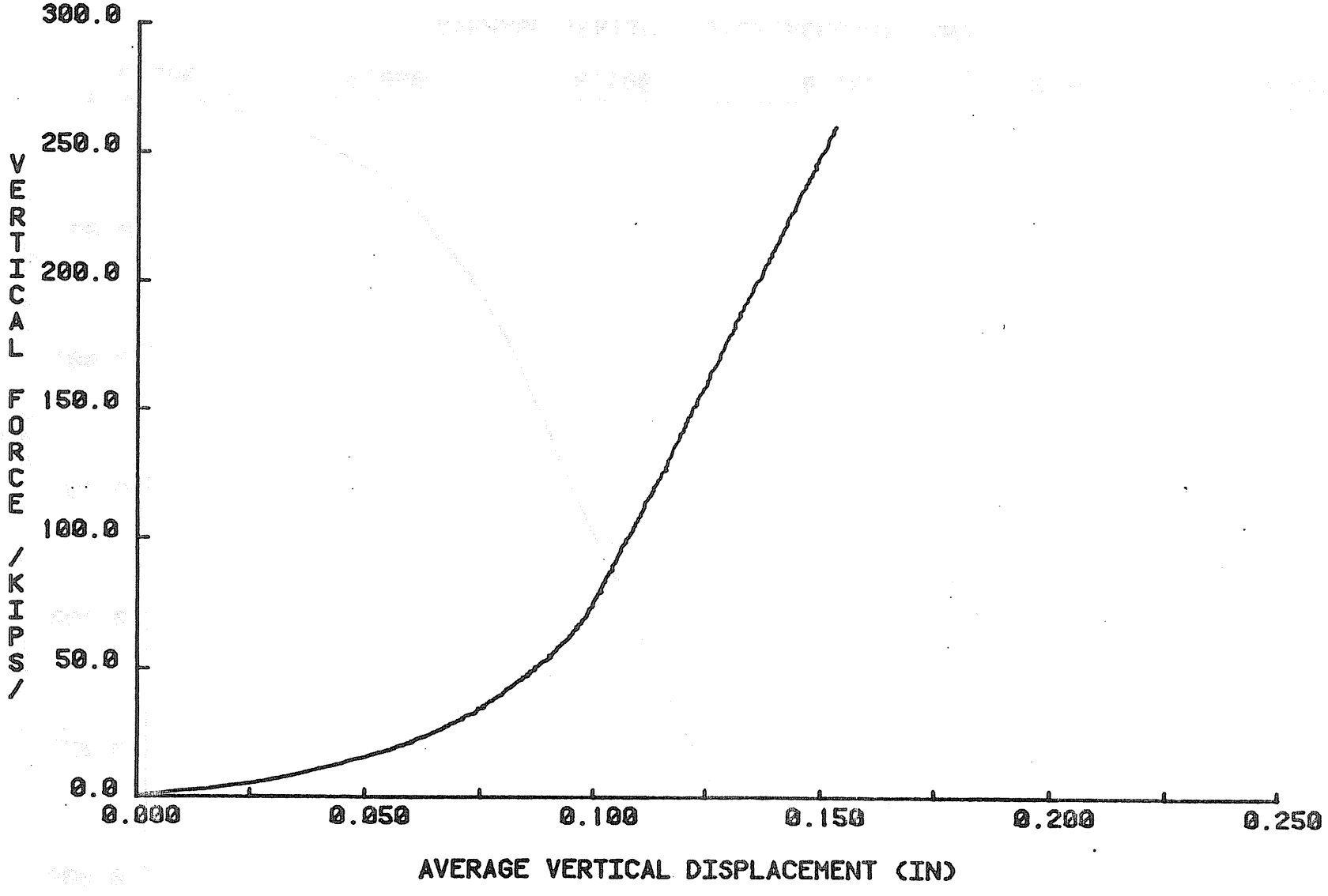

Figure C.5 Bearing D45, Pre-Fatigue Compressive Stiffness Test

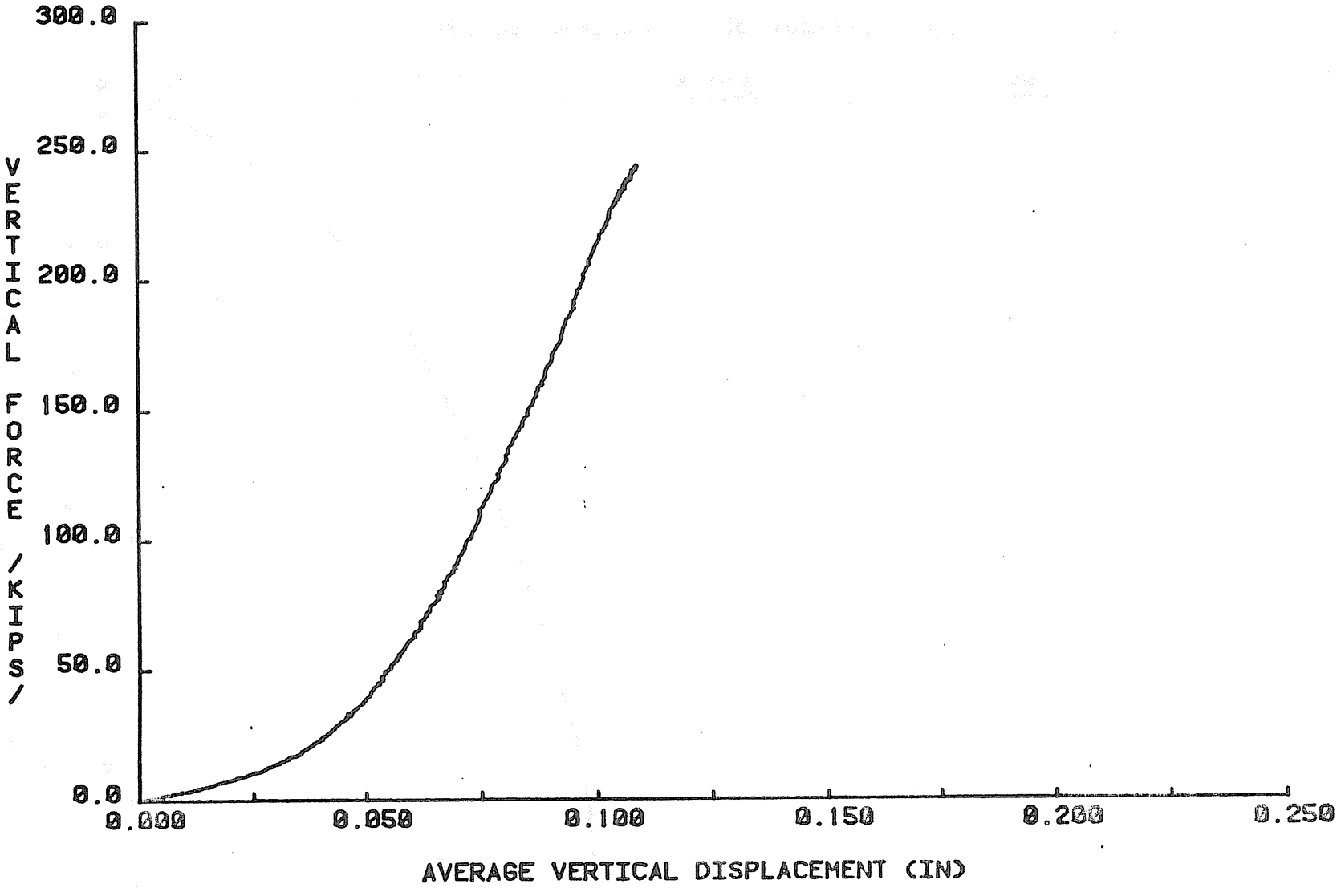

Figure C.6 Bearing D30, Pre-Fatigue Compressive Stiffness Test

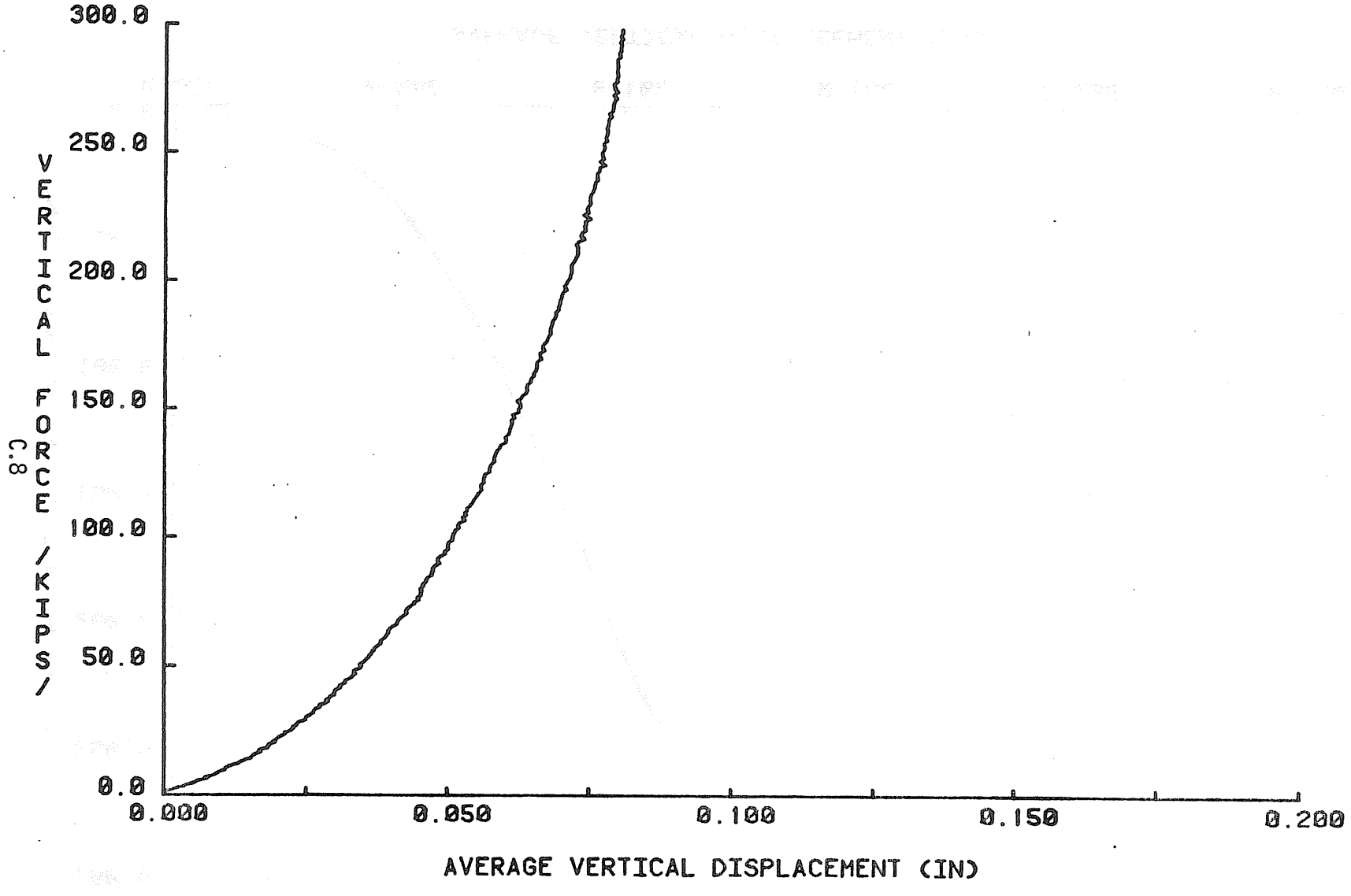

Figure C.7 Bearing E90, Pre-Fatigue Compressive Stiffness Test

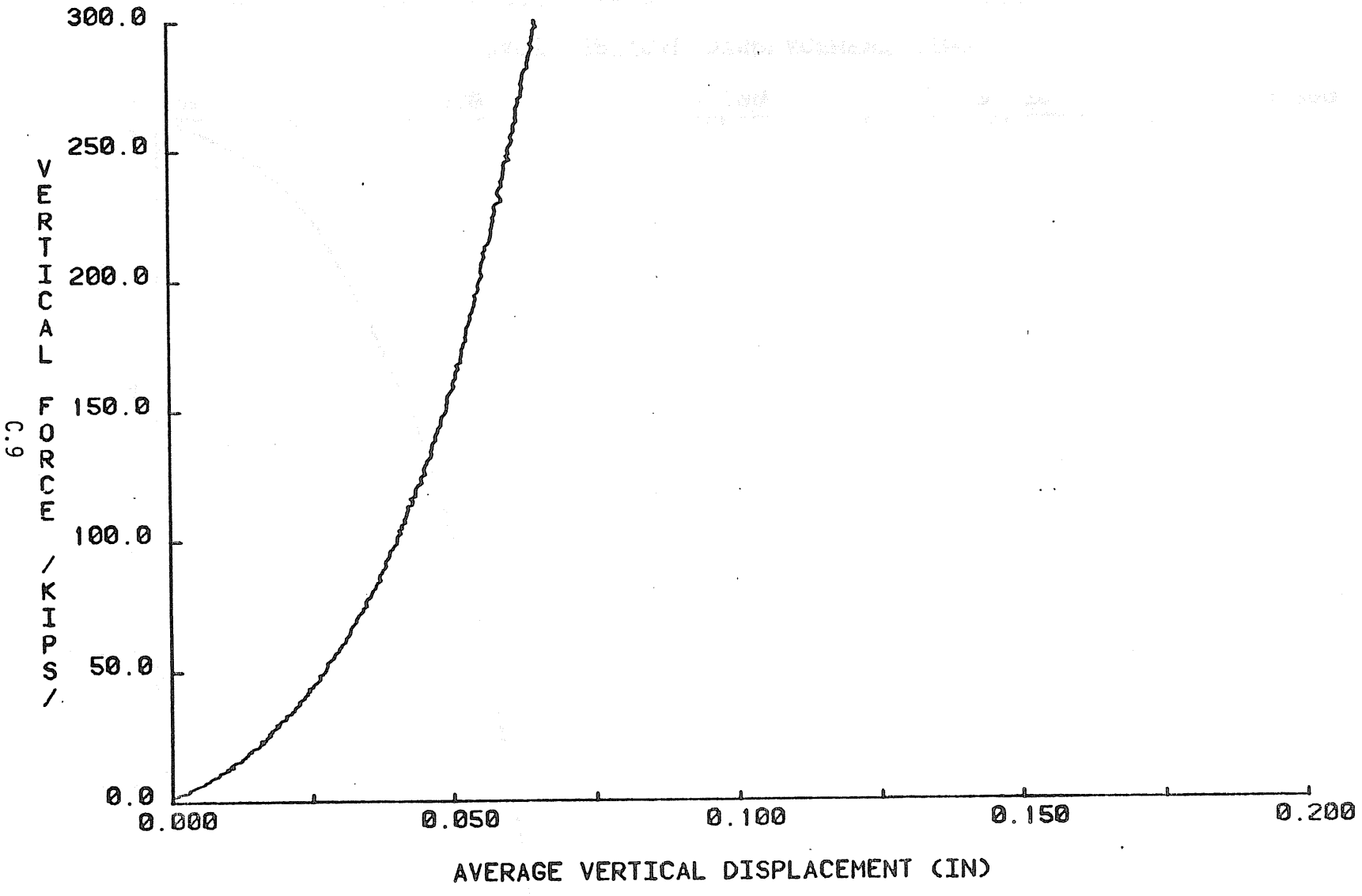

Figure C.8 Bearing E60, Pre-Fatigue Compressive Stiffness Test

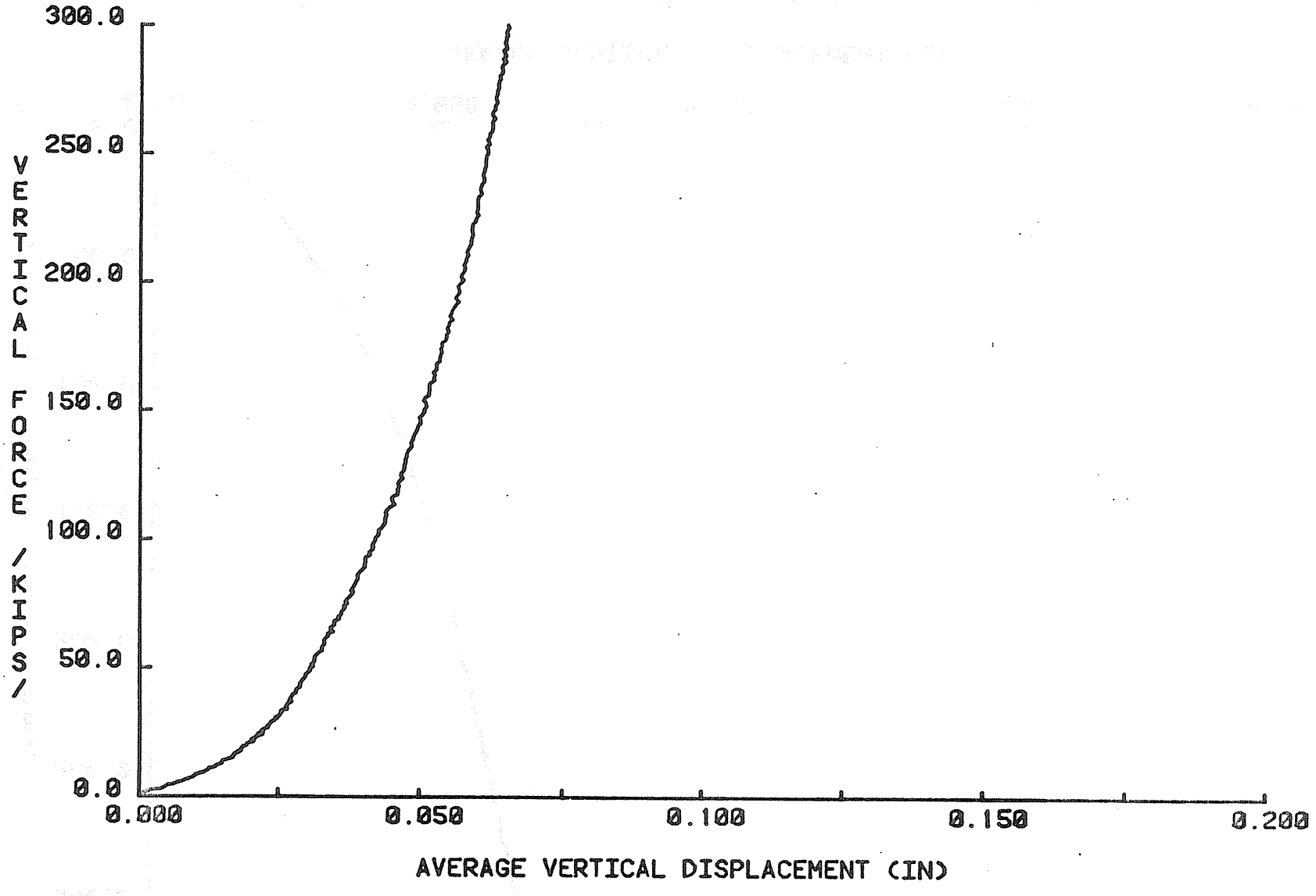

C.10

Figure C.9 Bearing E45, Pre-Fatigue Compressive Stiffness Test

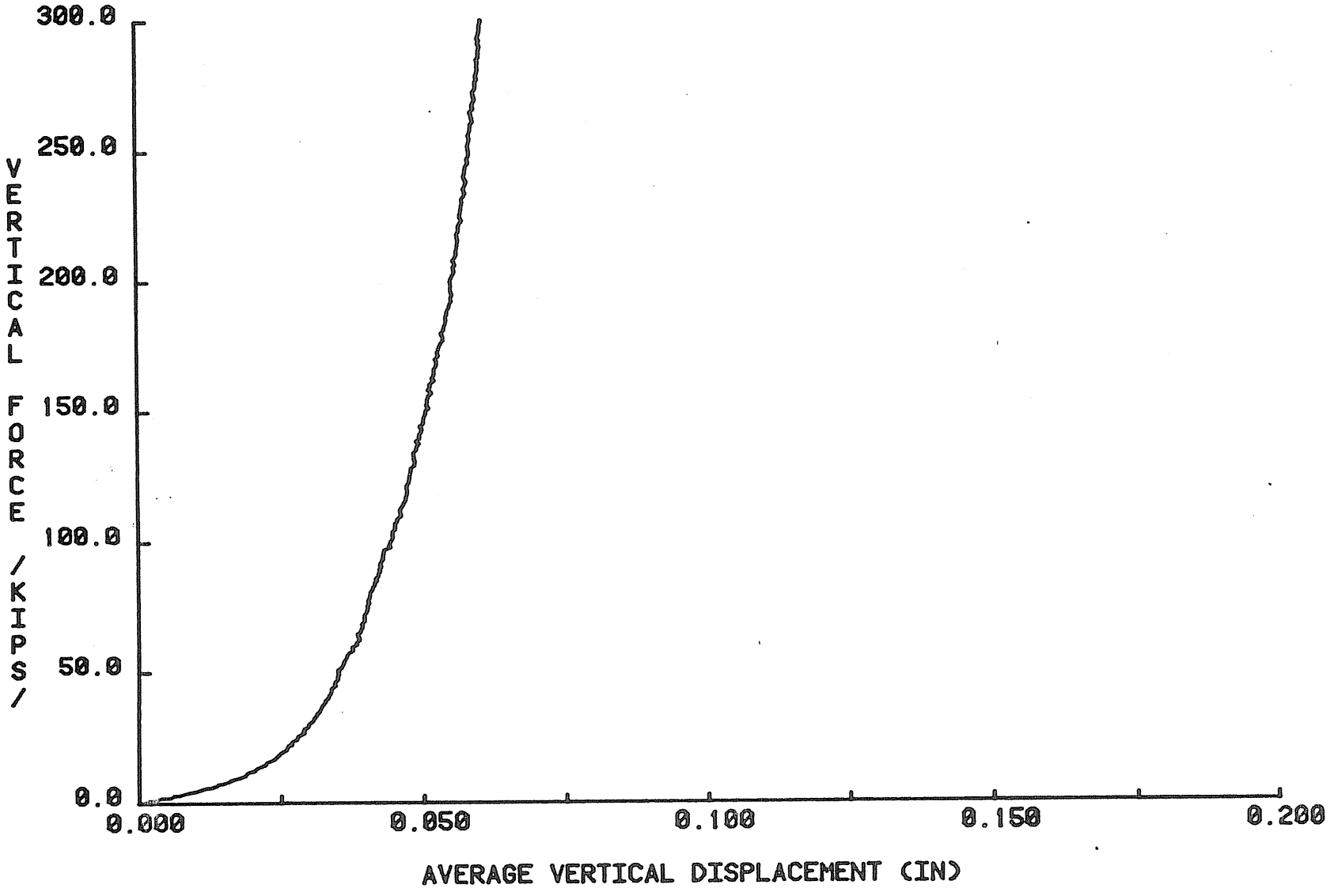

Figure C.10 Bearing E30, Pre-Fatigue Compressive Stiffness Test

APPENDIX C.2

POST-FATIGUE (PARALLEL) COMPRESSIVE STIFFNESS TESTS

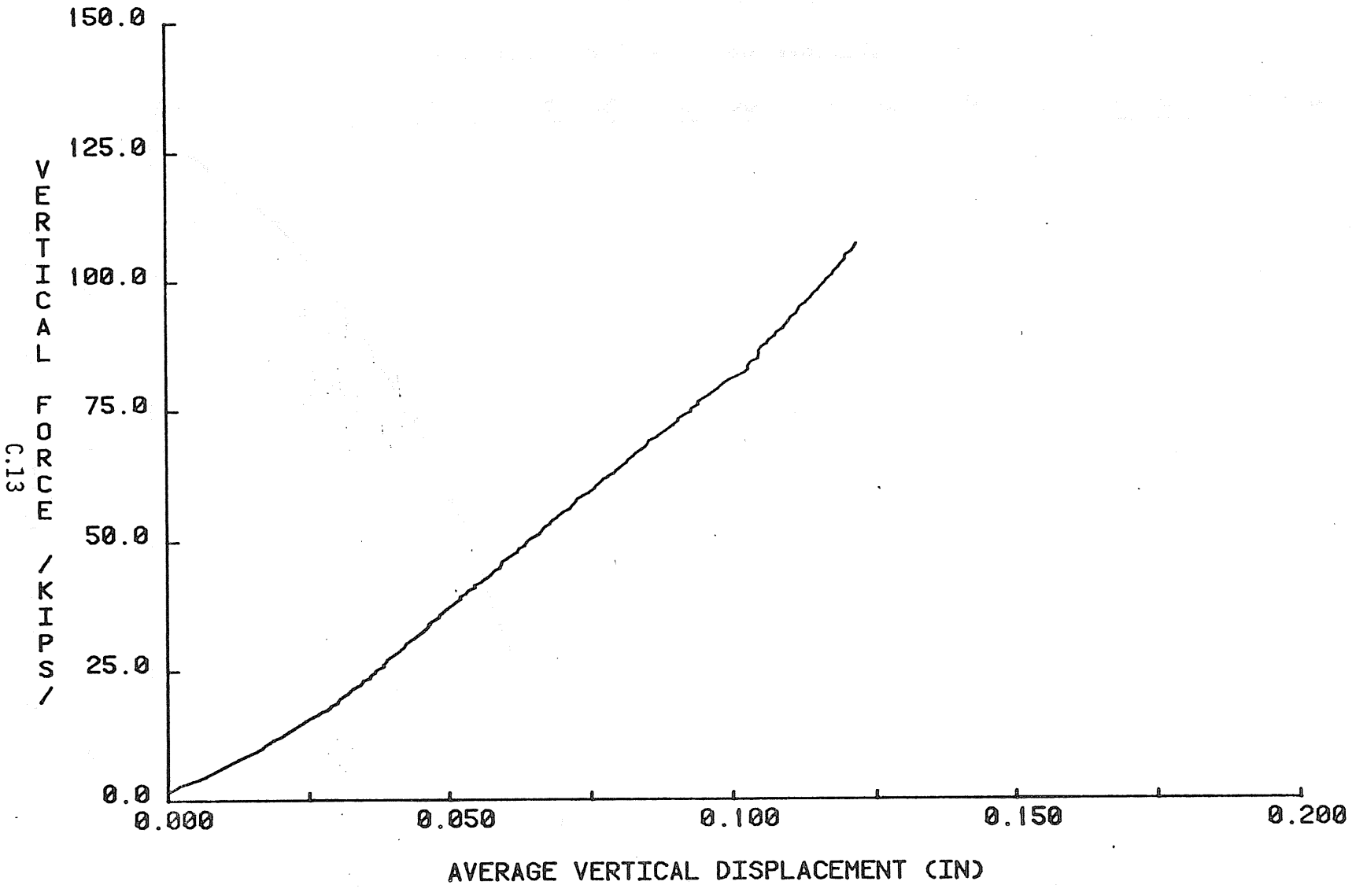

Figure C.11 Bearing A90, Post-Fatigue (Parallel) Compressive Stiffness Test

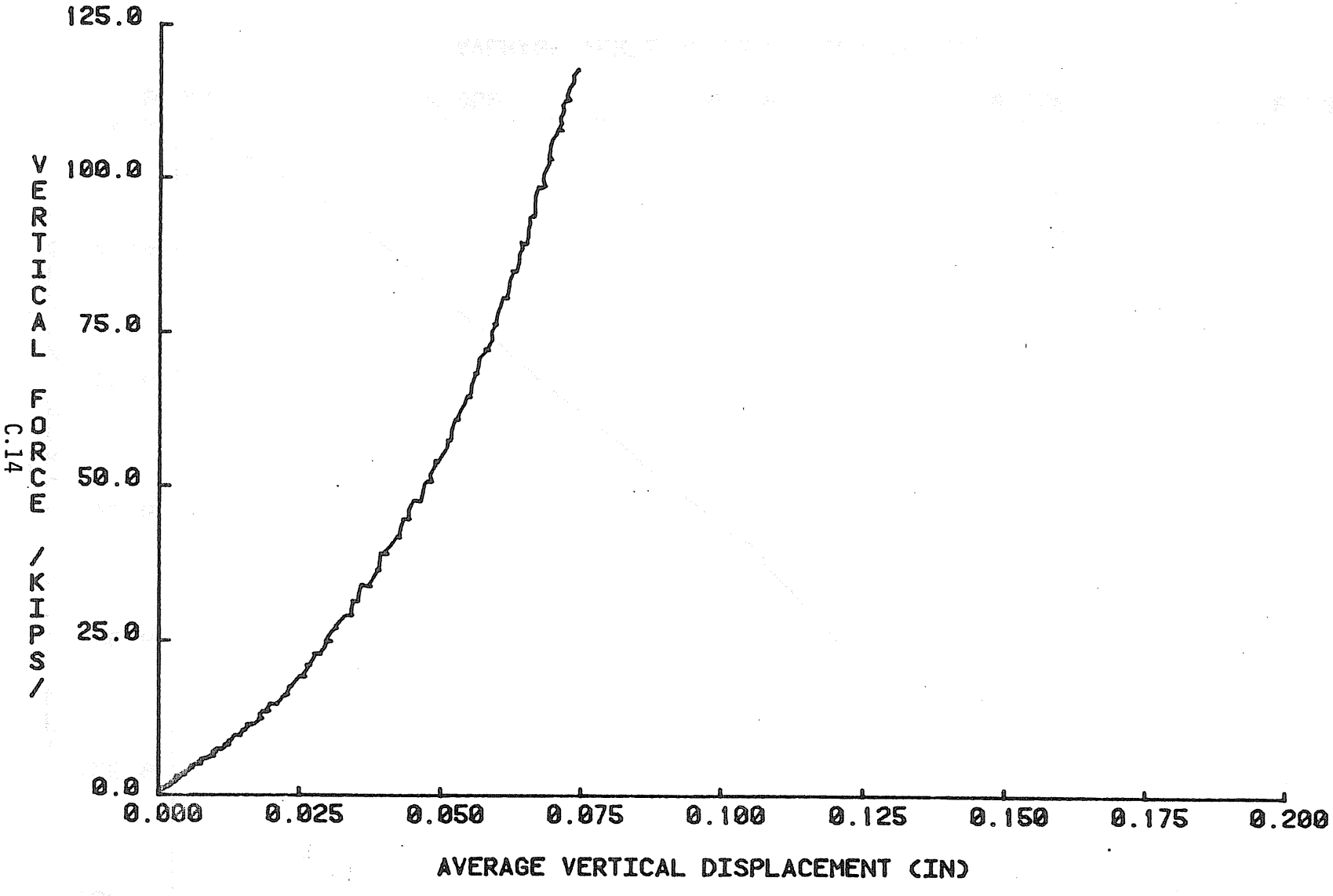

Figure C.12 Bearing A60, Post-Fatique (Parallel) Compressive Stiffness Test

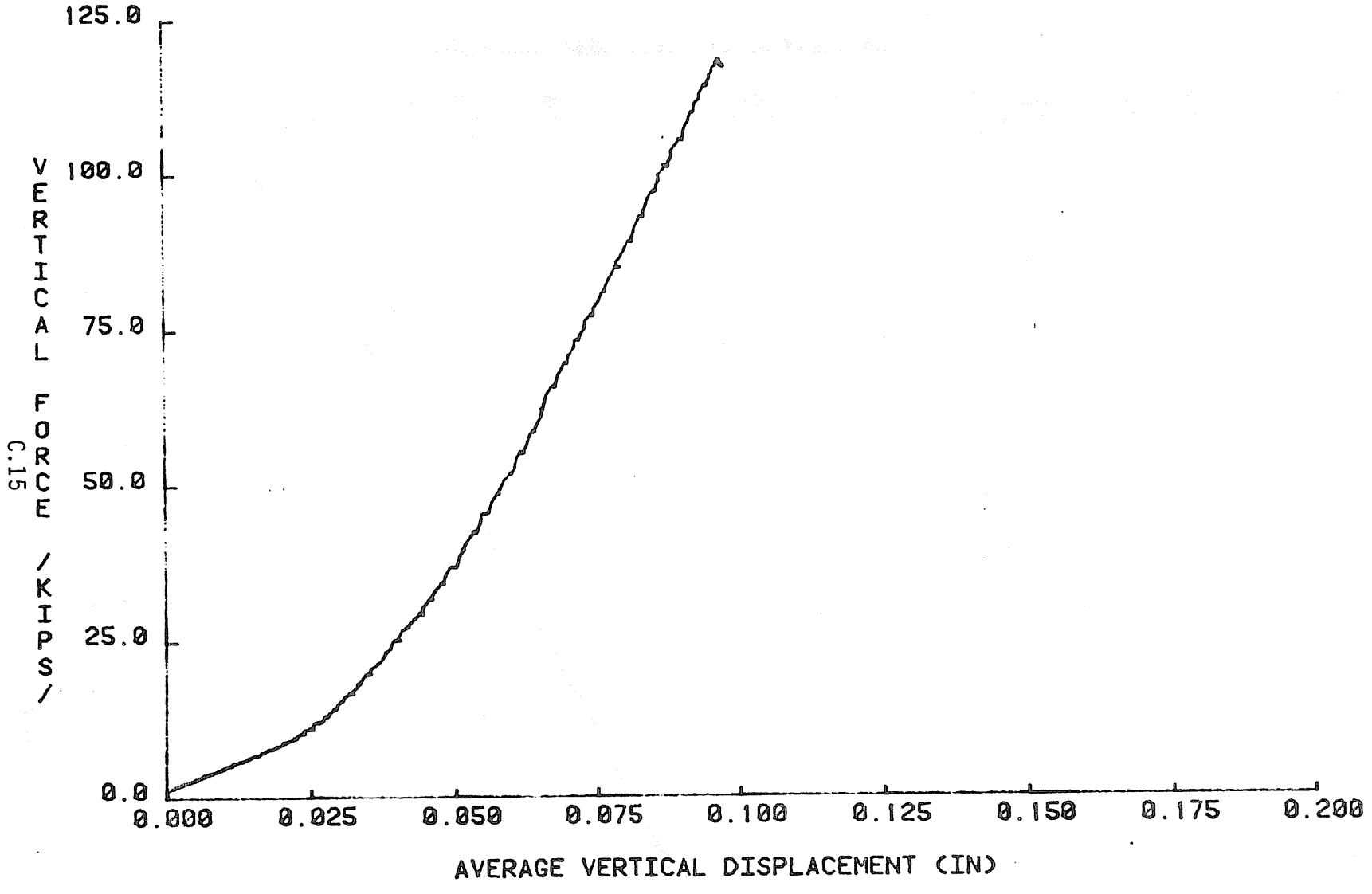

Figure C.13 Bearing A45, Post-Fatigue (Parallel) Compressive Stiffness Test

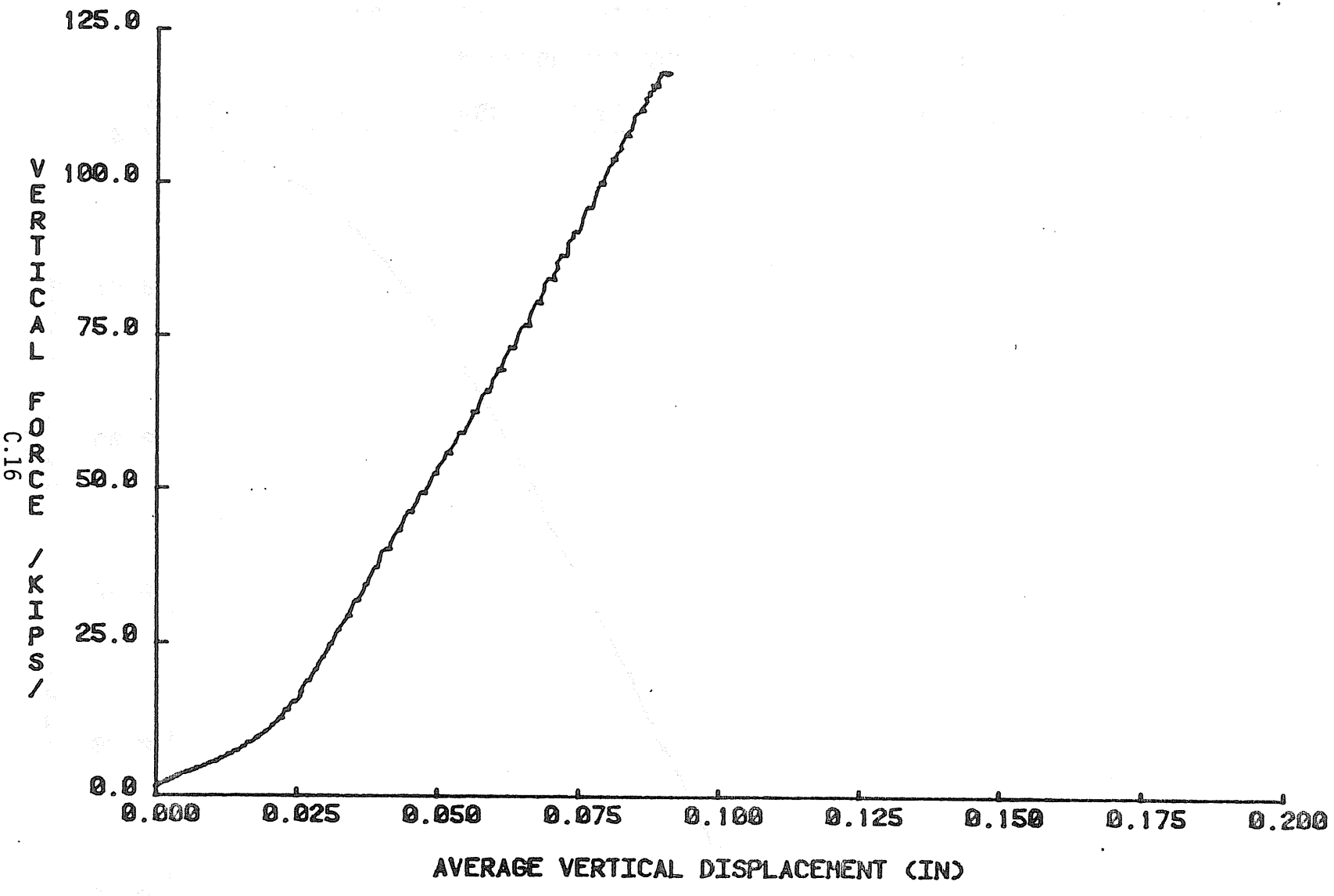

Figure C.14 Bearing A30, Post-Fatigue (Parallel) Compressive Stiffness Test

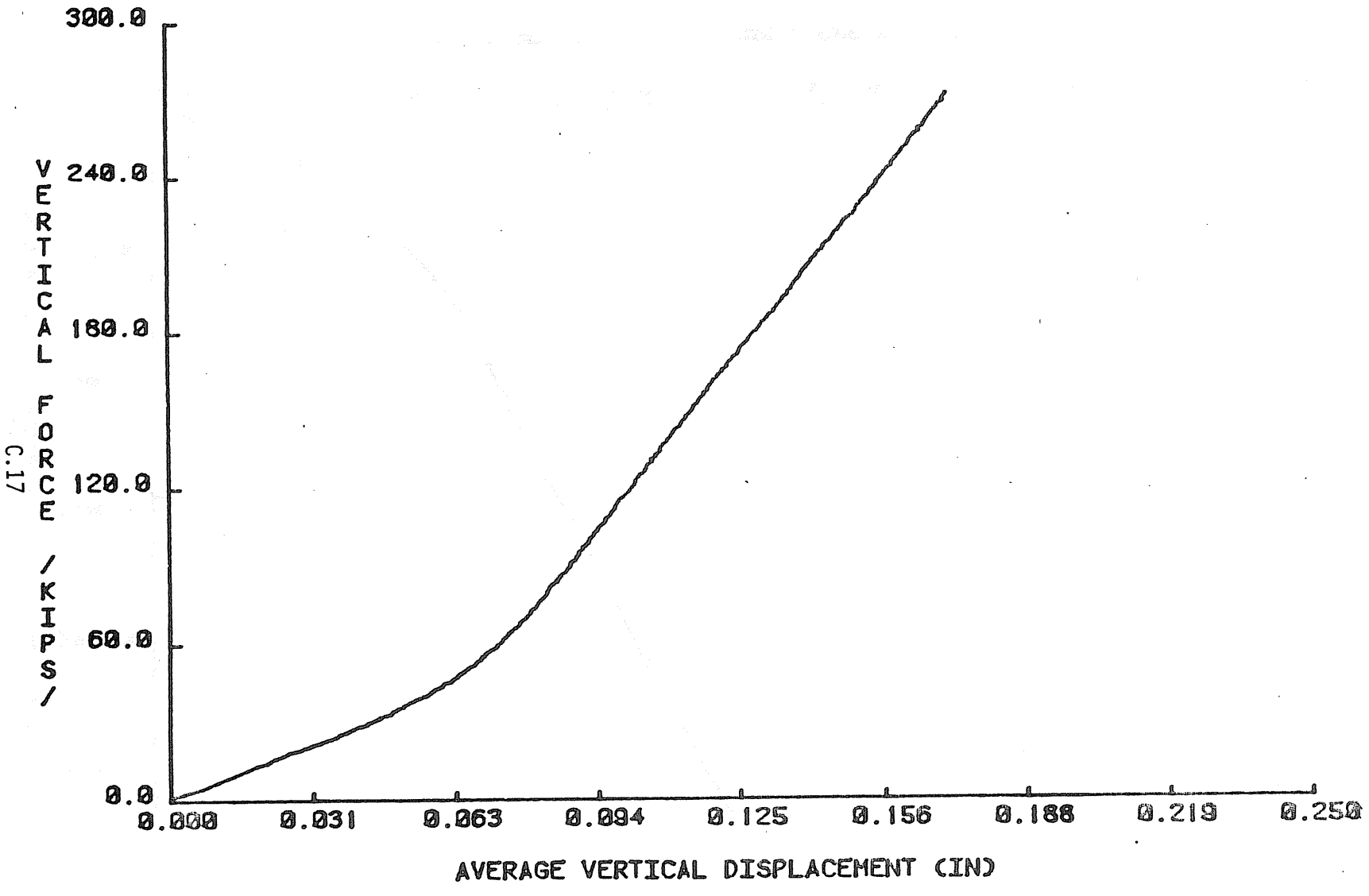

Figure C.15 Bearing D90, Post-Fatigue (Parallel) Compressive Stiffness Test

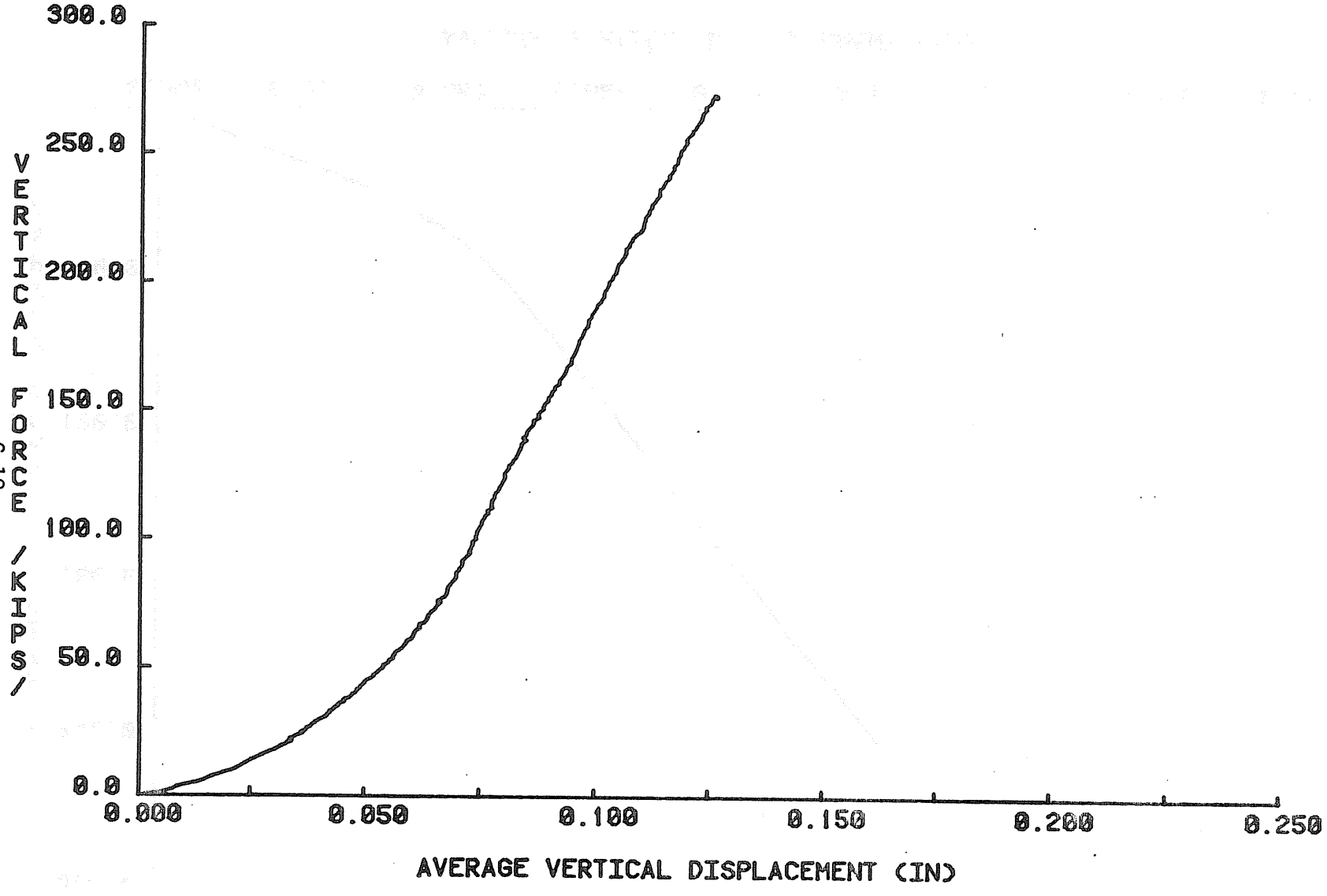

C.18

Figure C.16 Bearing D60, Post-Fatigue (Parallel) Compressive Stiffness Test

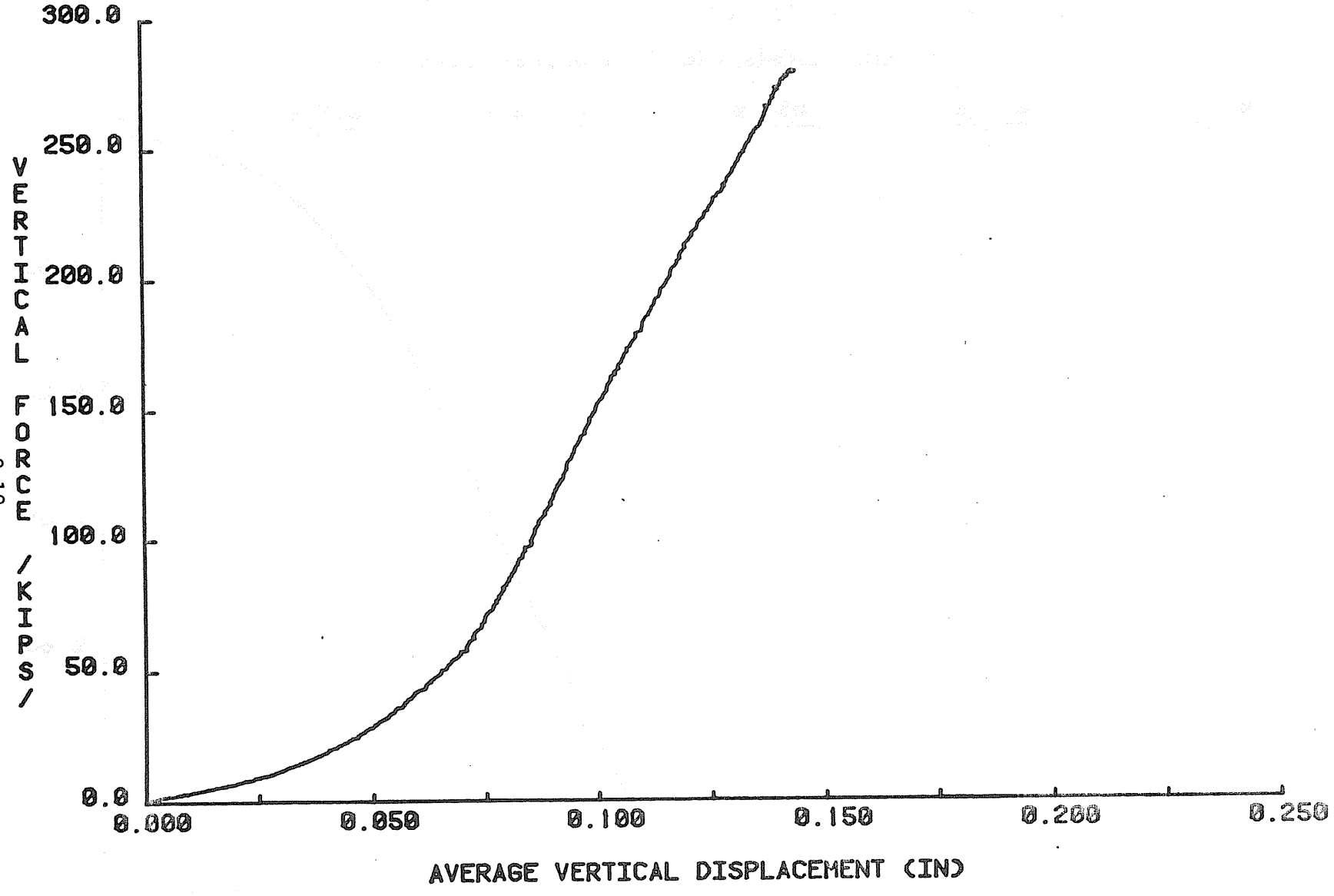

Figure C.17 Bearing D45, Post-Fatigue (Parallel) Compressive Stiffness Test

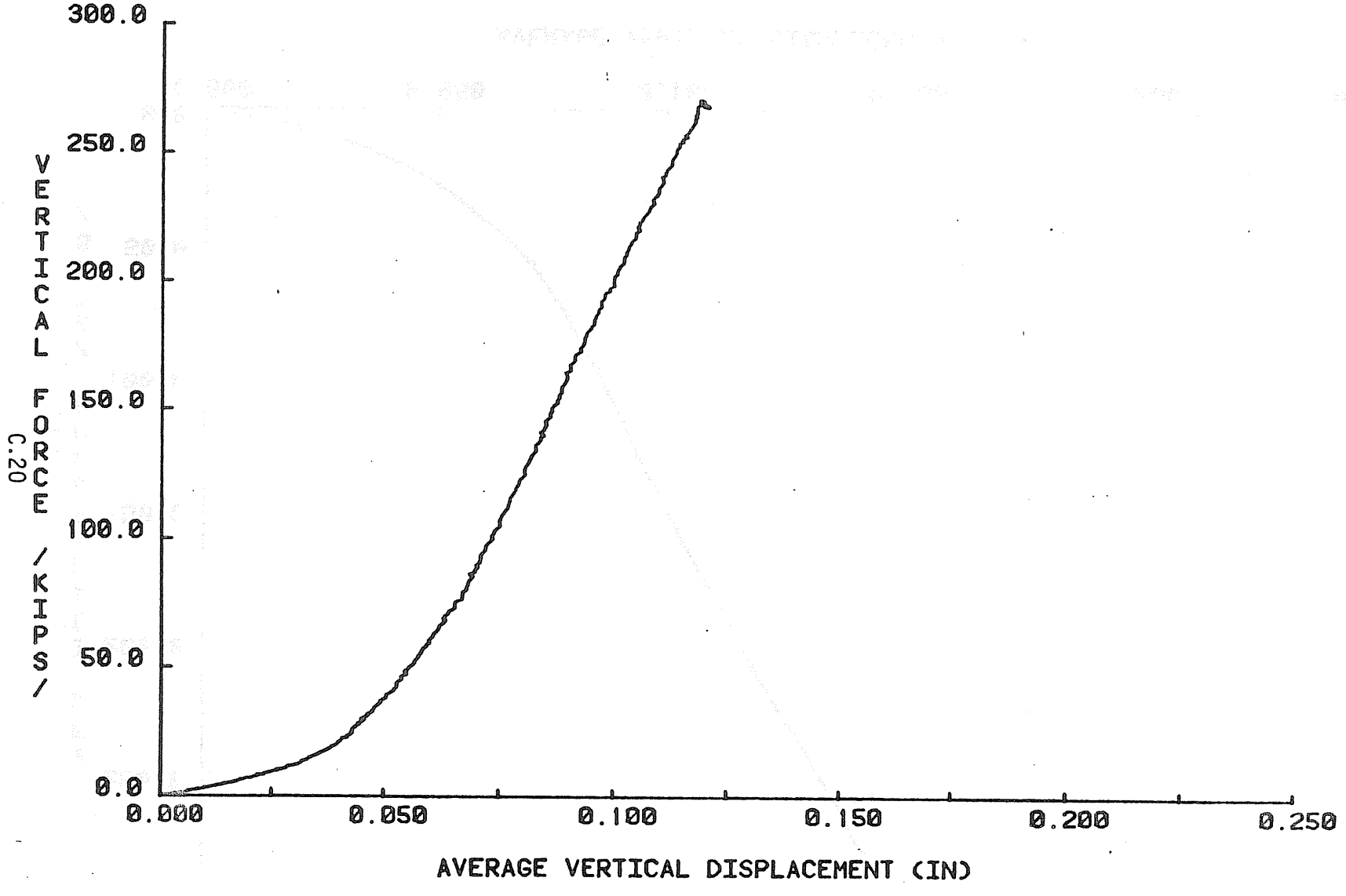

C.20

Figure C.18 Bearing D30, Post-Fatigue (Parallel) Compressive Stiffness Test

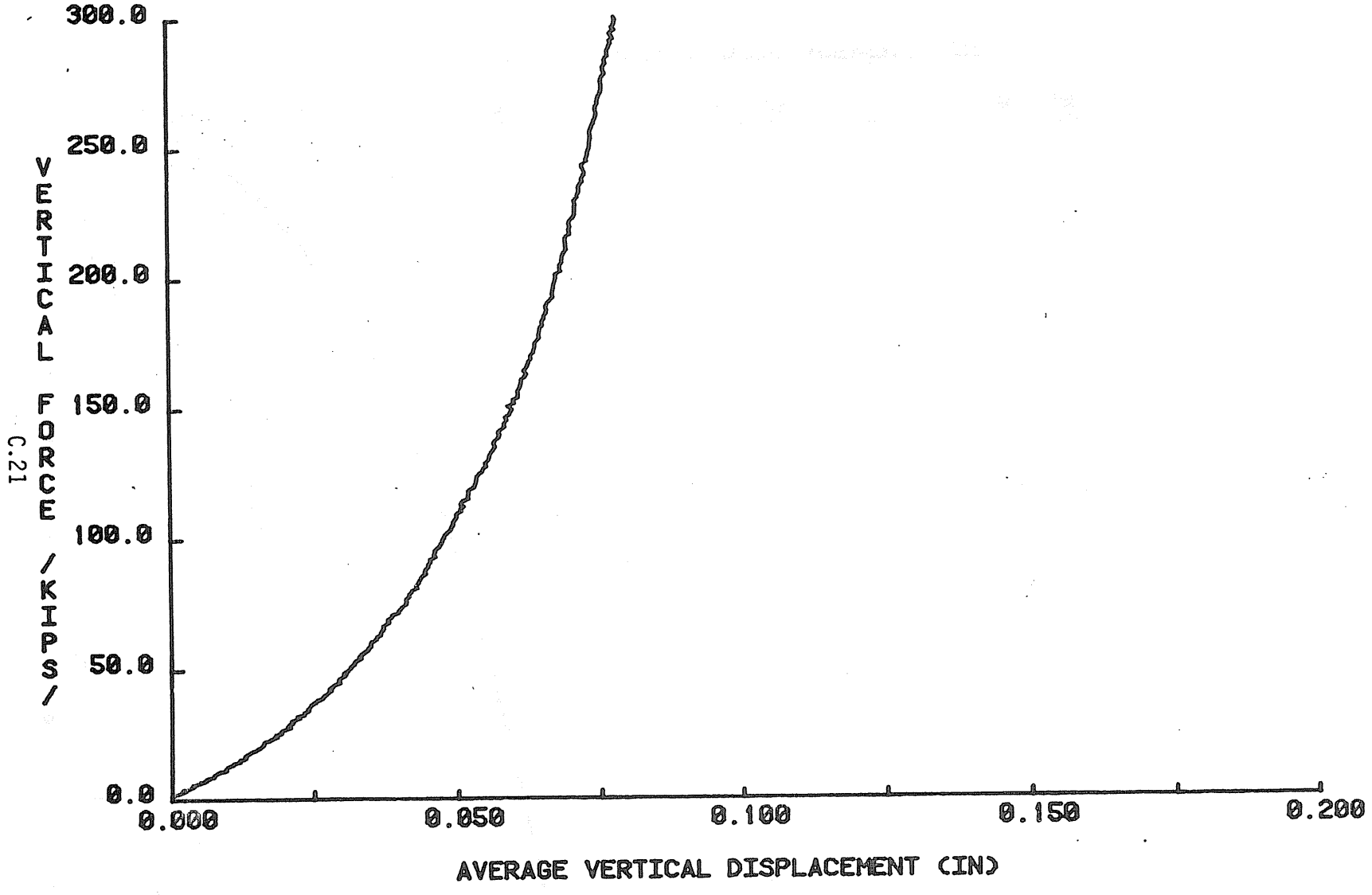

Figure C.19 Bearing E90, Post-Fatigue (Parallel) Compressive Stiffness Test

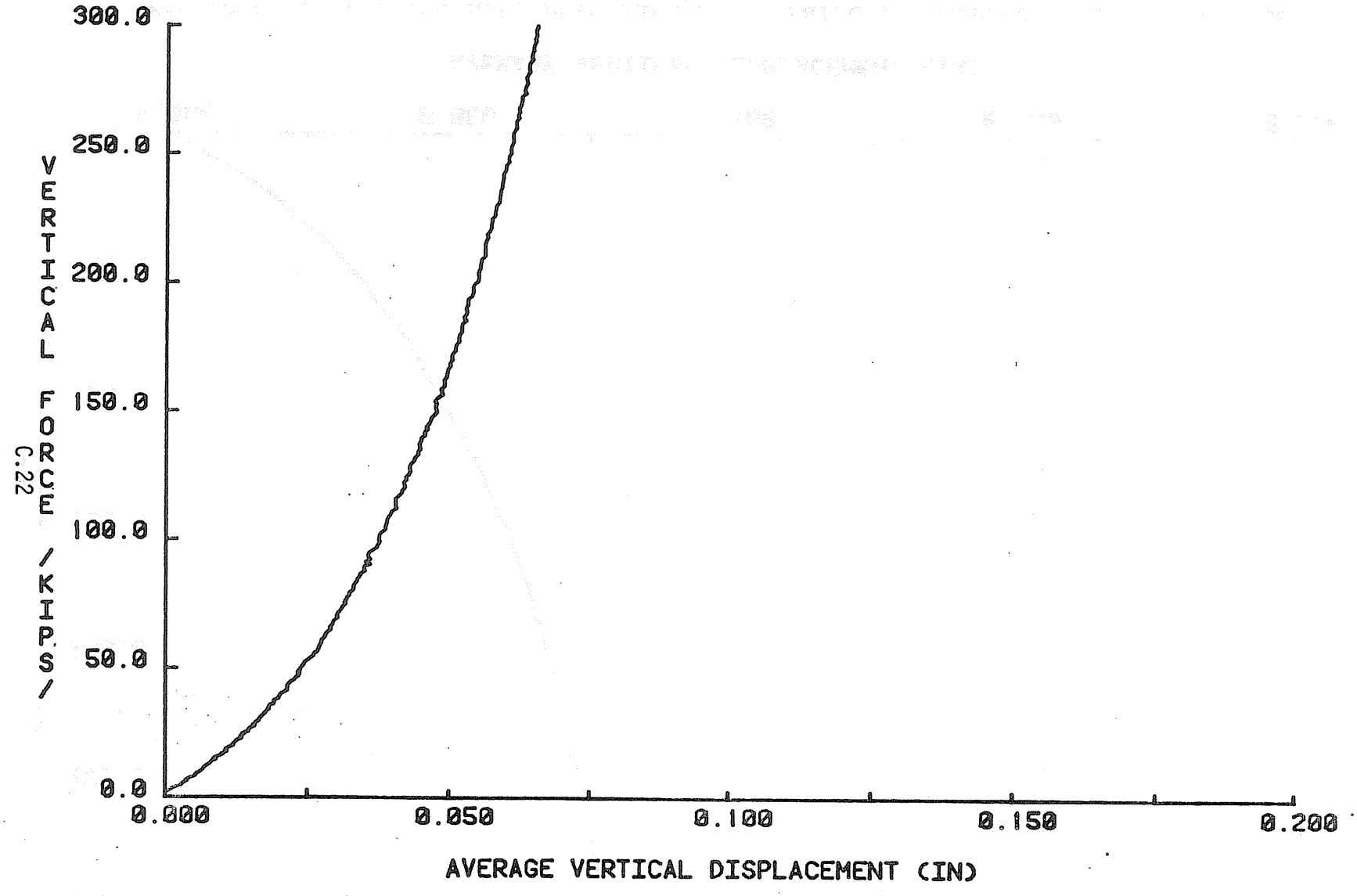

Figure C.20 Bearing E60, Post-Fatigue (Parallel) Compressive Stiffness Test

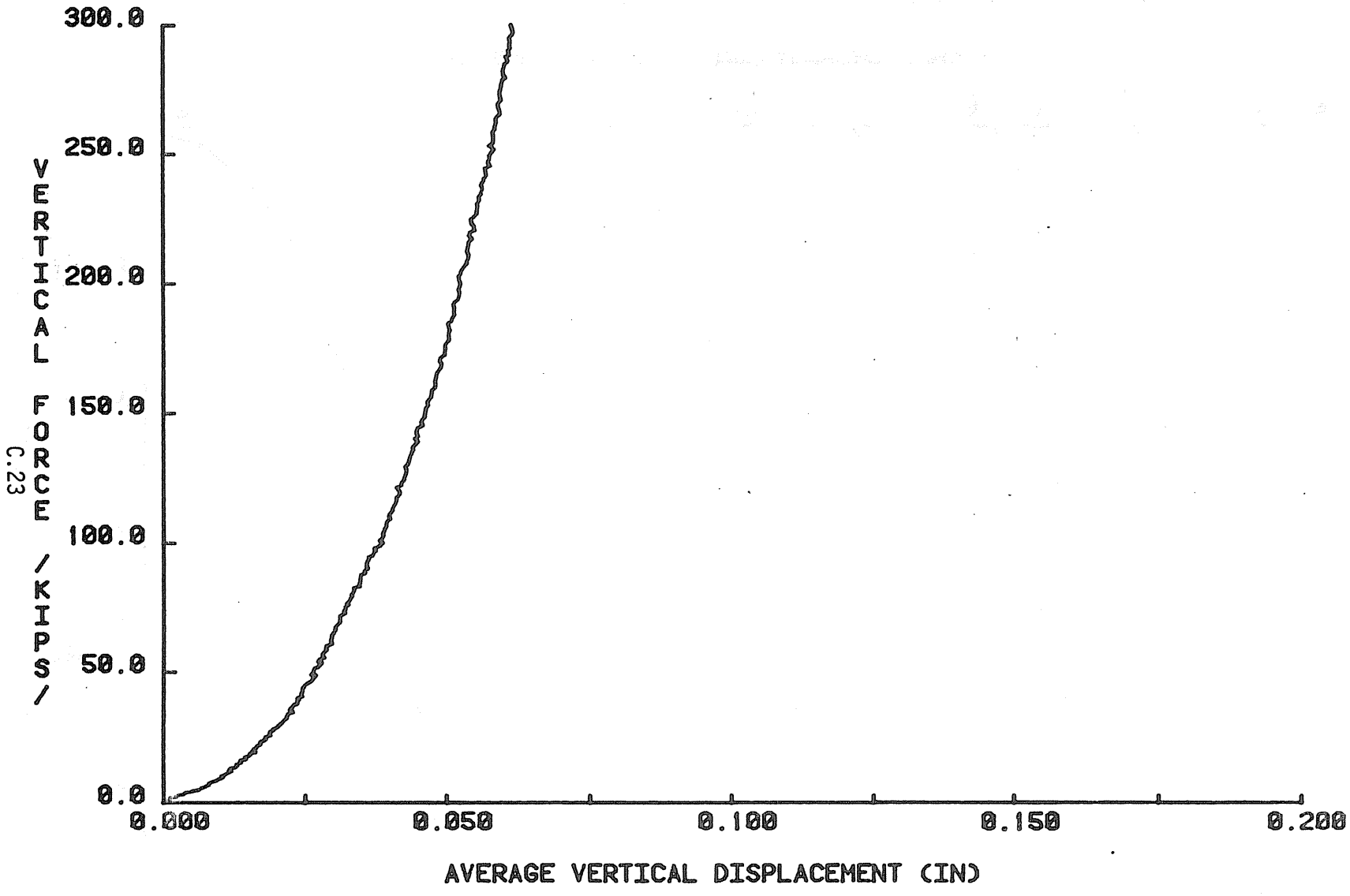

Figure C.21 Bearing E45, Post-Fatigue (Parallel) Compressive Stiffness Test

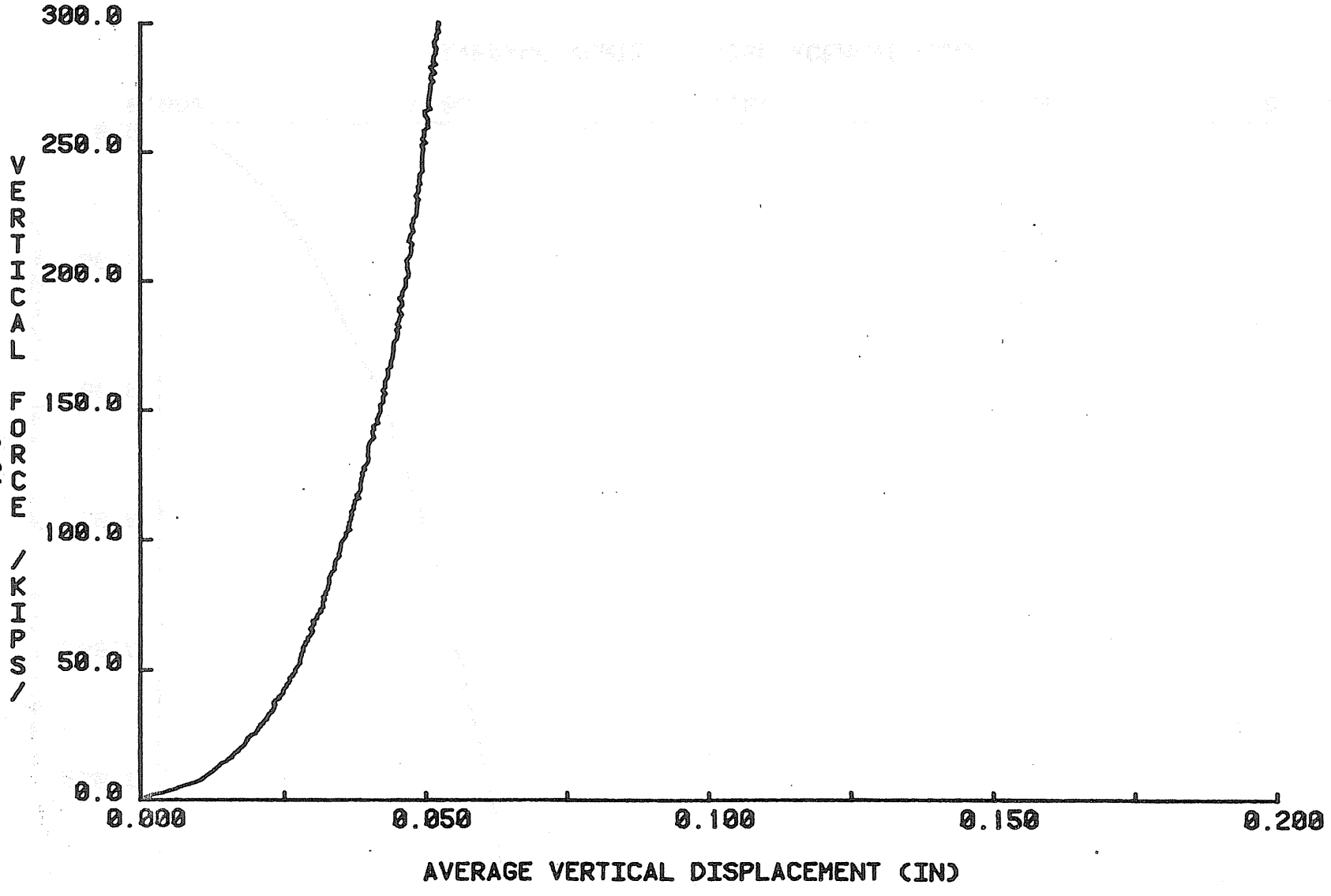

Figure C.22 Bearing E30, Post-Fatigue (Parallel) Compressive Stiffness Test